UTS UNIVERSITY OF TECHNOLOGY SYDNEY

Numerical and Experimental Investigations on Static Behaviour of Composite Cold-Formed Steel and Timber Flooring System

by Dheeraj Karki

Thesis submitted in fulfilment of the requirements for the degree of

Doctor of Philosophy

under the supervision of Dr Harry Far and
A/Prof Shami Nejadi

University of Technology Sydney
Faculty of Engineering and Information Technology

September 2023

Certificate Of Original Authorship

I, *Dheeraj Karki*, declare that this thesis is submitted in fulfilment of the requirements for the award of *Doctor of Philosophy* in the *School of Civil and Environmental Engineering* at the University of Technology Sydney.

This thesis is wholly my own work unless otherwise referenced or acknowledged. In addition, I certify that all information sources and literature used are indicated in the thesis.

This document has not been submitted for qualifications at any other academic institution.

This research is supported by the Australian Government Research Training Program.

Signature: Production Note:
Signature removed prior to publication.

Date: 12/09/2023

Acknowledgments

I want to express my sincere gratitude to my supervisors, Dr Harry Far, A/Professor Shami Nejadi and Dr Ali Saleh, for their exceptional guidance and insightful counsel during this research project. I am grateful for their sincere interest in my progress and appreciate their ongoing assistance, without which this thesis would not have been possible.

My sincere thanks go to the University of Technology Sydney for allowing me to conduct this research supported by the Australian Government Research Training Program. I want to thank all of the technical officers in the Structural and Material Testing Facility of UTS Tech Lab, especially Peter Brown, for his continuous assistance and technical expertise, which made this project's experimental component feasible.

I am also thankful to my peers and colleagues in the faculty, especially Suleiman Al-Hunaity, who helped me during the experimental phase of the project and valuable project discussions.

Finally, I would like to express my deepest gratitude to my wife, Elisha, for standing beside me, supporting my decisions, and always encouraging me. I am indebted to my family for their love and support.

Table of Contents

List of Figures

List of Tables

Notations

Abbreviations

AISI	American iron and steel institute
AS/NZS 4600	Australian standard for the design of cold-formed steel structures
BSI	British standards institution
CFS	Cold-formed steel
CFST	Cold-formed steel and timber
CLT	Cross-laminated lumber
CS	Coach screw
DSM	Direct strength method
EBA	Eigen buckling analysis
EWM	Effective width method
FEA	Finite element analysis
FEM	Finite element model
LVL	Laminated veneer lumber
NB	Nut and bolt
SDS	Self-drilling screw
STC	Steel timber composite
TCC	Timber concrete composite

Symbols

A_f	Cross-sectional area of fastener
A_s	Cross-sectional area of CFS joist
A_{sc}	Cross-sectional area of CFS section in compression
A_{st}	Cross-sectional area of CFS section in tension
A_p	Cross-sectional area of plywood sheathing
b_{eff}	Effective width of plywood
C	Compressive force in plywood
d_f	Diameter of fastener
D	Ductility of shear connectors
E	Elastic modulus
$E_{0.2}$	Tangent modulus at 0.2% proof stress
$(EI)_{exp}$	Flexural stiffness of composite beam measured from experiment
$(EI)_{eff}$	Effective flexural stiffness of the composite beam
$(EI)_{fea}$	Flexural stiffness of composite beam predicted by finite element analysis
F_{cp}	Compressive strength of plywood
F_{tp}	Tensile strength of plywood
I_{comp}	Second moment of area of composite system
K	Slip modulus of shear connector
$K_{0.4}$	Initial stiffness of shear connectors
$K_{0.6}$	Pre-peak stiffness of shear connectors
$M_{pl,r}$	Theoretical plastic moment capacity of composite beam

M_{bare}	Moment capacity of bare CFS joist
$M_{u,exp}$	Ultimate moment capacity of composite beam measured in experiment
$M_{u,fea}$	Ultimate moment capacity of composite beam predicted by FEA
M_{ol}	Elastic local buckling moment
M_{od}	Elastic distortional buckling moment
M_y	Yield moment
N_f	Total number of fasteners in overall span of composite beam
P_u	Ultimate load
Q	Longitudinal shear force that can be resisted by shear connectors
S_{ol}	Imperfection multiplier for local buckling
S_{od}	Imperfection multiplier for distortional buckling
T	Tensile force in CFS joist
V_b	Bearing resistance of timber floorboard
V_f	Shear capacity of fastener
y_c	Distance from the bottom fibre of composite section to the centroid of CFS section
y_{el}	Distance from the bottom fibre of CFS joist to the centroid of composite section
Z	Section modulus
ε	Engineering strain
ε_{true}	True strain
$\varepsilon_{0.2}$	Strain at 0.2% proof stress

$\varepsilon_{1.0}$	Strain at 1% proof stress
m	Strain hardening component
n	Ramberg-Osgood strain hardening component
$n'_{0.2,1.0}$	Ramberg-Osgood strain hardening component between $f_{0.2}$ and $f_{1.0}$
$f_{0.2}$	0.2% proof stress
$f_{1.0}$	1% proof stress
f_y	Yield strength of steel
f_u	Ultimate tensile strength of steel
f_{ol}	Elastic local buckling stress
f_{od}	Elastic distortional buckling stress
f_{uf}	Ultimate strength of fastener
γ	Shear bond coefficient
η	Attained degree of shear connection
h_s	Height of CFS section
t_s	Thickness of CFS section
t_p	Thickness of plywood

Abstract

Currently, the use of Cold-Formed Steel (CFS) joists with timber-based floorboards for constructing lightweight flooring systems in residential buildings is widespread. However, the potential benefits of composite action that arise due to the interaction of the top flange of cold-formed steel joist and the bottom surface of timber floorboard due to shear connection are not considered in the design of such a flooring system. As a result, it led to conservative designs of cold-formed steel joists. This thesis presents a comprehensive experimental and numerical investigation into the flexural behaviour of composite cold-formed steel and timber flooring systems considering the beneficial effect of composite action. As a part of an experimental program, thirteen full-scale composite beam tests were carried out. CFS C-sections with dimensions of 254mm depth and 2.4mm thickness were sheathed with structural plywood panels using four different types of mechanical fasteners as shear connections. For all the tested composite specimens, improvements in the ultimate loading capacity and stiffness were found as a result of the mobilisation of composite action. A three-dimensional (3D) finite element model was developed in ANSYS software and validated against the experimental results. The validated numerical model was used for parametric studies to investigate the influence of various factors that affect the structural behaviour of the composite CFS flooring system. Simplified analytical models are proposed to predict the elastic bending capacity and flexural stiffness of the composite CFS and timber beams. The proposed design methodology discussed herein enables to design for enhanced structural performance to be achieved in CFS flooring systems by utilising the potential benefits of composite action to establish the practical design rules to be used by practising engineers.

Connecting timber floorboard sheathing to CFS joists using mechanical fasteners (e.g. screws and bolts) is a novel method for developing a hybrid and prefabricated eco-friendly floors. This study, through experimental and numerical investigations, has demonstrated the feasibility of composite action to be considered in designing the load-carrying capacity of such lightweight floors. The conducted research shows the substantial gains in structural performance and the influence of key parameters for the composite construction. The findings from the presented study highlights the enhanced structural performance of CFS-plywood composite beams floor system and is an excellent potential option to be utilised in sustainable modular building construction.

1 Introduction

1.1 Background

Buildings consume a significant amount of energy, both embodied and operating, and therefore have a considerable impact on our environment (Newton et al., 2001). Embodied energy is consumed by most of the procedures associated with building construction, from using natural resources to final consumption, including manufacturing of materials and equipment, transportation and other functions (Newton et al., 2001). Energy consumption impacts the environment through its usage of non-renewable resources and emission of greenhouse gases (Omer, 2009). A study conducted by the Australian Bureau of Statistics (ABS) found that the construction industry within Australia had relatively small direct emissions from the consumption of fuels but significantly more embodied emissions, making it one of the major indirect emitting sectors (Yu et al., 2017). Apart from the environmental impacts, the construction industry is of great significance because of its important economic position and contribution to Australia's gross domestic product (GDP) (Hassanieh, 2017). Therefore, there is a need to develop some sustainable and economical structural system with minimum impact on the environment.

Most recently, there has been an increasing interest in the building construction industry to minimise energy consumption throughout the building's lifecycle. As a part of the sustainable development process, over the most recent years, there has been a developing enthusiasm for reducing the resources and materials used in building construction (Loss and Davison, 2017). Some growing interests are arising among architects, builders, and engineers to limit the energy demand

during the whole building life cycle as a prime demand for green and eco-friendly buildings (Chan et al., 2017). As a result of an innovative structural system, different composite structures that fulfil performance criteria emerged and contributed to a more sustainable built environment. Combining two or more materials in a structural member is known as a composite structure (Loss et al., 2016). The main advantage of composite structure over non-composite structure is that they generally provide overall more significant performance than the sum of their individual parts, which means an increase in structural capacity and contribute to the minimal utilisation of resources by decreasing the size of structural members (Loss and Davison, 2017).

Steel is one of the most used materials in composite construction due to the strength and stiffness that can be achieved with the least utilisation of materials (Dickof et al., 2014; Hassanieh, 2017). Two main types of structural steel are commonly used in construction; hot-rolled steel and CFS (Kankanamge, 2010). Hot-rolled steel, which requires heat while manufacturing, is more popular and used for many applications in construction. However, in the last decade, the use of CFS as load-bearing and non-load-bearing members for residential, commercial and industrial buildings has significantly increased (e.g., Rondal, 2000; Hancock, 2003). Cold-formed steel (CFS) members are made from structural quality sheet steel formed into various shapes by press braking or roll forming through a series of dies without heat (Kankanamge, 2010). Figure 1.1 shows the different cross-sectional shapes of CFS sections used in the construction (Yu, 1999).

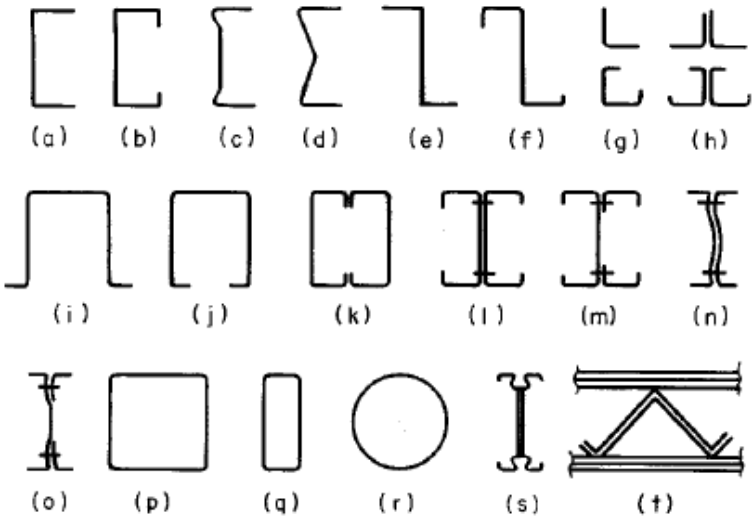

Figure 1.1: Various shapes of cold-formed steel sections (Yu, 1999).

CFS members are chosen over their hot-rolled counterparts for constructing structural systems because of their high strength-to-weight ratio, ease of fabrication, ease of transportation, and rapid installation (Hancock, 1998; Wang and Young, 2014). The increasing interest of building professionals in using cold-formed steel members over other construction materials, such as hot-rolled steel or timber, is because of the following reasons (NASH, 2007);

- Lightweight- CFS is made of thin gauge, high tensile steel making them light and strong.
- Cost-effective –CFS framing provide cost-effective benefits over the entire life cycle of construction due to shorter project cycles, accuracy of steel components and improved design efficiency.
- Durable- CFS framing offers resistance to corrosion, mould and termite.
- Sustainable-CFS framing is 100% recyclable and meets the highest sustainability requirements for green building standards.

- Non-combustible and resilient-CFS framing is non-combustible and resistant to extreme environmental loads like wind, seismic, snow
- Easy installation- CFS framing is light, making it easy to transport, handle and assemble.
- Pre-fabrication and modular construction-CFS wall, floor or roof sections can be assembled off-site to minimise wastage of material and ensure better quality control.

Steel framing has been in Australia for over 50 years and is firmly established in residential and low-rise commercial construction (Australian steel institute, 2019). The use of cold-formed steel joists for the construction of lightweight flooring system is widespread in residential buildings in Australia (NASH, 2007), but it should be borne in mind that there are no design equations for the composite cold-formed steel flooring systems that considers the influence of composite action on flexural capacity.

1.2 Cold-Formed Steel Flooring Systems

The demand for a lightweight flooring system consisting of cold-formed steel joists in the building construction industry has increased over the years because of the high strength-to-weight ratio and ease of construction (Raffoul et al., 2019). Initially, the application of cold-formed steel joists is limited to domestic floors. However, increasing urbanisation is forcing a shift in housing to mid-rise apartments, making it the best alternative to conventional timber floor joists (Australian steel institute, 2019). Figure 1.2 below shows a typical raised floor construction in a domestic building in Australia using cold-formed steel joists.

Figure 1.2: A typical domestic raised floor system using cold-formed steel joists (Stratco Australia, 2019).

Lightweight flooring systems consisting of cold-formed steel joists and timber-based floor panels can be an economical and durable solution for the construction of flooring systems in the construction industry due to mass production and speed of construction (Kyvelou, 2017). Composite cold-formed steel and timber flooring systems can be assembled off-site and fixed on-site in a modular way, reducing the construction time. Such flooring system also offers the advantage of a high strength-to-weight ratio, which eventually reduces the self-weight of floors and less imposed load on the foundation(Loss and Davison, 2017). A typical reference construction system and sequence of assembly for the prefabricated composite floor components is shown in Figure 1.3 and assembly method of the prefabricated components is demonstrated in Figure 1.4. Installation of the modular components could be in sequential order as depicted and a close dimensional tolerances can be achieved. This type of construction technology

permit the design of open space structures giving freedom in floor layout and architectural style.

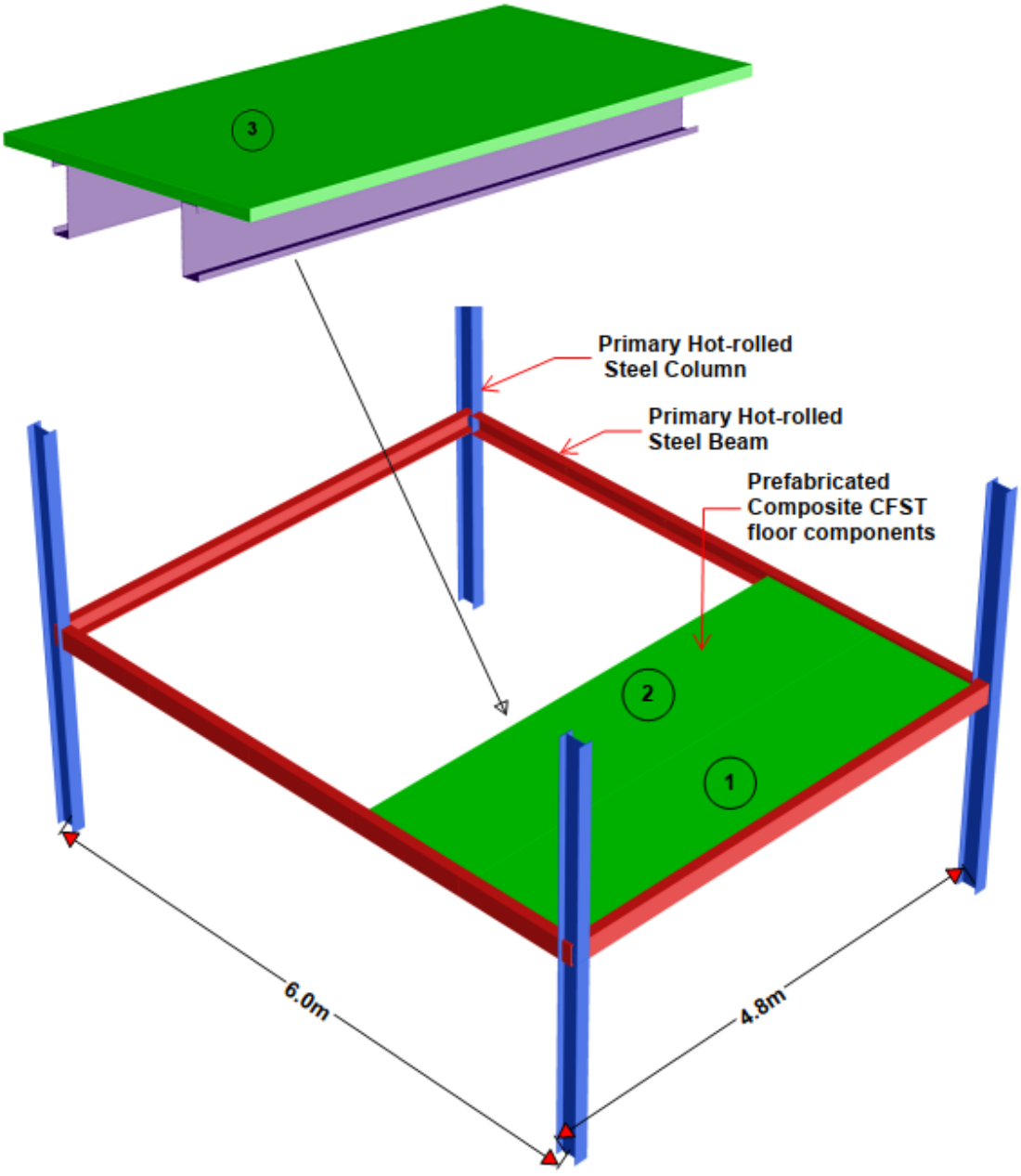

Figure 1.3: Typical reference construction system and sequence of assembly for prefabricated composite floor components

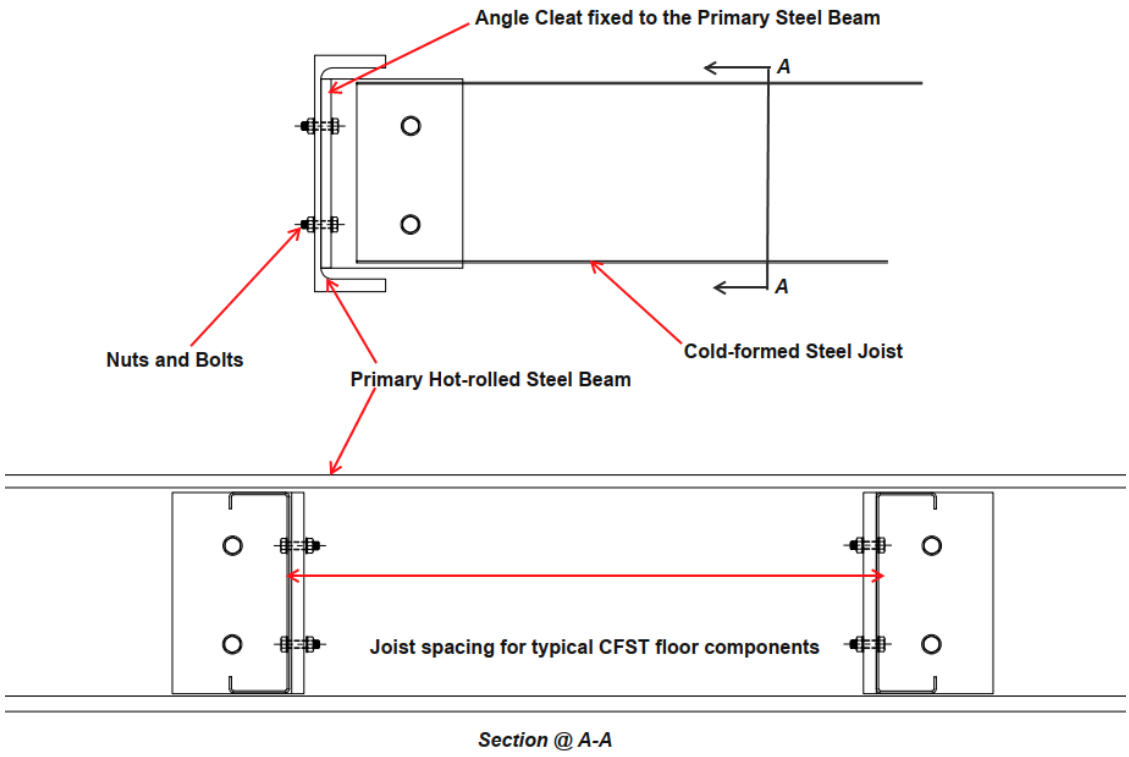

Figure 1.4: Typical connection methodology for the CFST floor components to the priamry steel beam

A few recent studies (e.g. Kyvelou, 2017; Zhou et al., 2019) have been carried out to investigate the structural behaviour of composite flooring systems comprising cold-formed steel and different type of timber floorboards. The results obtained from both experimental and numerical investigation seem promising regarding the improved structural behaviour of the flooring system through the composite action achieved. Overall, the research findings have shown that such a flooring system is feasible to adopt by the building industry for the design and construction of lightweight floors.

1.3 Research Significance and Innovation

Considering the impact of buildings on energy consumption and greenhouse gas emissions, numerous types of research have been done to create an efficient composite floor structure utilising the materials like hot-rolled steel and concrete (e.g. Valente and Cruz, 2004; Mirza and Uy, 2009; Ataei et al., 2016), and timber and concrete (e.g. Ceccotti, 2002; Steinberg et al., 2003; Yeoh et al., 2009). The application of cold-formed steel joist and timber-based floorboard is recently explored in some studies (e.g. Kyvelou et al., 2017b; Zhou et al., 2019; Far, 2020) highlighting the importance of composite action that arise between CFS joists and timber floorboards. There are well-developed design methods for traditional hot-rolled steel beams and reinforced concrete slabs, and timber concrete composite floors; but no theoretical formulations and guidelines have been established yet for the lightweight cold-formed steel and timber flooring systems in Australia. To overcome the current knowledge gaps, this study aims to investigate the composite action of the lightweight floor system with CFS C-shape joists and structural plywood panels.

The composite cold-formed steel and timber floors are relatively lighter than other composite floors and can significantly increase the speed of construction (Kyvelou et al., 2017b; Zhou et al., 2019). The use of CFS joist and structural plywood panels, both recyclable, make this flooring system a novel and sustainable solution that has a minimal impact on the environment. The sustainability of composite CFS and plywood floors can be further enhanced by designing it for future deconstruction and allowing structural components or members to be reused. Since the interaction between cold-formed steel joists and timber-based floorboards plays a vital role in the overall strength and stiffness

of the system, the influence of shear connections on these floors must be well understood. Hence, several methods of shear connections will be studied, considering the ease of assembling and disassembling the floor components.

It is important to note that previous cold-formed steel and timber-based floorboard investigations were carried out on typical cold-formed steel joists without holes on the web. However, this study aims to conduct static tests on composite flooring systems comprising cold-formed steel joists with and without holes in the web. The reason for investigating joists with holes is that plumbing and other service installations will take place through the ceiling in a finished building, and the provision of holes will also help to minimise overall floor depth.

1.4 Aims and Objectives

The main aim of this research project is to investigate the structural performance of lightweight composite flooring systems comprising CFS joists and timber-based floorboards. The specific objectives of this study can be summarised as follows:

- Evaluation of material characteristics and load-slip response of the components of the flooring system by conducting material tests and push-out tests, respectively.
- Conducting full-scale four-point bending tests to investigate the structural behaviour of CFS and timber flooring systems.
- Validation of finite element models with experimental results and conducting parametric studies to investigate the influence of various

factors that affect the structural behaviour of the composite flooring system.

- Assessing the degree of composite action of the flooring systems when a fastening arrangement is used and evaluate the potential of increasing composite action through connection changes. A relationship for the design of shear connectors for complete shear interaction is also discussed.
- Quantifying the attained results and providing practical design guidelines and theoretical formulations to determine flexural capacity and the deflection for the studied CFS and timber flooring systems to be used by practising engineers in Australia.

1.5 Research Methodology

A holistic approach that consists of experimental, numerical and theoretical studies is implemented in this research study.

Four-point bending tests on a full-scale prototype of the composite cold-formed steel flooring system comprising cold-formed steel joist and structural plywood is carried out to study the strength and stiffness of the flooring system. Four different types of shear connectors, including self-drilling screws, coach screws, and nuts and bolts, were investigated as shear connectors in this study. Material tests were carried out to determine the mechanical properties of the materials, and push-out tests were performed to determine the load-slip response of the shear connectors. The experiments were conducted at the UTS tech lab.

Physical tests alone are insufficient to supplement this research; hence, a finite element software package ANSYS is employed to do the numerical analysis.

Numerous researchers have used ANSYS to predict the structural behaviour and ultimate strength of cold-formed steel members in the past (Majdi et al., 2014; Zhou et al., 2019). It is crucial to model all the materials and their characteristics precisely so that the numerical simulations demonstrate similar behaviour as obtained from the physical tests (Bakker and Peköz, 2003). Once the model validation was successful, parametric studies were performed to investigate the influence of various parameters. The influence of thickness and depth of cold-formed steel sections and spacing of the fastener arrangements are investigated on the structural behaviour of composite cold-formed steel and timber (CFST) beams.

A design equation to predict the bending moment capacity and deflection of the CFST beam is presented, considering the composite action phenomenon.

1.6 Thesis Outline

The introductory chapter features the structural applications and benefits of the cold-formed steel members. Also, the significance and objectives of this research are presented in this chapter.

State-of-the-art on composite cold-formed steel flooring system is outlined in Chapter 2. The mechanical properties and the structural behaviour of CFS members are also reviewed and underlined.

In Chapter 3, an experimental program consisting of material tests of the flooring system components and push-out tests of the mechanical fasteners is comprehensively presented. The load-slip performance of different mechanical fasteners utilised in the composite beams is thoroughly described.

The flexural behaviour of the cold-formed steel and timber (CFST) flooring system is investigated by conducting four-point bending tests on the full-scale specimens, which is fully illustrated in Chapter 4. The summary of experimental findings and degree of the achieved composite action is provided.

Chapter 5 discusses the numerical investigation of composite cold-formed steel and timber (CFST) beams. The finite element model is validated against the experimental results described in chapter 4. Parametric studies are conducted after successful validation of the model, and the influence of various factors on the structural behaviour of CFST beams is presented.

An analytical model is proposed for the calculation of the ultimate elastic load-carrying capacity and mid-span deflection of composite CFST beams in Chapter 6. The design equation is assessed against the experimental and numerical investigation results reported in Chapters 4 and 5, respectively.

Chapter 7 summarises the major findings of this research, and recommendations for further studies are provided.

2 Literature Review

2.1 Introduction

This chapter gives a brief overview of existing research on several types of composite flooring systems, such as hot-rolled steel and concrete, timber and concrete, and hot-rolled steel and timber, emphasising the importance of shear connection in the composite flooring system. The present findings on the structural performance of a composite floor system comprising cold-formed steel joists form the primary basis for this chapter. Moreover, the review of recent research conducted on composite floor systems using cold-formed steel and timber-based floorboard is studied, and the outcomes are highlighted while discussing the contribution of this research which was not covered in the previous work of this type. Initially, the material properties of cold-formed steel are briefly discussed, and then their susceptibility to local instability is explained. The flexural behaviour of cold-formed steel members is underlined, and the design method for cold-formed steel members based on AS/NZS 4600:2018 is also briefly presented in this literature.

2.2 Cold-Formed Steel (CFS)

Cold-formed steel members, in recent years, have significantly grown in the construction industry because of higher strength materials and a broader range of structural applications compared to conventional hot-rolled members (Hancock, 2003; Keerthan and Mahendran, 2013). Recent studies (e.g. Far et al., 2017; Saleh et al., 2018) have highlighted the benefits of using cold-formed steel members in the building industry. However, cold-formed steel members are

usually thinner than hot-rolled sections and have modes of failure and deformation that are not commonly found in ordinary steel members (Yang and Liu, 2012). Hence, design specifications are required that guide the design of cold-formed steel structures or thin-walled members. In Australia, AS/NZS 4600 (Standard Australia, 2018) sets out the minimum requirements for the design of cold-formed steel members.

2.2.1 Material Properties

The cold-forming process for manufacturing cold-formed steel members can change its mechanical properties. The cold-forming process increases yield and ultimate tensile strength and reduces ductility (Yu, 1999). The mechanical properties of flat and corner parts are different in a cross-section due to differences in the degree of cold working, mainly in the region of the bend (Hancock, 1998). In these regions, the ultimate tensile strength and yield stress are enhanced with a proportionate reduction in ductility. The studies conducted on the influence of cold work by Chajes et al. (1963) showed that the alterations of mechanical properties due to cold working are primarily due to strain hardening and strain ageing, as shown in Figure 2.1.

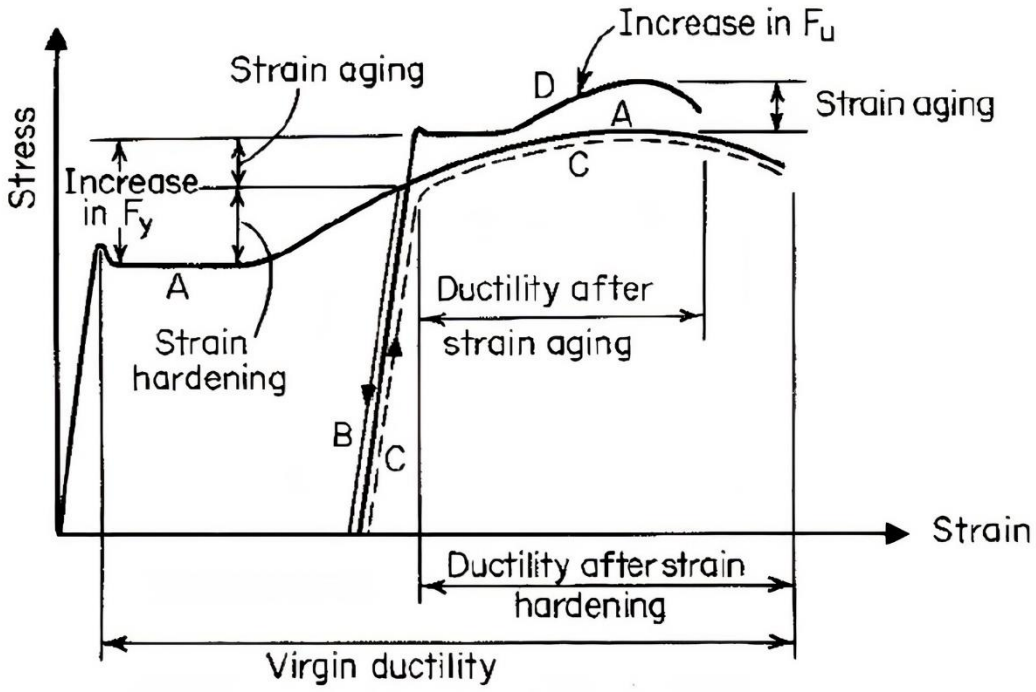

Figure 2.1: Effects of strain hardening and strain ageing on stress-strain (Chajes et al. (1963))

Design codes like AS/NZS 4600:2018 (Standard Australia, 2018), American Iron and Steel Institute Specification (AISI, 2007), and British standard (BSI, 1998) allow the inclusion of increased strength due to cold-forming and provide the equations to determine the increased yield strength. In Australia, AS/NZS 4600:2018 provide limitations and methods to compute average design yield stress (f_{ya}). The average design yield stress can be determined either from the experimental tests or from design equations that determine the tensile yield strength of bends (f_{yc}) and the average design yield stress of the steel in the full flange section of flexural members (f_{ya}).

Numerous researchers (Abdel-Rahman and Sivakumaran, 1997; Young and Rasmussen, 1998; Kyvelou et al., 2017b) conducted tensile coupon tests to determine material characteristics of cold-formed steel. The stress-strain

behaviour of cold-formed steel was found to exhibit a round curve without a distinct yield point. As the materials with a rounded stress-strain behaviour have no distinct yield point, the 0.2% proof stress $f_{0.2}$, determined according to the offset method at 0.2% strain, has been accepted as the "yield stress" (f_y)for this type of material. Figure 2.2 shows a typical stress-strain curve for cold-formed steel and the yield stress at 0.2% strain.

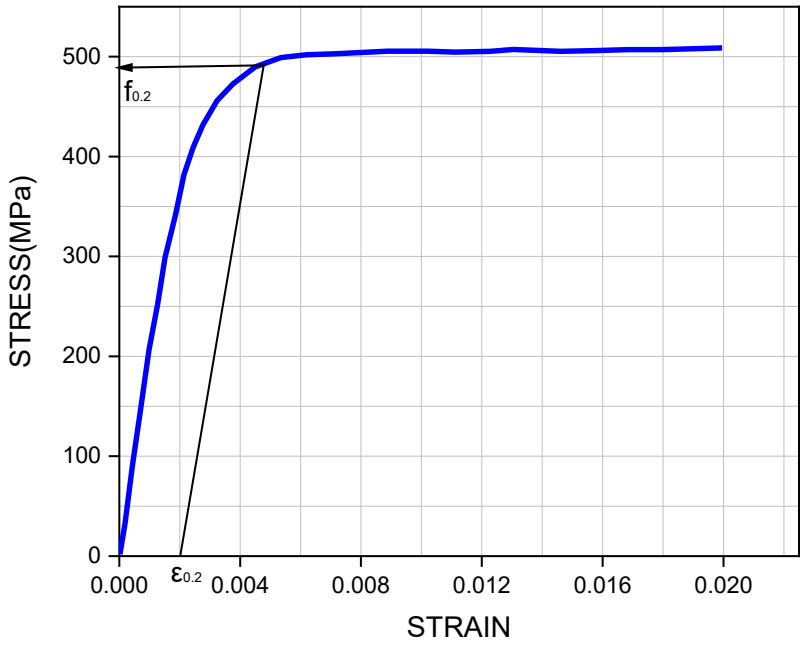

Figure 2.2: Typical stress-strain curve of cold-formed steel

It is imperative to assign the approximate material characteristics of any material in a numerical model to study the behaviour of a system. Several equations have been developed and used in past studies to predict the stress-strain model of cold-formed steel. The Ramberg-Osgood model, which was developed for aluminium, uses three parameters-Young's modulus (E), yield strength (f_y, 0.2% proof stress), and strain hardening component n as shown in equation (2.1).

$$\varepsilon = \frac{f}{E} + 0.002\left(\frac{f}{f_y}\right)^n \quad (2.1)$$

Where *f* and ε are the engineering stress and strain, respectively.

Some modifications to the Ramberg-Osgood expression were done to employ the model for other non-linear metallic materials, as equation (2.1) could not accurately capture the full stress-strain curve. Mirambell and Real (2000) and Rasmussen (2003) proposed a two-stage model as an extension to the Ramberg-Osgood model to determine the stress-strain relationship for stainless steel. Recently, Kyvelou et al. (2018) chose the two-stage Ramberg-Osgood model proposed by Gardner and Ashraf (2006) for the modelling of cold-formed steel, as shown in equations (2.2) and (2.3), and the model was found to be sufficient to replicate the behaviour of cold-formed steel.

$$\varepsilon = \frac{f}{E} + 0.002\left(\frac{f}{f_y}\right)^n, f \leq f_{0.2} \quad (2.2)$$

$$\varepsilon = \frac{f - f_{0.2}}{E_{0.2}} + \left(\varepsilon_{1.0} - \varepsilon_{0.2} - \frac{f_{1.0} - f_{0.2}}{E_{0.2}}\right)\left(\frac{f - f_{0.2}}{f_{1.0} - f_{0.2}}\right)^{n'_{0.2,1.0}} + \varepsilon_{0.2}, f_{0.2} < f < f_u \quad (2.3)$$

Where $f_{0.2}$ is 0.2% proof stress, $E_{0.2}$ is the tangent modulus, $f_{1.0}$ is 1.0% proof stress, $\varepsilon_{0.2}$ and $\varepsilon_{1.0}$ are the strains at 0.2% and 1.0% proof stresses, and $n'_{0.2,1.0}$ is strain hardening component.

More recently, a comprehensive study was undertaken on 700 experimentally obtained stress-strain curves worldwide on cold-formed steel of different grades,

thicknesses, and section sizes by Gardner and Yun (2018) and proposed an expression to predict the engineering stress-strain response of the cold-formed steel. The predicted stress-strain curves are in excellent agreement with the test data. They adopted equations proposed by Mirambell and Real (2000) as a basis for developing their expression, as shown in equation (2.4). An explanatory detail and formula for calculating the key input parameters required for the two-stage model can be found in the literature.

$$\varepsilon = \begin{cases} \dfrac{f}{E} + 0.002\left(\dfrac{f}{f_y}\right)^n, f \le f_y \\ \dfrac{f - f_y}{E_{0.2}} + \left(\varepsilon_u - \varepsilon_{0.2} - \dfrac{f_u - f_y}{E_{0.2}}\right)\left(\dfrac{f - f_y}{f_u - f_y}\right)^m + \varepsilon_{0.2}, f_y < f \le f_u \end{cases} \quad (2.4)$$

2.2.2 Residual Stress

Due to the cold work of forming, cold-formed steel sections undergo plastic deformations, resulting in residual stresses that may cause premature yield and ultimate strength reduction (Kyvelou, 2017). Residual stress is the sum of flexural and membrane stress, as in Figure 2.3(a). Membrane residual stresses are generally small compared to flexural residual stresses; therefore, membrane residual stresses can be ignored (Schafer and Pekoz, 1998a). Figure 2.3(b) shows the distribution of flexural residual stress for roll-formed and press-braked cold-formed steel lipped channel sections as a percentage of yield strength (f_y). It can be seen that though the channel section underwent the same cold working, there is a significant difference in residual stress in the web and flange.

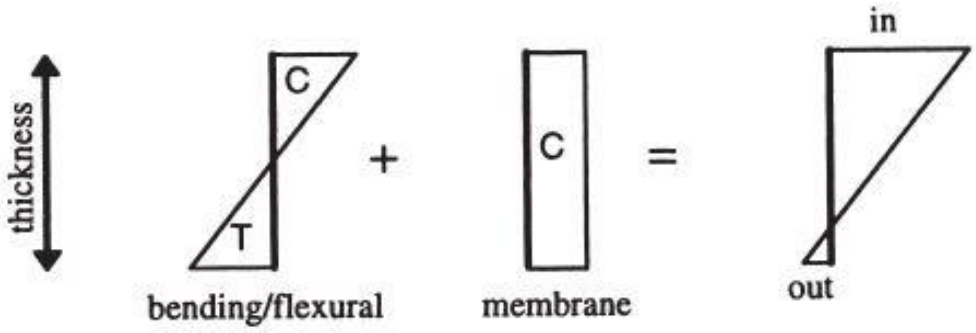

(a) Definition of flexural and membrane residual stress

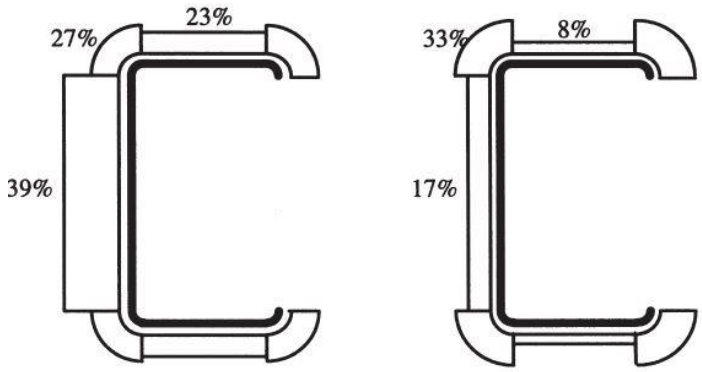

Roll-formed Press-braked

(b) Average bending residual stress (%fy)

Figure 2.3: Flexural and membrane residual stresses (Schafer and Pekoz, 1998a)

Quach et al. (2006) presented a paper in which a finite element based method was carried out to predict residual stresses in press-braked thin-walled sections. Their numerical result demonstrated a close agreement with laboratory measurements which showed that the maximum residual stress occurred in the corner region and away from the flat surface. The enhancement of strength in the corner region is because of the amount of cold-worked required to form the curve, than flat is considerably more during the manufacturing process.

Schafer and Pekoz (1998a) mentioned that adequate computational modelling of residual stresses could cause difficulty; hence, residual stresses are often excluded, or the stress-strain characteristic of the material is adjusted to estimate the effect of residual stress. So, modelling suggestions were provided by them to assess the influence of residual stress. They even pointed out that the residual membrane stress may be ignored if the corner region is of little importance, but the flexural residual stresses should be modelled to get an accurate result. Kankanamge and Mahendran (2012) studied the effect of residual stresses on cold-formed steel beams subjected to lateral-torsional buckling by investigating the moment capacities with and without the inclusion of residual stress, and the result shows that there is an insignificant influence of residual stress. Cold-formed steel structures standard, AS/NZS 4600:2018, states that residual stresses can be modelled directly or indirectly through a stress-strain curve. Hence, the effect of residual stress can be neglected in finite element modelling if the material property is taken from the coupon tests of the member as the residual stresses are inherently embedded in the member.

2.2.3 Geometric Imperfections

Cold-formed steel beams are not flawlessly straight and generally associated with geometric imperfections, affecting the ultimate strength and buckling behaviour (Seo et al., 2008). The deviation of a member from perfect geometry is geometric imperfection and includes bowing, warping, and twisting (Schafer and Pekoz, 1998a). Geometric imperfections are usually divided into two groups; cross-sectional imperfection and global (overall) imperfection. The cross-section change from its ideal shape is called cross-sectional imperfection, while the member deviation from its straightness is called overall imperfection. For cross-

sectional imperfections, the most common approach is to consider the thickness of the cross-section as a magnitude of imperfection. Generally, L/1000 is used as the imperfection magnitude for global imperfections (Gendy and Hanna, 2017).

In the last two decades, several studies have been done to study the effect of geometric imperfections on the strength of cold-formed steel members. Schafer and Pekoz (1998a) categorised the cross-sectional geometric imperfections as type 1 (local) and type 2 (distortional) imperfections and provided a rule of thumb as a factor of a thickness (t) or width (w) of the section as shown in Figure 2.4.

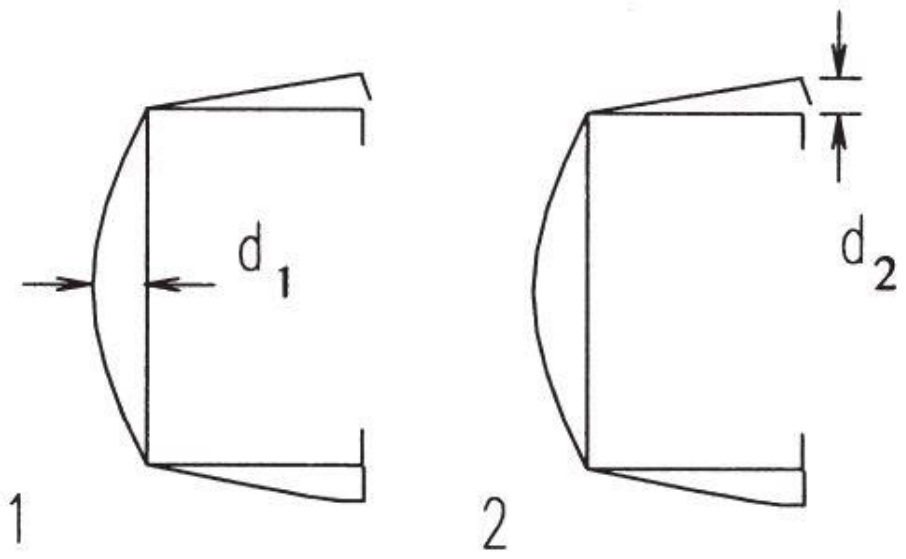

$d1 \approx 0.006w$ Or $d1 \approx 6te^{-2t}$ $\qquad$ $d2 \approx t$

Figure 2.4: Type 1 and Type 2 geometric imperfections (Schafer and Pekoz, 1998a)

The rule of thumb is applicable to w/t less than 200 for type 1 imperfection and w/t less than 100 for type 2 imperfection, and thickness t should be less than 3mm. Since the rule of thumb is not accurate in providing a complete characterisation of imperfection magnitude, cumulative distribution function (CDF) values based on their probabilistic analysis are provided by Schafer and

Pekoz (1998a). Yu and Schafer (2007) developed a non-linear finite element model to simulate the experimental tests (Yu and Schafer, 2003, 2006) of local and distortional buckling on cold-formed steel beams. The geometric imperfections included in the finite element analysis were the CDF values, as mentioned by Schafer and Pekoz (1998a), and the numerical analysis result was found to be in good agreement with experimental tests.

The imperfection amplitude of the CFS beam can also be measured experimentally in the laboratory or using the different CDF values proposed by Schafer and Pekoz (1998a). According to AS/NZS 4600:2018, for member imperfections (out-of-straightness), the critical value is taken as 1/1000 of member length, while the member's length is considered the distance between the supports and for cross-section imperfections that include local and distortional buckling shall be included in numerical analysis. The shape of the imperfections for local and distortional buckling shall be incorporated in the numerical model by multiplying the local and distortional modes assuming peak unit deformation by imperfection multipliers and superimposing these scaled imperfections onto the ideal geometry.

For local buckling, the imperfection multiplier (S_{ol}) can be calculated as follow:

$$S_{ol} = 0.3t\sqrt{\frac{f_y}{f_{ol}}} \tag{2.5}$$

t= plate thickness

f_y = yield stress

f_{ol} =elastic local buckling stress

For distortional buckling, the imperfection multiplier (S_{od}) can be calculated as follow:

$$S_{od} = 0.3t\sqrt{\frac{f_y}{f_{od}}} \tag{2.6}$$

t= plate thickness

f_y = yield stress

f_{od}=elastic distortional buckling stress

Dubina and Ungureanu (2002) selected the tests carried out by Young and Rasmussen (1998) on plain and lipped channel members to study the influence of the size and shape of geometrical imperfections in FEM analysis. They concluded that the member buckling strength is affected by various shapes of local-sectional imperfections and further highlighted the sensitivity of distortional buckling to sectional imperfections as the distortional mode has lower post-buckling strength than the local mode. Several researchers (Kwon and Hancock, 1993; Chou et al., 2000) have shown that the inclusion of initial geometric imperfections in finite element analysis is very important as they greatly influence the strength of cold-formed steel members. The most common way used by researchers for the inclusion of geometric imperfections is to perform eigenvalue buckling analysis (EBA) firstly to obtain an appropriate buckling mode shape, which is then included in the nonlinear analysis to define initial imperfection (Wang and Zhang, 2009; Seo et al., 2008). Nevertheless, the study conducted by Haidarali and Nethercot (2011) showed that utilising EBA to determine initial imperfections can be challenging for some sections when the interaction between

local-distortional buckling arises. So a finite strip software CUFSM and sinusoidal functions were used in their study to generate the initial geometric imperfections. A similar approach was followed by Kyvelou et al. (2018) on her study and a very good agreement of the experiment and numerical results in terms of ultimate strength and buckling behaviour of the CFS beam was found. However, the studies by Wang and Zhang (2009) and Laím et al. (2013) employed EBA to obtain appropriate mode shapes and then included them in the non-linear analysis, which also reported an excellent agreement between the experimental and numerical results. Hence it is seen that the inclusion of geometric imperfection can be made using the conventional method of feeding the Eigenmodes from EBA into non-linear analysis or the method adopted by Haidarali and Nethercot (2011).

2.2.4 Flexural Behaviour of Cold-formed Steel Beams

Due to their thin-walled nature, cold-formed steel (CFS) members are susceptible to the failure mode not commonly found in conventional steel design. The failure of the CFS beam is generally due to material yielding, local buckling, distortional buckling, and lateral-torsional buckling (Wang and Zhang, 2009; Laím et al., 2013; Yang and Liu, 2012)

2.2.4.1 Buckling Modes of CFS Beams

Figure 2.5 represents the result of a finite strip buckling analysis which demonstrates the different ways in which a channel section may buckle when subjected to a major axis bending moment (Hancock, 2003), and the description of the points is briefly outlined below;

The first minimum point (A) is a Local buckling mode involving the web, compression flange and lip stiffener. The second minimum point (B) is Flange

distortional buckling, where the compression flange and lip rotate about the flange web junction with some elastic restraint to rotation provided by the web. At long-wavelength (C), where the channel section is unrestrained, a flexural torsional buckle occurs, often known as Lateral buckling. However, if the tension flange is subjected to a torsional restraint, lateral distortional buckling will occur at point (D) as shown.

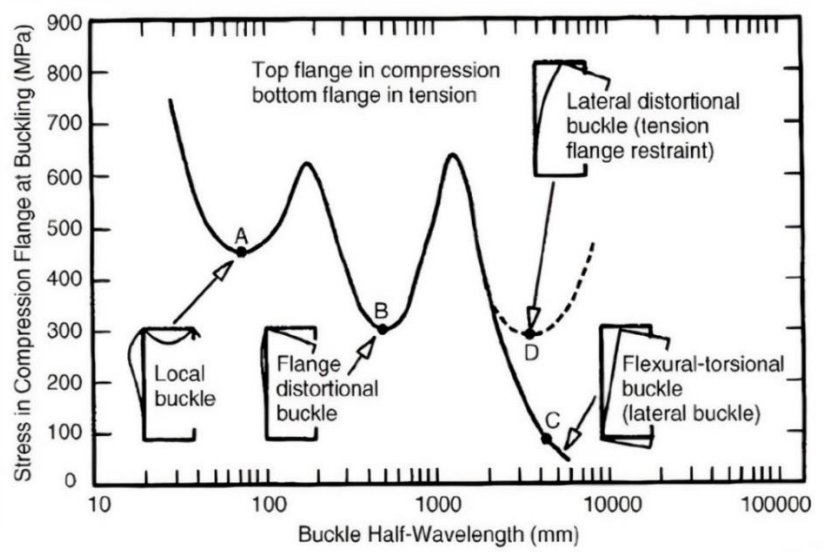

Figure 2.5: Channel section buckling stress versus half-wavelength for major axis bending (Hancock, 2003).

(i) Local buckling and post-local buckling of thin plate elements

Local buckling involves only rotation, not the translation, at internal fold lines of a cross-section. This deformation occurs due to the instability of a slender plate constrained between two stiffening elements. A typical local buckling mode for a channel section is shown in Figure 2.6. Local buckling does not normally fail the section. If a beam can carry an increasing load even after local buckling, the beam is known to have the post-buckling capacity. A post-buckling reserve is permitted in design to achieve an economical solution (Hancock, 1998).

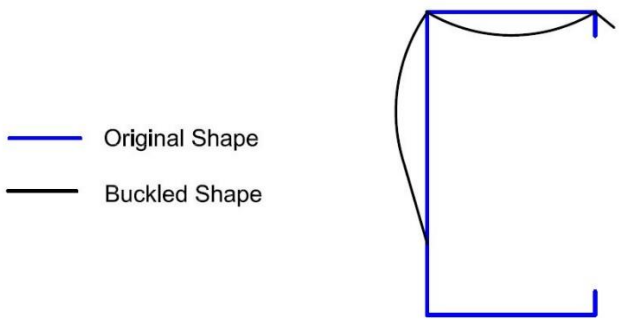

Figure 2.6: Local buckling mode

(ii) Distortional Buckling

Distortional buckling involves rotation and translation at one or more internal fold lines of a cross-section. The mode can occur for members in both compression and flexure.

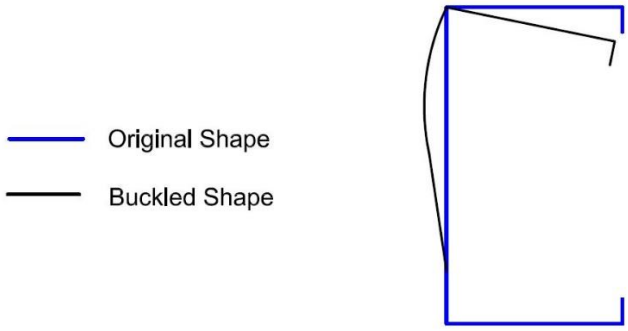

Figure 2.7: Distortional buckling mode

Distortional buckling of flexure members like C- and Z- sections usually involves rotation of only compression flange and lip about the flange-web junction in opposite directions, as in Figure 2.7. The web undergoes flexure at a similar half-wavelength as the flange buckle, and the compression flange may translate slightly in a direction normal to the web at a similar half-wavelength as the flange and web buckling deformations (Hancock, 1998).

The post-buckling capacity of the distortional buckling mode is less than the local buckling mode. Even when local buckling is at a lower critical elastic moment than distortional buckling, failure due to distortional buckling mode occurs because of reduced post-buckling strength (Schafer and Peköz, 1999).

(iii) Lateral Distortional Buckling

If the tension flange of the beam is subjected to torsional restraint, it causes transverse bending of the vertical web, resulting in lateral distortional buckling mode (Hancock, 1998).

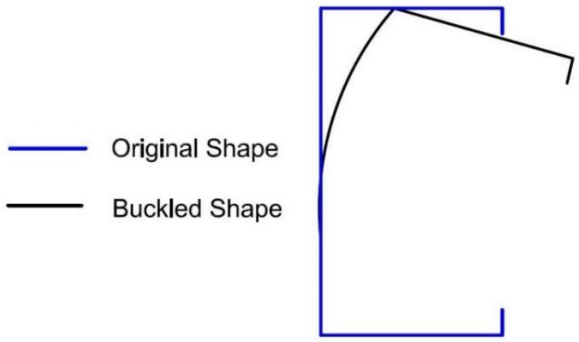

Figure 2.8: Lateral distortional buckling mode

(iv) Flexural Torsional (Lateral) Buckling

Lateral buckling does not involve deformation of the cross-section. Instead, the entire cross-section sways and twists simultaneously. This instability occurs when a member is restrained insufficiently along its length (Hancock, 1998). Due to the geometry of open cross-section, cold-formed steel beams give high flexural rigidity about a single axis at the expense of low flexural and torsional rigidity

about other axis and are generally susceptible to flexural torsional buckling (Chu et al., 2004).

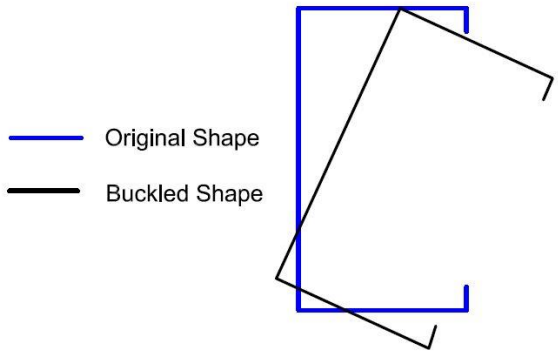

Figure 2.9: Flexural torsional buckling mode

2.3 Design Methods for Cold-formed Steel Beams

Currently, two main design methods for cold-formed steel members are available in design specifications: Effective Width Method (EWM) and Direct Strength Method (DSM). EWM was introduced by Von Karman et al. (1932) and was later modified by Winter (1947) for cold-formed steel members. It has been adopted in design specifications such as AS/NZS 4600:2018 (Standard Australia, 2018), Eurocodes and American Iron and Steel Institute (AISI, 2007). An alternative method developed by Schafer and Pekoz (1998b) called the direct strength method (DSM) has been included as an alternative method in North America and Australia/New Zealand.

The idea of EWM is that local plate buckling causes a reduction in the effectiveness of the plates that comprise a cross-section. Moreover, the loss in the effectiveness of plates is an approximate means to account for equilibrium in an effective plate under a simplified stress distribution against the full plate with

a non-linear longitudinal stress distribution due to buckling (Schafer, 2008). In Australia, Section 2 of AS/NZS 4600:2018 (Standard Australia, 2018) contains the design requirements and formulae for calculating the effective width of various elements with different edge support and loading conditions. The cross-section is divided into its comprising elements (i.e. flats, corners). The effective width of each flat element (plate) is calculated based on the slenderness (b/t), degree of edge stiffening (k) and stress level (f*) of the element. Buckled portions are neglected; the remaining portions form an “effective” section. Effective section properties (e.g., I_{eff}, Z_{eff} & A_{eff}) are used to predict the stiffness and strength of the member. The limitation with the EWM is that for simpler cross-sections, such as the Hat section without intermediate stiffeners, the method is relatively easier, but for recent complex cross-sections, the effective section properties can become complex to calculate. Hence, DSM was developed as an alternative method to deal with the limitation of EWM.

DSM uses member elastic buckling solutions based on gross properties rather than individual elements. DSM does not rely on effective width calculations. In DSM, all elastic instabilities, i.e. local, distortional and global buckling, are determined. Section 7 of AS/NZS 4600 covers the direct strength method (DSM) of cold-formed steel design. Finite strip software like THINWALL or CUFSM is a tool based on DSM and helps design cold-formed steel members.

Both EWM and DSM give a simplified solution to a complicated non-linear problem, allowing Engineers to have a working method to design without the requirement of experimental testing of every individual member. In any case, it is significant to understand that neither EWM nor DSM is thoroughly correct, as the formulae expressed are based on limited experimental test data. Schafer (2008)

claims that the long-term goal for cold-formed steel member design should be a fully non-linear computational analysis. Therefore in this research, more emphasis will be drawn to the numerical modelling using Finite element analysis to study the flexural behaviour of cold-formed steel (CFS) floor joists sheathed with structural plywood panels.

2.4 Composite Flooring Systems and the Importance of Shear Connection

Composite construction is popular because it combines structural efficiency with the speed of construction to give an economical solution to a wide range of building types (Rackham et al., 2009). The overall performance of a composite system is commonly higher than the sum of its individual components (Loss and Davison, 2017). The structural performance and integrity of the system are crucial to its connection because the fasteners establish the bond between individual components, preventing them from working separately and further improving the load-carrying capacity and stiffness of the system (Kyvelou et al., 2017a). Numerous research has been done for composite systems that commonly include a combination of steel with concrete, timber with concrete, timber with timber and steel with timber. This section will provide a general overview of the different types of composite flooring systems widely utilised in the construction industry and highlights the importance of shear connection on the structural performance of such flooring systems.

Conventional composite floors that combine hot-rolled steel beams and reinforced concrete slabs are designed to utilise both materials through composite action that occurs at the interface employing shear connectors (Yam, 1981; Asiz and Ahmed, 2013). This type of composite floor is efficient because

they exploit the strength of concrete in compression and steel in tension, which is achieved by the force transfer mechanism between the top flange of the steel beam and concrete (Couchman, 2016). The force transfer is achieved using shear connectors, which are normally welded studs and can transfer force due to their stiffness and ability to accommodate the slip between steel and concrete (Couchman, 2016). The strength and ductility of shear connectors between the steel beam and concrete slab were found to have a significant influence on the flexural strength of the composite beam (Mirza and Uy, 2009; Valente and Cruz, 2004). An increasing amount of research has already been done on composite steel-concrete floors, and nowadays, it is widely used in many construction applications like buildings and bridges (Crisinel and O'Leary 1996; Rackham et al., 2009). In Australia, the composite structures standard, AS/NZS 2327.1 (Standard Australia, 2017), sets out the design requirements and construction of simply supported composite beams comprising a steel beam interconnected to a concrete slab by shear connectors, including the applications in which the slab incorporates profiled steel sheeting. In a composite beam, the behaviour of the shear connection depends upon the relationship between the shear force per connector and the longitudinal slip between the interfaces. While designing steel and concrete composite beams, it is essential to consider the slip capacity, which is exhibited by mechanical shear connectors, not only the required strength of shear connectors (Johnson and Molenstra, 1991; Oehlers and Sved, 1995). More recently from the viewpoint of sustainable development, which is related to the deconstructability and recycling of building infrastructure, studies have been done in composite beams where shear connectors can be unbolted to deconstruct or modify the existing condition of slabs. The study carried out by Ataei et al. (2016)

based on the tests undertaken on full-scale beams and joints focusing on the sustainable and deconstructable system shows the potential of this type of system which can contribute to minimising carbon emissions in comparison to the conventional steel-concrete composite system. Liu et al. (2015) carried out numerical investigations based on push-out tests to investigate the behaviour of high-strength friction grip bolted shear connectors and geopolymer concrete slabs and found the model capable of efficiently predicting the ultimate strength and load-slip curve for shear connection. Despite the fact that concrete based floors are most commonly used, and several types of research being carried to make the system more eco-friendly, the utilization of non-renewable resources that require a high amount of energy consumption over its life cycle and the difficult recycling process makes it unsuitable for sustainability.

Timber concrete composite (TCC) floor is a viable and lightweight alternative to reinforced concrete floors that have the potential for cost savings and sustainability (e.g., Steinberg et al. (2003); (Ceccotti, 2002)). The TCC system is lighter in contrast to the traditional concrete system, which will fundamentally decrease the weight of the overall structure. The reduced weight will prompt a lower measure of seismic action (Yeoh et al., 2011). Due to the negligible friction between the timber beam and concrete slab, each component will act independently when subjected to flexural action. As a result, a slip will occur between the components upon loading. Hence the use of shear connectors is a critical component in this system. Shear connectors allow the transfer of shear between timber and concrete. The strength and stiffness of the system mainly rely on the properties of shear connectors (Hailu, 2015). Commonly two types of connection mechanisms are used, which are mechanical connections, such as

nails, screws, and bolts and glued connections, such as steel lattices glued into the timber and punched metal plates. An experimental and numerical investigation carried out by Ahmadi and Saka (1993) shows that composite action was achieved by using inexpensive nails as shear connectors between timber joists and cast-in-place concrete slabs, which can result in a composite floor system that is easy to construct and cost-effective in comparison to non-composite floors. Bathon and Graf (2000) studied steel mesh as a shear connector, inserted into a continuous slot within a timber beam and connected by adhesive action. Gelfi et al. (2002), based on their studies on stud shear connection for the concrete slab and wood beams, point out that weak connection reduces the strength of composite beams, and hence care should be taken to design connections concerning spacing, length and diameter of stud connectors. Benítez (2008) studied and performed a testing and analytical evaluation of three different types of shear connectors: plain steel dowels at an angle of 60^0, a circular hollow section inserted into a fitted slot in timber and fixed to it by a coach screw and a small UC section fixed by coach screws into the timber. The results have indicated that the degree of composite action depends upon the stiffness of the connector and system, timber condition and initial slip. Similarly, Deam et al. (2008) assessed different types of connection systems to provide composite action between the concrete slab and LVL support beams to compare the stiffness, strength and performance of connectors. Laboratory tests by Gutkowski et al. (2008) show that a higher degree of composite action can be achieved in a layered solid-wood concrete beam using notched shear key/anchor detail rather than ordinary nails. Some researchers even carried out investigations to find out the influence of concrete on TCC floors. Kieslich and Holschemacher (2010)

focused their study on the influence of high-performance concretes like Fiber Reinforced Concrete (FRC), Self-Compacting Concrete (SCC), High Strength Concrete (HSC) and presented the advantages and disadvantages of concretes for use in TCC. Some common problems like poor compaction of concrete, shrinkage cracks in the concrete, wood swelling and moisture loss from concrete which previous researchers faced were studied by LeBorgne and Gutkowski (2010) and presented methods to mitigate those problems to increase the efficiency of the wood-concrete composite system. Though the TCC floor offers numerous advantages, using concrete slab does not make them eco-friendly, considering the impact of buildings on greenhouse gas emission and energy consumption.

Steel-timber composite floor combines timber as a slab and steel as a beam connected by mechanical fasteners. Previous research studies have shown that it is feasible to replace conventional concrete slabs with CLT or LVL (e.g. Hassanieh, Valipour and Bradford, 2016; Asiz and Smith, 2009). The main advantage of this type of flooring system over steel-concrete or timber-concrete is that it uses timber, which is commonly known to be a sustainable construction material over concrete, and it is relatively lightweight, which can significantly improve the speed of construction and accordingly reduce the cost of buildings (Hassanieh, 2017). Steel-timber prefabricated construction technology permits the design of open-space structures and can be easily replaced or reused during the lifecycle of a building (Loss et al., 2016). After investigating the behaviour of screw-type fasteners to join CLT slabs to a steel frame, Asiz and Smith (2011) concluded that using screw fasteners as a shear connection is feasible. It is demonstrated that the use of steel in a building is much reduced by using a CLT

slab relative to a reinforced concrete slab without compromising its structural performance, such as drift due to lateral loads. Likewise, the reaction load to structural supports are essentially reduced because of the lighter CLT slab, as CLT has a mass of about 33% to 50% of the reinforced concrete slab resulting in lower inertial response produced from the seismic load (Asiz and Ahmed, 2013). Hassanieh et al. (2016a) studied the composite behaviour of steel timber composite (STC) beams, and three types of connections were studied. They were coach screws, bolts or a combination of glued and screwed connectors. It was found that STC beams with bolted connectors have higher initial stiffness than STC beams with coach screw connectors. Furthermore, applying glue in combination with mechanical connectors provided near full composite action in STC beams and remarkably increased the initial stiffness of STC connections and STC beams.

Moreover, Hassanieh et al. (2017a) investigated the load-slip behaviour of steel and cross-laminated timber (CLT) slabs for different types of shear connectors by doing push-out tests. Analytical models were used and presented for all connection types after calibration against laboratory results. Recent studies (Yang et al., 2021; Liu et al., 2022; Yang et al., 2020) conducted to study the flexural behaviour of steel timber composite beams have demonstrated the importance of shear connectors on the load-carrying capacity of composite beams.

As discussed in the above paragraphs, the choice of suitable shear connectors in a composite floor system is very important for the effective structural performance and unity of the system. The behaviour of shear connection in a composite beam relies primarily on the relationship between shear force per

connector and the longitudinal slip at the interface between the top flange of the steel section and the composite slab (Johnson and Molenstra, 1991). The shear connector must have enough stiffness and ductility (slip capacity) to accommodate whatever slip occurs. The more shear connectors are present, the higher the degree of shear connection and the less slip (Couchman, 2016). Hence, it is very important to specify a minimum degree of shear connection in composite design (Johnson and Molenstra, 1991; Gelfi et al., 2002). If sufficient shear connectors are present to either fully exploit the steel section or concrete section, then the composite beam is said to have a full shear connection. When less force is required to be transferred between steel and concrete to achieve the necessary beam moment resistance, a reduced number of shear connectors may be used, and the composite beam is said to have a partial shear connection (Couchman, 2016).

2.5 Composite Flooring Systems made up of Cold-formed Steel Beams

There has been increasing popularity and demand for lightweight cold-formed steel flooring systems over the last decades (Parnell et al., 2010; Kyvelou et al., 2017b). As a result, the choice of cold-formed steel beams over other structural members for the construction of flooring systems is due to their high strength-to-weight ratio, modular construction, easy transportation and quick installation on site. However, the use of composite flooring systems that integrate cold-formed steel sections, regardless of the market possibilities for residential and light commercial construction though it offers the advantage of reduced slab thickness and flexibility in combinations of the section, has little research and available design specifications (Lakkavalli and Liu, 2006; Hanaor, 2000).

Studies have been conducted on using cold-formed steel sections with concrete as an alternative solution to replace hot-rolled steel and reinforced concrete in residential buildings (Hanaor, 2000; Bamaga et al., 2019). Karki and Far (2021) have presented a comprehensive review of the state of the art in composite cold-foremd steel flooring systems highlighting the importance of shear connectors. The composite beam design relies mainly on shear interaction between the concrete slab and steel beam by shear connectors. Because cold-formed steel is thin-walled, the use of headed studs to the top flange of the steel beam as in traditional composite system does not apply to cold-formed steel composite beams (Hanaor, 2000; Lakkavalli and Liu, 2006). So, careful attention should be given to the design of shear connectors in composite flooring systems comprising cold-formed steel sections to allow the maximum shear connection (Hanaor, 2000). Hanaor (2000) and Lakkavalli and Liu (2006) carried out experimental investigations to study the flexural behaviour of composite cold-formed steel joists and concrete slab systems and evaluate the viability of the shear transfer mechanism. Both studies show several ways of achieving shear transfer mechanisms by employing different types of shear connectors, and the results showed an increase in strength and a decrease in deflection of the composite system with the best-performing shear connector type. Irwan et al. (2009; 2011) conducted experimental studies carrying out push-out tests and full-scale symmetric cold-formed steel-concrete composite beams where a new type of shear connector called bent-up triangular tab shear transfer (BTTST) was employed for shear enhancement. The result shows that the proposed shear transfer mechanism has sufficient strength and is viable, resulting in a composite floor system with adequate strength and stiffness. Wehbe et al. (2011) conducted

a study to develop cold-formed steel and concrete composite flexural members. They investigated flexural strength, stiffness and shear connection. Hsu et al. (2014) carried out composite beam tests having cold-formed steel beams and concrete slabs to assess the flexural behaviour of the system. The composite beam in their study consists of three elements: concrete slab on a corrugated cold-formed metal deck, cold-formed steel beams joined back to back, and a continuous furring channel as a shear connector. While Majdi et al. (2014) did the numerical investigation of the experimented composite beam system, the results were found to be within acceptable limits from finite element analysis with the experimental results. More recently, parametric studies conducted by Shamayleh and Far (2022) highlighted the importance of the ductility of mechanical fasteners as shear connectors to achieve lightweight composite cold-formed steel and reinforced concrete flooring systems.

It is clear that efforts have been made to utilise and validate cold-formed steel sections with concrete as a composite beam to replace conventional composite beams, and the existing research proved it to be feasible. Although there have been various investigations looking at the viability and potential of cold-formed steel flooring systems comprising concrete, it is only recently that the use of cold-formed steel joists with timber-based floorboards has drawn the interest of researchers to study its structural behaviour to make it an innovative and eco-friendly flooring system.

Some earlier studies (Xu et al., 2000; Xu and Tangorra, 2007; Parnell et al., 2010) investigated the dynamic performance of this type of floor and showed their acceptability to be used as a lightweight floor. Moreover, investigations have been carried out on lipped channel joists (Sakumoto et al., 2003; Baleshan and

Mahendran, 2010) and hollow flange channel joists (Jatheeshan and Mahendran, 2016) in the past to study the fire performance of cold-formed steel flooring system. So far, there has been limited research on the structural performance of cold-formed steel flooring systems using timber-based floorboards. Li et al. (2012) examined the potential of lightweight bamboo and cold-formed steel composite slab through the full-scale experimental testing and discovered the importance of connection to the system's stiffness. Based on their experimental tests, loss and Davison (2017) demonstrated that the composite system's stiffness is crucial to the type of connection used. Kyvelou et al. (2017b, 2018) studied the structural behaviour of the composite flooring system through experimental and numerical investigations on 5.8m long beams. They formulated a design rule for composite cold-formed steel flooring systems lacking in Eurocodes. The studies showed that considering the benefits of composite action provided by mechanical fasteners joining wood-based floorboards on cold-formed steel joist significantly improved the structural performance and load-carrying capacity of the flooring system. Zhou et al. (2019) recently conducted full scale experimental and numerical investigations on 2.4m (width) and 4.8m (length) floor layout to determine the composite action of the light-weight flooring system built with cold-formed steel joist and oriented strand board (OSB), which is not well covered in design standard in China. Parametric studies were carried out to study the influence of screw spacing, joist spacing and floorboard thickness and finally design formula is proposed to calculate the flexural capacity of the floors taking account of composite action after validating with experimental and numerical results. Numerical investigations conducted by Navaratnam et al. (2021) highlighted the enhancement in moment capacity of CLT-CFS composite

beam due to the mobilisation of composite action and further recommended prefabricated composite floor components to use in sustainable modular building construction. A typical cold-formed steel and timber based flooring system for the construction of mezannine floor is shown in Figure 2.10.

Figure 2.10: Construction of a mezannine floor using CFS joist and timber floorboard sheathing (Ayrshire Metals Ltd UK, 2022)

As discussed above, a few studies have been carried out to investigate the structural behaviour of composite flooring systems comprising cold-formed steel

and a certain type of timber floorboards. The results obtained from both experimental and numerical investigation seem promising regarding the improved structural behaviour of the flooring system through the composite action achieved. Overall, the research findings have shown that such a flooring system is feasible to be adopted by the building industry to design and construct lightweight floors.

2.6 Literature Review Findings and Contribution to the Current Research

The findings from previous works on the flexural behaviour of cold-formed steel members, residual stress and geometrical imperfections, the importance of shear connection in composite flooring systems and the structural behaviour of cold-formed steel flooring systems were very useful in understanding the boundaries and focused areas for the current research. A summary of the key findings, which are directly related to the current research from the literature review, is outlined below.

- Because of its thin-walled nature, cold-formed steel members are subjected to instabilities like local, distortional and lateral (flexural-torsional) buckling. Local buckling and post-buckling strength of cold-formed steel members subjected to bending play a vital role in the design. So, it is necessary to include these buckling effects to achieve an economical and effective design of cold-formed steel members.
- Earlier researchers have extensively used Finite Element Analysis (ANSYS or ABAQUS) to study the structural behaviour of cold-formed steel members. They have demonstrated that the behaviour of cold-formed steel members can be precisely examined if geometric

imperfections, mechanical properties, boundary conditions, element types, and mesh density are included in the finite element model accurately.

- A considerable reduction in the ultimate strength of cold-formed steel members is because of geometric imperfections. Hence, it is very important to consider the influence of geometric imperfections in the calculations of design capacity and finite element analysis to capture the failure mode and post-buckling mechanism accurately.
- Experimental and numerical investigations on cold-formed steel and timber-based flooring systems carried out by Kyvelou et al. (2017a, 2017b, 2018) and Zhou et al. (2019) have shown that it is possible to use such lightweight flooring systems in buildings as the structural behaviour and load-carrying capacity can be improved by taking into account the composite action between the cold-formed steel beam and timber floorboards. Careful consideration should be given to the type and spacing of shear connectors as they greatly influence the ultimate strength capacity of the composite flooring system.

Although there have been few investigations for composite cold-formed steel flooring systems with timber floorboards around the world, research on this type of composite flooring system comprising cold-formed steel beams and timber-based floorboards is being done for the first time in Australia. There are well-developed design methods for traditional hot-rolled steel beams and reinforced concrete slabs, and timber concrete composite floors, but no theoretical formulations and guidelines have been established yet for the lightweight

composite cold-formed steel and timber flooring systems. Hence this research project aims to provide a simplified approach to calculate the flexural capacity and stiffness of the composite flooring systems that can be used by practising engineers in Australia. As these types of flooring systems can be manufactured off-site, modular construction and ease of installation are two of the great benefits this flooring system can offer to address the increasing housing demands in Australia effectively. It is important to note that previous cold-formed steel and timber floor investigations were carried out on typical cold-formed steel joists without holes. This research project will perform static tests on the composite flooring systems comprising cold-formed steel joists with and without holes in the web and structural plywood. The reason for investigating joists with holes is that plumbing and other service installations will take place through ceiling in a finished building and the provision of holes will also help minimise overall floor depth. Since the interaction between the cold-formed steel beam and timber floorboard plays a vital role in the overall strength and stiffness of the system, the influence of shear connections on these floors must be understood. Hence, four types of shear connections will be studied considering the ease of assembling and disassembling of the floor components and the ductility of fasteners. This study, for the first time, will experimentally investigate the influence of different type and size of mechanical connections (e.g. screws and bolts) on the composite efficiency of the floors. Because of its lightweight, use of eco-friendly materials like steel and timber, and potential for modular construction, this flooring system is an innovative and sustainable system to be used for varying span floors in residential and light commercial buildings.

2.7 Concluding Remarks

A literature review on the behaviour of cold-formed steel sections and the design method for cold-formed steel flexural members has been presented in this chapter. A general review of different types of composite flooring system with an accentuation on the significance of the choice of shear connectors followed. The cold-formed steel and flooring system is the main basis of this chapter, and hence finally, emphasis has been drawn to a composite flooring system that comprises cold-formed steel joists as a structural member. Recent research findings carried out in the UK and China on a cold-formed steel beam, and timber floorboard (Particle board and OSB) were presented, and attention has been drawn to the contribution to the existing knowledge that this study will offer.

3 Load-Slip Behaviour of CFS Joists and Plywood Panels

3.1 Introduction

As discussed in Chapter 2, the role of shear connectors in the efficient design of hot-rolled steel and timber flooring systems has been demonstrated through a series of push-out tests on connection joints (Hassanieh et al., 2017a, 2016b) and four-point bending tests on a large scale steel-timber composite beams (Hassanieh et al., 2016a; Loss and Davison, 2017). Moreover, Hassanieh et al. (2017b) suggested that the structural behaviour of a steel-timber composite system is significantly influenced by the stiffness and load-carrying capacity of connections. The strength and stiffness of the composite beam were found to rely mainly on the shear interaction.

Li et al. (2012) examined the potential of lightweight bamboo and cold-formed steel composite slab through full-scale testing and highlighted the importance of shear connection to the stiffness of the composite system. Recent experimental studies (Kyvelou et al., 2017b; Zhou et al., 2019), which utilised self-drilling screws as a shear connection, demonstrated the benefits of composite action on the moment capacity and flexural stiffness of the composite cold-formed steel and timber flooring system. Numerical studies (Karki et al., 2021; Far, 2020a) into the structural behaviour of composite cold-formed steel and timber flooring system also demonstrated the beneficial effect of composite action on the load-carrying capacity of the composite beams. More recently, experimental analysis (Vella et al., 2020) into cold-formed steel-to-timber connections with inclined screws was carried out by conducting push-out tests. It was found that inclined screws at 45^{o} resulted in higher stiffness than 0^{o} screws. Although the findings

from these investigations on cold-formed steel and timber composite system look promising, those studies seem to be focused on screws only as shear connectors. Furthermore, there is necessary to develop and investigate different shear connectors with higher stiffness and ductility to enhance the composite efficiency and load-carrying capacity of cold-formed steel and timber flooring systems.

Nowadays, the prefabricated building construction method is gaining popularity and has reduced environmental impacts during construction and provided cost and material-effective houses while decreasing the construction time (Navaratnam et al., 2021; Navaratnam et al., 2019; Lacey et al., 2018). Cold-formed steel and engineered timber products make the right choice in prefabricated construction industries as they are sustainable and lightweight. Modular units like cold-formed steel and timber composite floors can be fabricated off-site and joined on-site. Hence, it is crucial to understand the behaviour of connections used to join timber panels to the cold-formed steel joists. As part of the experimental investigation, a series of material and push-out tests were conducted to determine the mechanical properties of the employed materials and the response of shear connections.

In this chapter, the performance of the CFS-plywood composite connection is experimentally investigated. The means of shear connections adopted in this study were mechanical fasteners alone and adhesives and mechanical fasteners. The use of mechanical fasteners with adhesives is to investigate the composite performance of the system in comparison to the one with mechanical fixings only. Kyvelou et al. (2017b) reported the significant influence of structural adhesive on the moment capacity and flexural stiffness of the cold-formed steel and timber composite floor. As the results from the studies seem promising, it has become

apparent to further study the influence and behaviour of structural adhesive along with mechanical fixings to a further extent. Hence, by conducting push-out tests, this study investigates the short-term load-slip response, ultimate load carrying capacity, stiffness, and failure mode of CFS-plywood composite connections. Lastly, by carrying out the non-linear regression analysis of the experimental results, empirical formulae for the load-slip response of the CFS-plywood connections are proposed in this chapter.

3.2 Experimental Program

Material tests were conducted to determine the material characteristics of the structural components used in the composite system, and push-out tests were conducted to determine the load-slip response of the shear connectors. Figure 3.1 shows the cross-sectional dimensions of the CFS C-section joist utilised in the push-out tests. 45mm thick structural plywood panels (F11 structural grade) shown in Figure 3.2, made from radiate pine, were used as timber sheathing. Previous experimental investigations on the composite cold-formed steel and timber flooring system employs 1.5mm thick and 3mm thick CFS sections with oriented strand board or particle board (Kyvelou et al., 2017b; Zhou et al., 2019). However, it is very important to design and optimise such composite flooring system based on the availability of steel sections as well as the wood products in local regions around the world (Far, 2020a). Hence, considering the readily available materials in Australian context, 2.4mm thick CFS C-section and 45mm thick structural plywood panels is selected for the experimental specimens. It is important to note that structural performance of the selected materials to satisfy loading conditions based on the spacing of joists and span of floor. A

comprehensive testing program in accordance with the relevant Australian Standards was carried out to obtain the mechanical properties of the materials used in the push-out tests.

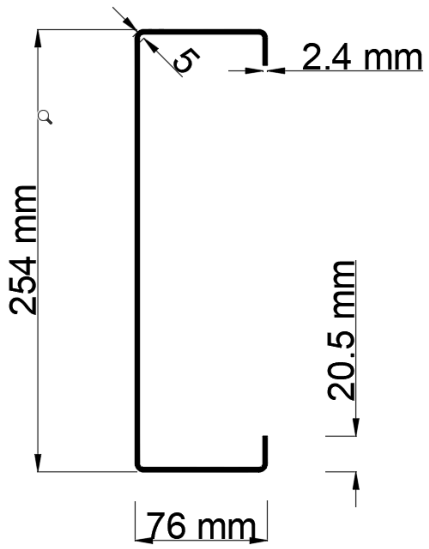

Figure 3.1: Cross-section dimensions of CFS joist

Figure 3.2: Tested plywood material

3.2.1 Material Tests

3.2.1.1 Cold-Formed Steel Tensile Tests

Tensile steel coupon tests were conducted to determine the mechanical properties of the cold-formed steel joists. All the cold-formed steel sections used in this study were supplied by Fielders Pty Ltd. The dimensions of the tensile coupon are illustrated in Figure 3.3. The coupons were extracted from the web and flange of the different CFS joists. Eight tests were carried out. The tensile coupon specimen before and after the test is shown in Figures 3.4 and 3.5 respectively.

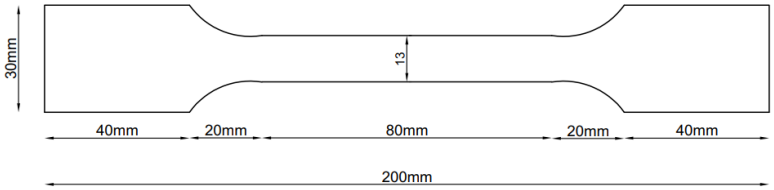

Figure 3.3: Dimension of the tensile coupon

Figure 3.4: Tensile coupon with strain gauge attached

Figure 3.5: Failure of CFS coupon during tensile testing

The coupon preparation and tests were carried out following AS1391:2007 (Standard Australia, 2007). Two strain gauges were attached to each side of the coupons to measure strain accurately. The tests were conducted using a 100 kN Shimadzu tensile testing machine (AGX-100 kN) under displacement control. The results obtained from the tensile coupon tests are presented in Table 3.1, and the stress-strain curves are shown in Figure 3.6.

Table 3.1: Mechanical properties obtained from the tensile coupon test

Specimens	Elastic modulus E (GPa)	Yield strength $\sigma_{0.2}$ (MPa)	Tensile strength σ_u (MPa)	Elongation at fracture ε_f (%)
SP-1	206	502	556	14
SP-2	202	509	560	18
SP-3	210	496	612	11
SP-4	205	512	564	9
SP-5	207	502	547	15

SP-6	208	507	572	14
SP-7	206	504	556	12
SP-8	210	501	564	12
Average	207	504	566	

Minimum yield strength according to the manufacturer is 450 MPa.

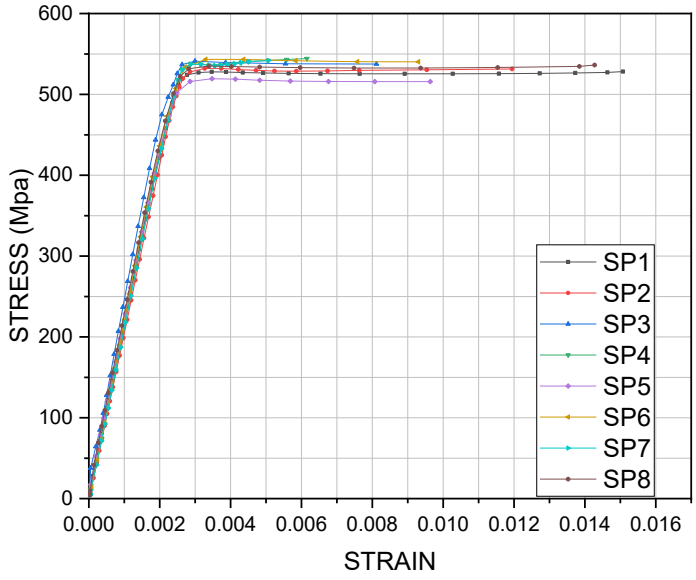

Figure 3.6: Stress-strain curve obtained from tensile coupon tests

3.2.1.2 Plywood Tests

Test samples obtained from 45 mm thick structural plywood panels were tested to determine their bending strength, compression strength, tensile strength and modulus of elasticity. All the plywood panels used in this study were made from Radiata Pine and were supplied by Big River Group Pty Ltd. The test specimen preparation and testing procedure were conducted following AS/NZS 2269-

1:2012 (Standard Australia, 2012). Four repeated tests were conducted for each test type.

Bending, compression and tensile test

Test pieces were cut from the plywood panels, as shown in Figure 3.7 in accordance with AS/NZS 2269.1. The cutting pattern allows for both the parallel (pa) and perpendicular (pe) specimens from the plywood panels of standard dimensions (2400 mm x 1200 mm). The test pieces for bending (shown as B_{pa} or B_{pe}) and compression (C_{pa} or C_{pe}) were 300 mm wide, and the tension (T_{pa} or T_{pe}) test pieces were 150 mm wide.

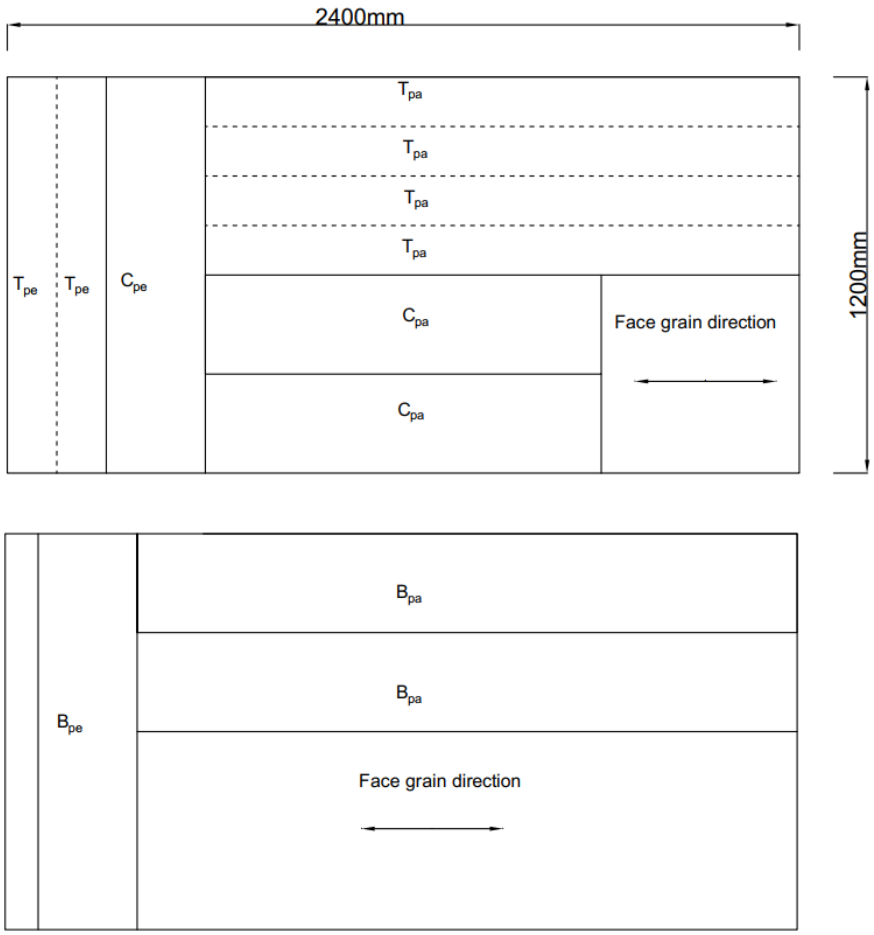

Figure 3.7: Cutting pattern for the structural plywood test panel

Four-point bending tests were conducted on the specimens cut from the plywood panels. The strength and stiffness properties of the plywood were determined for the panels cut in both parallel and perpendicular directions. The typical arrangement of the four-point bending test is shown in Figure 3.8. The load was applied through a 300 kN hydraulic actuator at a constant rate of 4mm/min until failure. Two lasers were used to measure the vertical deflections at mid-span. All the specimen failures occurred within 3-5 minutes as specified in the standard. Figure 3.9 illustrates a typical bending failure at about the mid-span of the specimen.

Figure 3.8: Four-point bending test setup

Figure 3.9: Typical bending failure on tensile face of plywood panel

The measured strength and modulus of elasticity in bending of the parallel and perpendicular cut specimens are presented in Table 3.2. In addition to the bending test, tensile and compressive tests on the parallel and perpendicular cut specimens were carried out per AS/NZS 2269-1:2012. As specified in the standard, the rate of load application was adjusted so that the failure of the test pieces occurred within the 4-5 minute range. The calculated compression and tensile strength are presented in Table 3.2. Parallel test pieces are labelled as 'Par'-followed by the specimen number, while perpendicular test pieces are labelled as 'Per'-followed by the specimen number.

Table 3.2: Measured strength and stiffness properties of tested plywood specimen

Specimen	Bending strength (MPa)	Compression strength (MPa)	Tension strength (MPa)	Modulus of Elasticity in bending (MPa)
Par-1	42.5	32	24.2	9877
Par-2	46	30.7	20.6	9780
Par-3	36	32	25	8497
Par-4	35.75	31.15	22.8	9006
Perp-1	46	29	16.2	9730
Perp-2	49.8	26.4	14	7738
Perp-3	50.15	29.1	17	8927
Perp-4	36	28	16.8	6796

3.2.2 Push-out Tests

3.2.2.1 Push-out Specimens

Laboratory push-out tests on eight major groups of CFS-plywood connections have been performed, and each group consist of three identical specimens. Hence, a total number of twenty-four push-out specimens were fabricated and tested. The push-out specimens utilised 2.4mm thick CFS C-section with 45mm thick structural plywood panels. The details of the push-out specimens are given in Table 3.3. In Table 3.3, the test series identification system adopted is a letter ‘P’, which indicates a push-out test, followed by connection types. For example, the ‘P-SDS’ label indicates a push-out test series that uses self-drilling screws as shear connectors. Similarly, any test series that utilised structural adhesive on the CFS flange and plywood interface used a letter ‘a’ at the end. For instance,

'P-CSa' indicates a push-out test series that used coach screws and adhesives as a means of shear connection.

Table 3.3: Summary of push-out specimen details

Test series	Type of connection	Number of specimens tested
P-SDS	#14 Self-drilling screw	3
P-SDSa	#14Self-drilling screw + adhesive	3
P-CS	M12 Coach screw	3
P-CSa	M12 Coach screw + adhesive	3
P-NB12	M12 Nut and bolt (without washer)	3
P-NB12a	M12 Nut and bolt (without washer)+ adhesive	3
P-NBW12	M12 Nut and bolt (with washer)	3
P-NBW8	M8 nut and bolt (with washer)	3
	Total tests	24

The geometry and set-up adopted for the tests are shown in Figure 3.10. The symmetric setup was adopted to ensure an even distribution of loading. To fabricate an economical size of the test specimens, 200 mm shear connector spacing was chosen, which is half of the construction industry practice. It is also worth mentioning that full-scale bending tests of the cold-formed steel and plywood flooring adopted 200 mm and 400 mm shear connector spacing. The load-slip behaviour of the shear connection from this push-out study is crucial for future numerical studies.

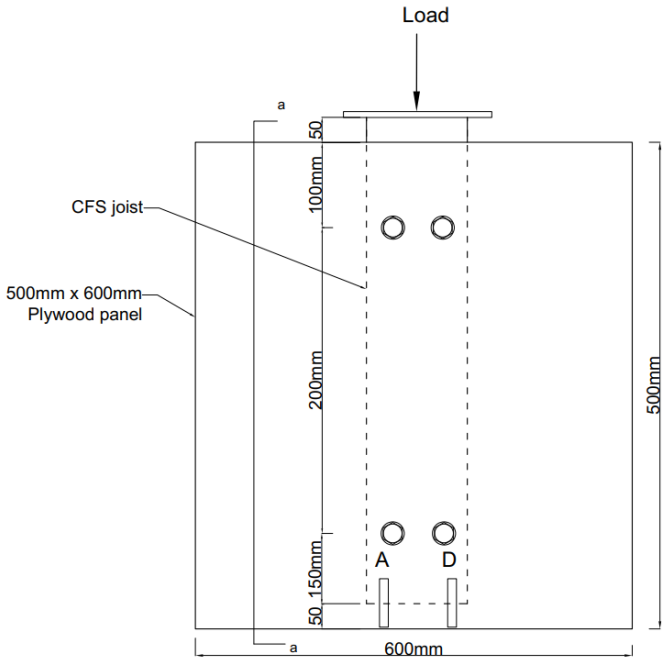

(a)

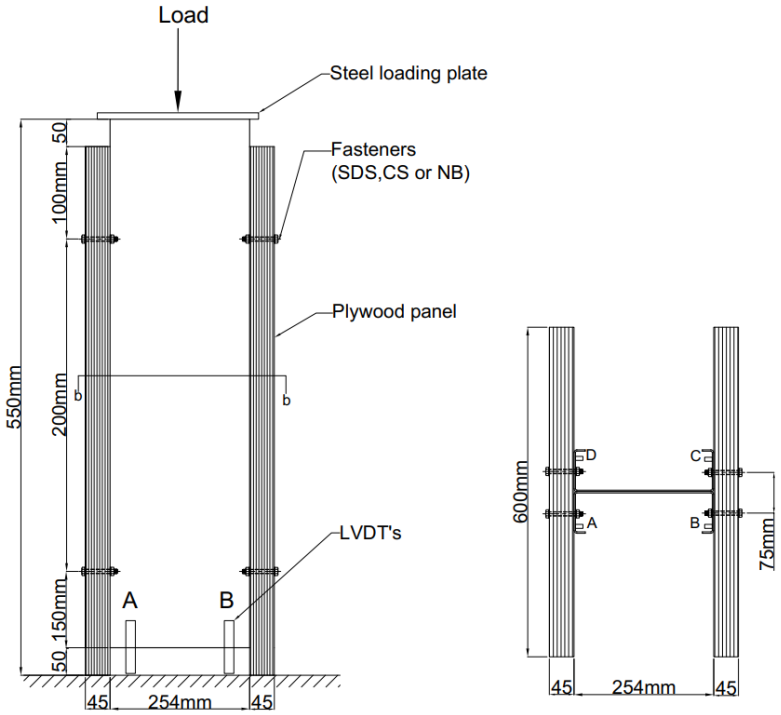

(b) (c)

Figure 3.10: Push-out specimen schematic view: (a) Elevation view; (b) Section view a-a ; (c) Plan view b-b

The primary variables considered in the experimental program were four different types of mechanical fasteners (e.g., self-drilling screws, M12 coach screws, M8 nut and bolt, M12 nut and bolt) and the use of structural adhesive along with fasteners. The effect of washers on the strength and stiffness of specimens with M12 nut and bolt connectors is also investigated. Size 14 self-drilling screws (6mm diameter), coach screws (Size M12), and nut and bolt (Size M8 and M12) were used in the testing as a means of shear connections. Coach screws and nuts and bolts were made of Grade 4.6 steel with nominal yield and ultimate strength of 240 MPa and 400 Mpa. Self-drilling screws, coach screws and bolts comply with the requirements of AS3566.1(Standard Australia, 2002), AS1393(Standard Australia, 1996), and AS1110.1(Standard Australia, 2000), respectively. The outline of fasteners used in the push-out tests is shown in Figure 3.11.

Figure 3.11: Shear connectors used in push-out tests

Structural adhesive (SikaBond-Contactfix) was used in the interface between cold-formed steel and plywood along with the mechanical fasteners in three of the test series shown in Table 3.3. The mechanical properties of the adhesive as per the manufacturer are provided in Table 3.4.

Table 3.4: Mechanical properties of structural adhesive

Tensile strength (MPa)	Compressive strength(MPa)	Shear strength (MPa)	Coefficient of linear expansion
30	70	15	$60x10^{-6}$ $mm^{o}c$

3.2.2.2 Test setup and fabrication

The push-out test configuration might impact the test results due to the uneven load distribution on the specimen caused by the mono-symmetric section geometry of CFS joists. Therefore, to guarantee a stable configuration, two CFS joists were joined back to back, and two plywood panels were connected on both sides of the flange, as illustrated in Figure 3.10.

After cutting the plywood panels to a required size of 500 mm × 600 mm, both the panels and the flange of the CFS C-section were pre-drilled except for the specimens with the self-drilling screws. The diameter of the pre-drilled holes in the plywood panels was 1 to 1.5 mm smaller than the diameter of the coach screws and 0.5 to 1 mm larger than the diameter of the bolts. The diameter of the pre-drilled holes in the flange of the C-section was 0.2mm to 0.6mm larger than the connectors (coach screws and bolts). The bolts were tightened using a manual torque wrench. The structural adhesive or glue was applied on both the CFS flange and plywood panel surface for the glued specimens. After mounting the plywood panel and CFS C-section together, the specimen was left to dry the glue for 24 hours before installing the screws or bolts.

The overall experimental setup is shown in Figure 3.12. All the tests were conducted using a 300 kN capacity Shimadzu universal testing machine. The relative displacement or slip between the CFS beam and plywood panels was measured using four LVDTs (linear variable differential transformers) with a 50 mm stroke. Four 60×6×6 mm steel brackets were fixed to the flange of the CFS joist, and the LVDTs were fixed to the plywood panels. The LVDTs were at an approximate level with contact in the steel bracket, so the relative slip between

the plywood panel and joist was measured when the load was applied to the CFS joist.

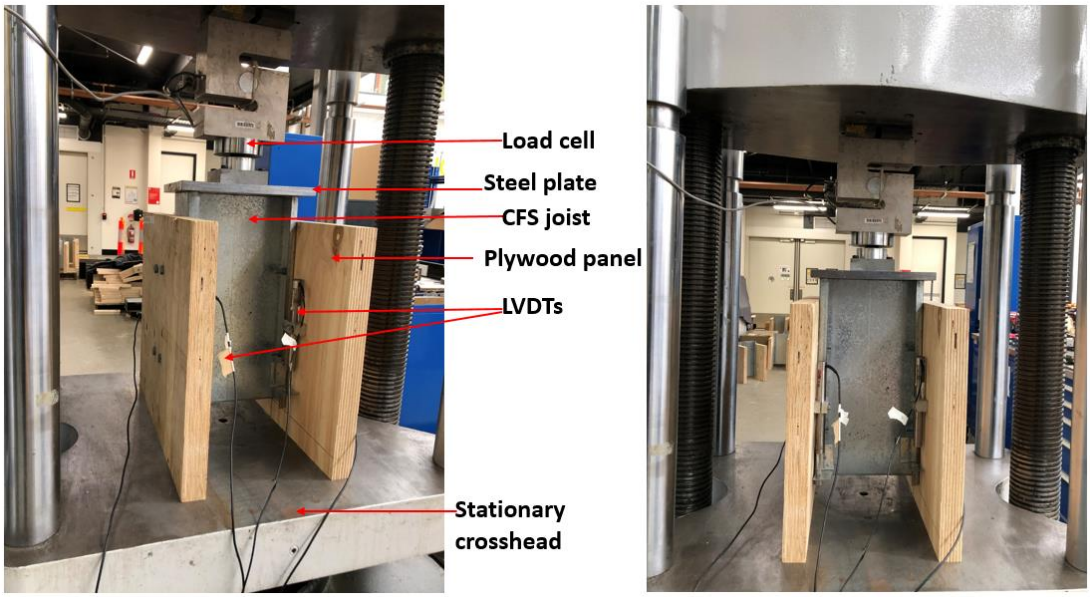

Figure 3.12: Experimental setup for push-out test in Shimadzu universal testing machine

3.2.2.3 Load application

All of the specimens were loaded according to the instructions given in BS EN 26891:1991(British Standard, 1991). Figure 3.13 shows the loading technique in line with the standard.

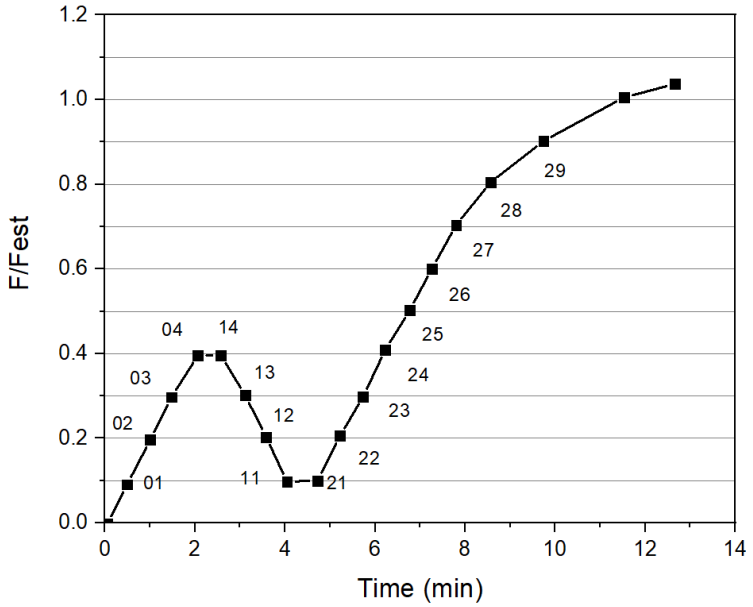

Figure 3.13: Loading procedure adopted in push-out tests as per BS EN 26891

A preliminary test was conducted from each series to determine the ultimate load, F_u. F_u is the load that corresponds to the failure of a specimen due to the connection failure or a 15 mm slip recorded during the test. Based on F_u (ultimate load) from the preliminary test, F_{est} (estimated failure load) was obtained. F_{est} is necessary for loading, unloading and reloading cycles as per the standard. The load was initially increased from 0 to $0.4F_{est}$ and was maintained at $0.4F_{est}$ for 30 s. Afterwards, the specimen was unloaded from $0.4F_{est}$ to $0.1F_{est,}$ and the load was sustained for 30 s at $0.1F_{est}$. Finally, a constant load rate was applied up to $0.7F_{est}$, and a constant rate of slip was applied above $0.7F_{est}$ until the specimen failed. The displacement rate for the self-drilling screw specimen was 1mm/min, whereas the displacement rate for the coach screw, nut, and bolt specimen was 2mm/min to make the specimens fail within 3-5 minutes. All the specimens failed at about 11 to 15 minutes, which aligns with the total testing time specified in the standard.

3.3 Discussion of Push-Out Test Results

Hassanieh et al. (2016b) reported that the structural behaviour of timber connections could be affected by the mechanical properties of materials and the fabrication method. Hence, three identical specimens for each type of CFS-plywood joint were fabricated and tested under similar loading conditions to ensure the accuracy and repeatability of the test results (e.g., stiffness, failure mode, and load-slip response). This section presents the distinct failure modes of the specimens and their load-slip responses from each test series.

3.3.1 Modes of Failure

3.3.1.1 Connections with self-drilling screws

Figure 3.14 demonstrates the failure mechanism of the specimens with SDS connection joints. The body of the screw was effectively restrained by the plywood preventing any rotation, and the head was under the flange of the CFS joist. As the loading was applied through the steel plate on CFS joists, the body of the screw was pressed into the plywood, and the region of the screw under the head at the CFS-plywood interface started to yield in bending. Upon further loading, the head of the screw detached from its body. All the specimens failed due to shear failure under the head of the screws, as depicted in Figure 3.15(a). The bending of the screws was also observed, as shown in Figure 3.15(b).

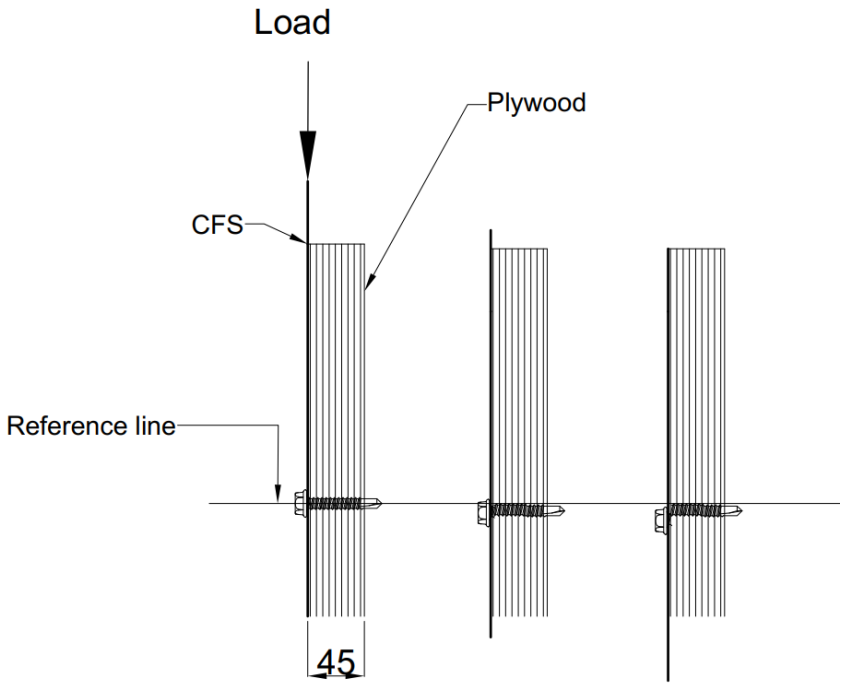

Figure 3.14: Failure mechanism of the specimens with self-drilling screws

(a)

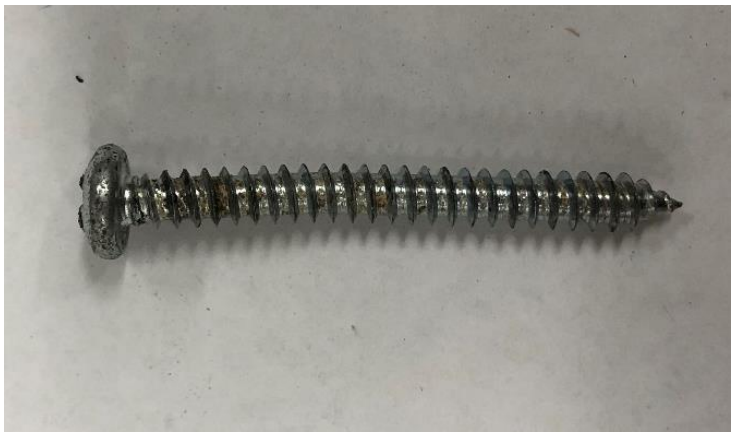

(b)

Figure 3.15: Failure modes of the specimens with self-drilling screws: (a) shear failure under head; (b) bending failure

3.3.1.2 Connections with coach screws

The failure mode of the push-out specimens with coach screw connections is shown in Figure 3.16.

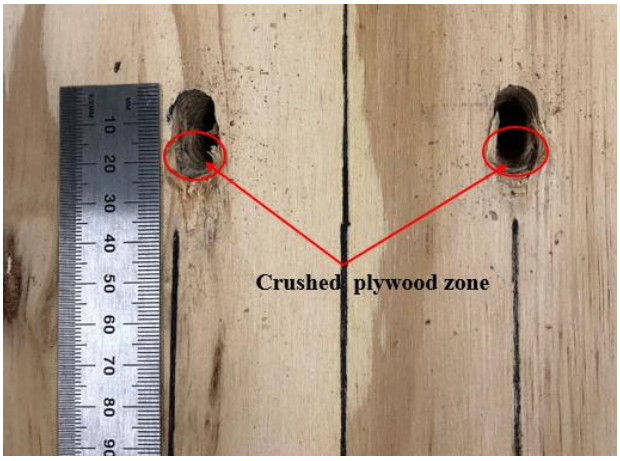

(a)

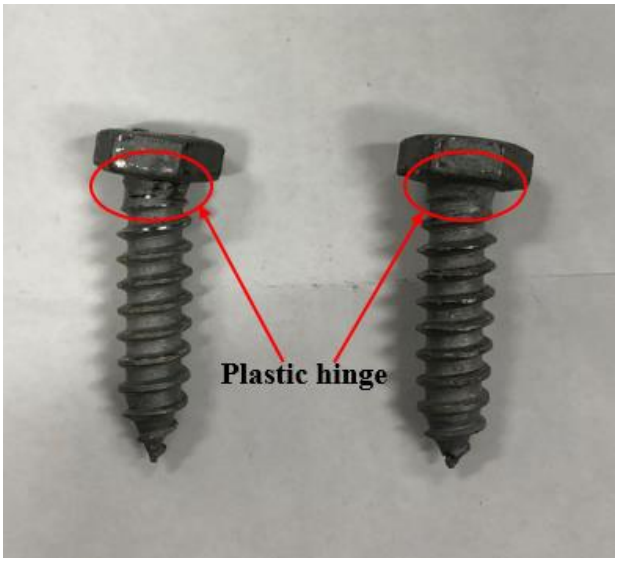

(b)

Figure 3.16: Failure modes of the specimens with coach screws: (a) crushing of plywood; (b) formation of plastic hinge

The formation of a plastic hinge occurred under the head of the coach screw almost on every fastener. When the push-out specimens were loaded, coach screws gradually rotated with the head moving towards the loading direction while the body was pressed into the plywood. The plywood panel was sufficient enough to restrain the bodily displacement of the coach screw even though significant bearing of the coach screw into the plywood was observed. The crushing of the

plywood panels was observed, which were almost double the size of the coach screw. A simplified failure mechanism of the specimens with CS connection joint is demonstrated in Figure 3.17.

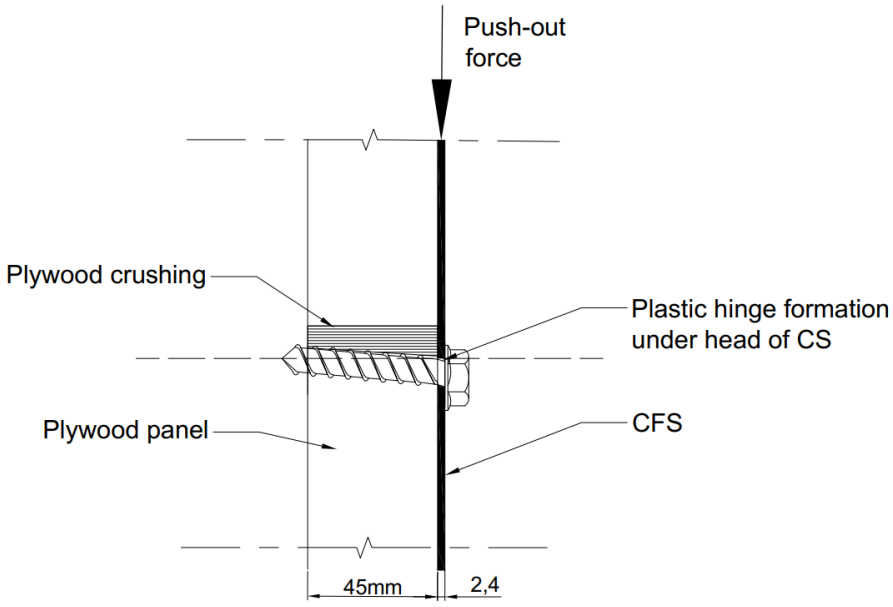

Figure 3.17: Failure mechanism of the specimens with coach screws

3.3.1.3 Connections with M12 nut and bolt (without washer)

The typical failure mode for the specimens with M12 nut and bolt (without washer) connections was the formation of the plastic hinge and crushing of plywood panels, as shown in Figure 3.18. When the push-out specimens were loaded, the load was perpendicular to the longitudinal axis of the bolt. With the gradual movement of the CFS joist due to the loading, plastic hinge formation took place near the threaded part of the bolt, which lies at the shear interface of the plywood and CFS joist. Because the plywood panels restrained the unthreaded body part of the bolt and the threaded part moved slowly along the loading direction, a plastic hinge formed at the shear interface. The illustration of the failure

mechanism of this connection type is shown in Figure 3.19. As mentioned earlier, the failure criteria for all the tested specimens were taken as a 15 mm joint slip as per BS EN 26891; loading was stopped at around 15 to 17 mm slip. The extent of the plywood crushed zone was double the size of the fastener, as observed in the coach screw connection.

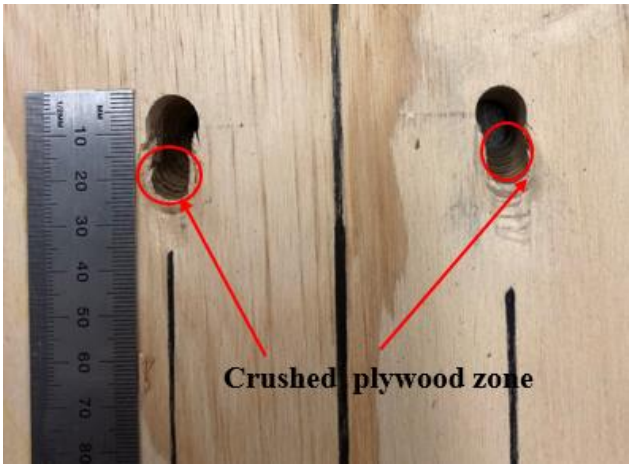

(a)

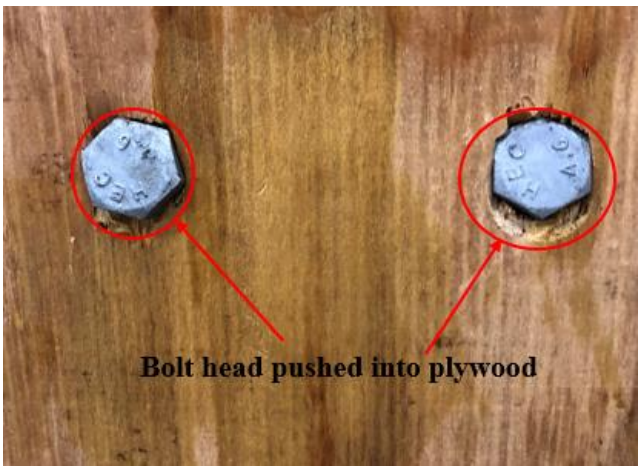

(b)

(c)

Figure 3.18: Failure modes of the specimens with M12 nut and bolts: (a) crushing of plywood; (b) bolt head bearing into plywood; (c) plastic hinge

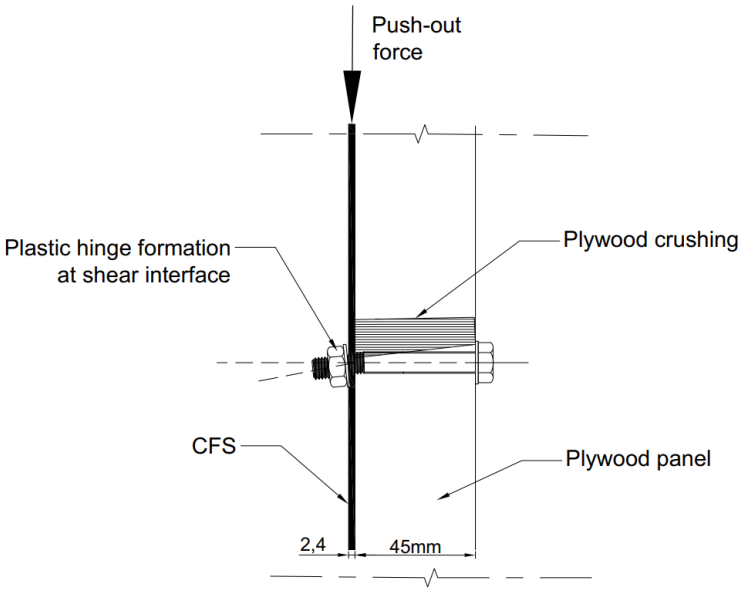

Figure 3.19: Failure mechanism of the specimens with M12 nut and bolt (without washer)

3.3.1.4 Connections with M12 nut and bolt (with washer)

The distinctive failure mode of the specimens with M12 nut and bolt with washer (P-NBW12) is shown in Figure 20. Two plastic hinges formed on the connector, one at the middle part (similar to the connections with M12 nut and bolt without washer) and the other near the bolt head, as highlighted in Figure 3.20(a). The crushing of plywood panels was similar to that of the P-NB12 test series specimen. With the increasing load on the push-out specimen, the bolt end on the CFS joist side gradually displaces in the load direction, and the unthreaded part restrained by plywood panels gets pressed into the plywood. Hence because of that phenomenon, a permanent deformation in the plywood panels, which had the size of washers, was observed, as shown in Figure 3.20(c). Local deformation around the fastener holes of the CFS joist was also found in these connection joints.

(a)

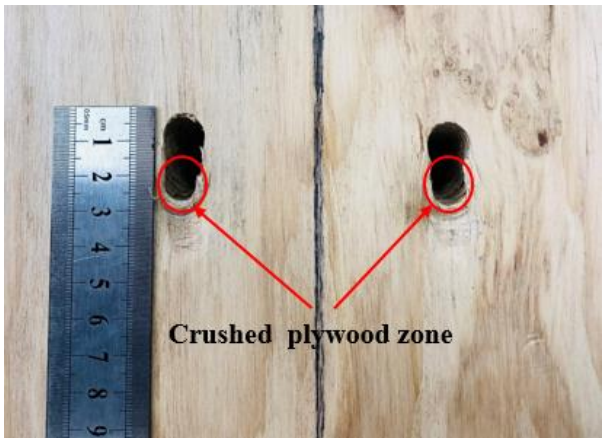

(b)

(c) (d)

Figure 3.20: Failure modes of the specimens with M12 nut and bolts (with washers): (a) plastic hinge formation; (b) crushing of plywood; (c) washer at bolt head pressed into plywood; (d) local deformation of CFS joist flange around holes

3.3.1.5 Connections with M8 nut and bolt (with washer)

Figure 21 shows the typical failure modes associated with the M8 nut and bolt connections. All the specimens on the test series P-NBW8 demonstrated the formation of a plastic hinge on the bolt and, ultimately, its fracture. At the initial loading stage, all the specimens were within the elastic range, and the slip of the connection joints showed a linear relationship with the loading. With the increasing load, bending of the bolts and formation of plastic hinge took place near the threaded part of the bolt, which lies at the shear interface of plywood and CFS joist. As the load was further increased, some connectors could not bear more loads and ultimately failed in the shear plane. The failure of these shear connectors was more of a brittle nature, while the coach screws and M12 nut and bolt demonstrated semi-ductile or ductile of its kind.

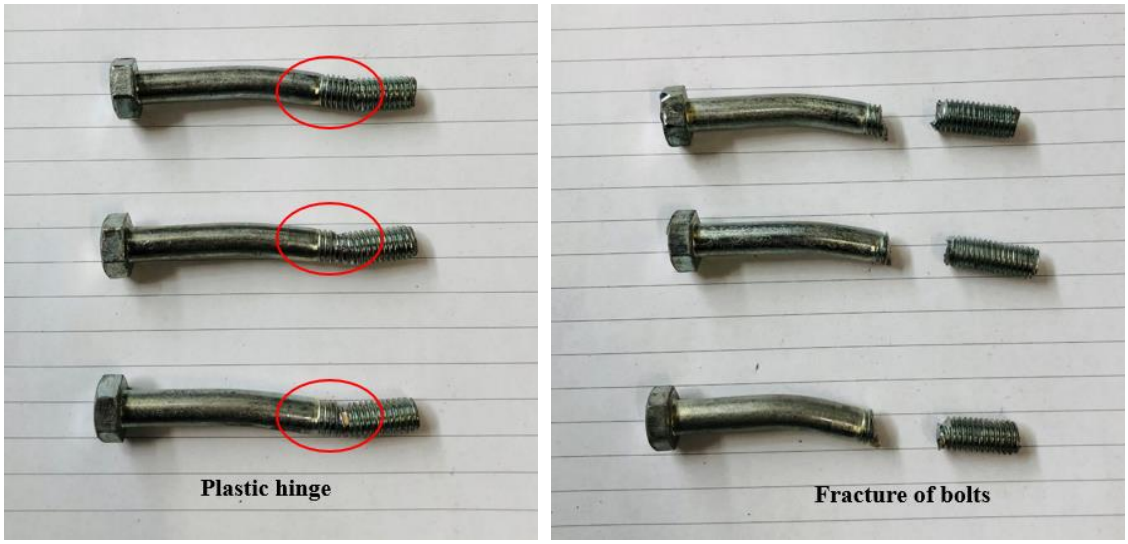

(a) (b)

Figure 3.21: Failure modes of the specimens with M8 nut and bolts (with washers): (a) plastic hinge formation; (b) fracture of bolts

3.3.1.6 Connections with structural adhesive+fasteners (self-drilling screw,coach screw or nut and bolt)

As can be seen in Table 3.3, three different test series: P-SDSa, P-CSa, and P-NB12a, that utilised self-drilling screws, M12 coach screws, and M12 nut and bolt, respectively, along with structural adhesives were tested. There was a sudden failure of the adhesives on the specimens with SDS and CS, meaning that debonding occurred at one point with the increasing load. This phenomenon was not observed for the nut and bolt connections. However, it should be noted that the failure mode of the specimens with and without adhesives was similar, which is already discussed in the above sections. Figure 3.22 shows the failure modes associated with fasteners and adhesives connection.

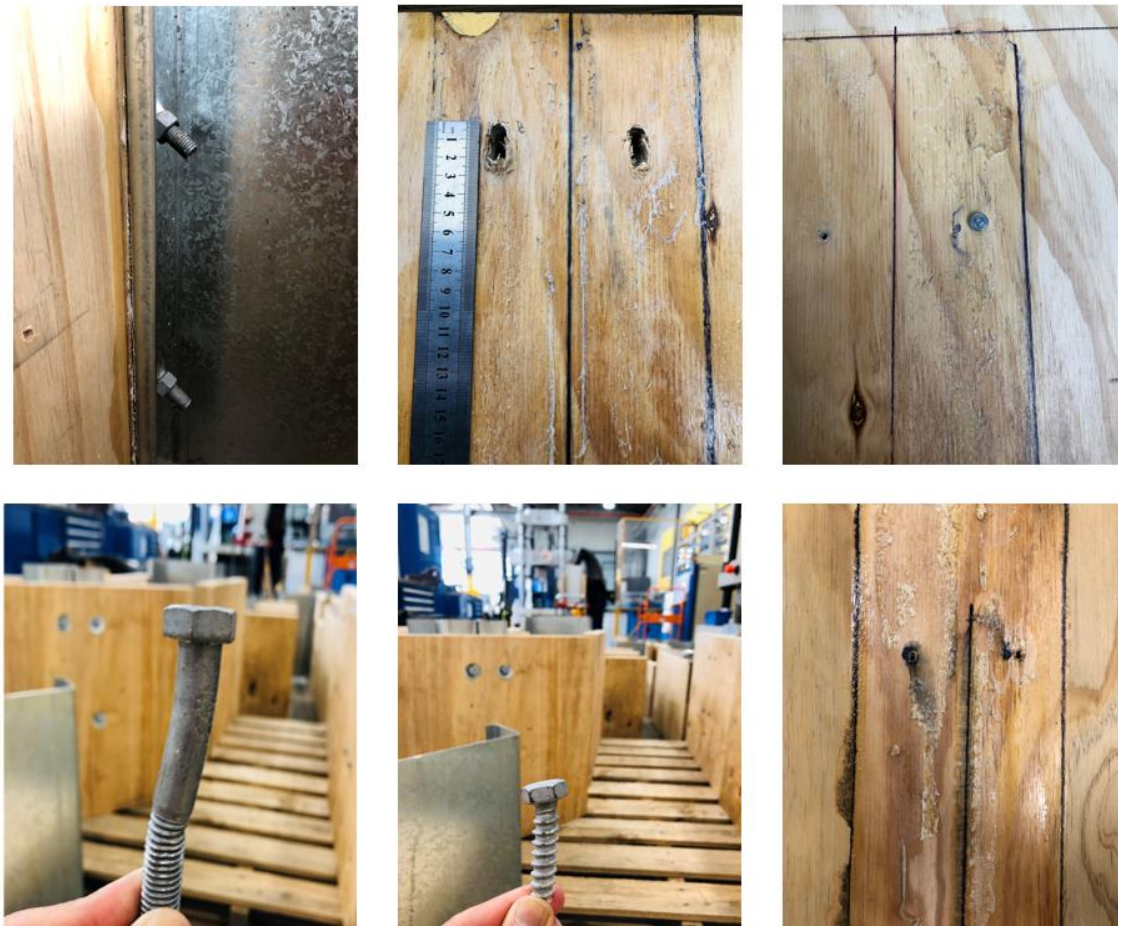

Figure 3.22: Failure modes of the specimens with fasteners + adhesives

3.3.2 Load-Slip Response of Connection Joints

When a composite CFS and timber beam assembly is loaded, the load is transferred from the timber sheathing through the shear connectors into the CFS beams beneath the sheathing. It is well known that the amount of load that can be shared depends on the amount of slip that arises between two members. This slip value, also known as slip modulus, helps to understand the extent of composite action that takes place in the assembly (Couchman, 2016). The load-slip responses of each connection type are discussed in this section. It should be noted that a joint slip of 15 mm is considered as the failure of connections

throughout the push-out tests. This is one of the failure criteria as outlined in BS EN 26891. And also the reason to record failure load at 15 mm slip rather than going up to the ultimate load of connectors (especially M12 nut and bolts) is that usually at around 15 mm slip, the bearing of the fastener into the plywood and crushing of plywood panel would have significantly taken place, even though the connection itself was taking a higher load. Hence adopting a 15 mm joint slip as a failure criterion was reasonable, considering the strength properties of the materials tested.

3.3.2.1 Connections with self-drilling screws only (Test series: P-SDS)

The load-slip behaviour of the connections with 6mm diameter self-drilling screws is shown in Figure 3.23. The load-carrying capacity P_u and stiffness $K_{0.4}$ and $K_{0.6}$ of the connections are provided in Table 3.5. The slip stiffness values $K_{0.4}$ and $K_{0.6}$ are the corresponding values at 40% and 60% of the peak load, respectively and are considered the initial and pre-peak stiffness of the connections. The slip modulus values $K_{0.4}$ and $K_{0.6}$ are calculated using the procedures given in BS EN 26891. It was found that the initial stiffness of the connections was higher than the pre-peak stiffness. In all specimens, a sudden drop in the load was observed once there was a breakage of the screw head.

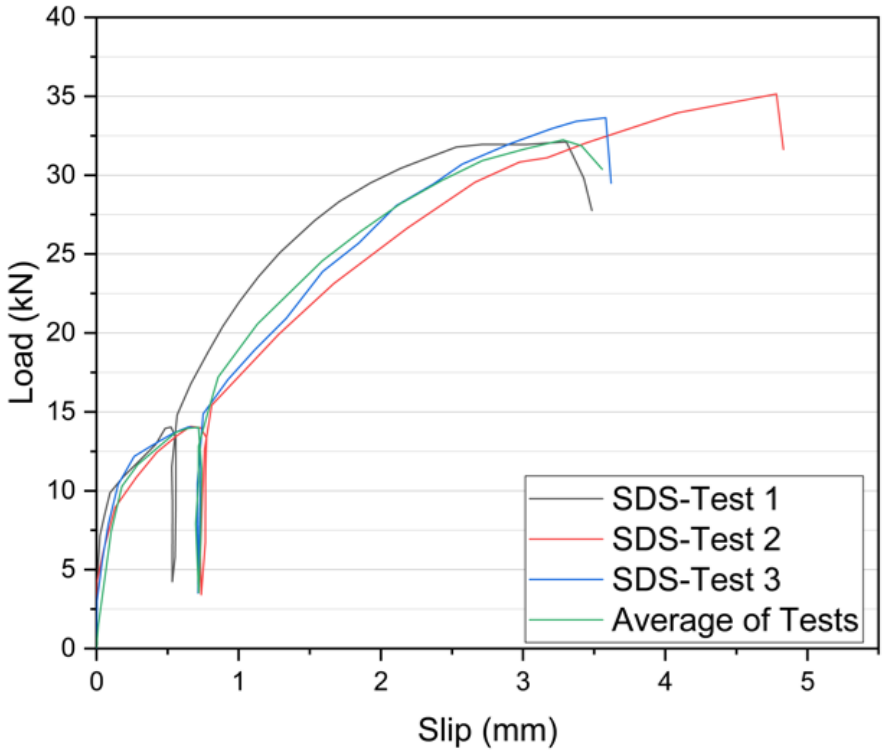

Figure 3.23: Load slip response of specimens with self-drilling screws (SDS)

Table 3.5: Load-carrying capacity and slip modulus of self-drilling screw

Self-drilling screw (SDS)	Load at failure, P_u (kN)	$K_{s,\,0.4}$ (kN/mm)	$K_{s,\,0.6}$ (kN/mm)
Test 1	32.2	22.1	20
Test 2	35.1	15.93	14.8
Test 3	33.6	17.63	14.92
Average of tests	32.26	17.59	16.99

3.3.2.2 Connections with coach screws (Test series: P-CS)

Table 3.6 summarises the test results of the connection joints with M12 coach screw connectors. Furthermore, the load-slip response of the connection is depicted in Figure 3.24.

Table 3.6: Load-carrying capacity and slip modulus of coach screw

Coach screw (CS)	Load at failure, P_u (kN)	$K_{s,0.4}$ (kN/mm)	$K_{s,0.6}$ (kN/mm)
Test 1	81.98	11.39	11.32
Test 2	82	10.63	10.6
Test 3	84.5	11.38	11.4
Average of tests	82.8	10.89	10.66

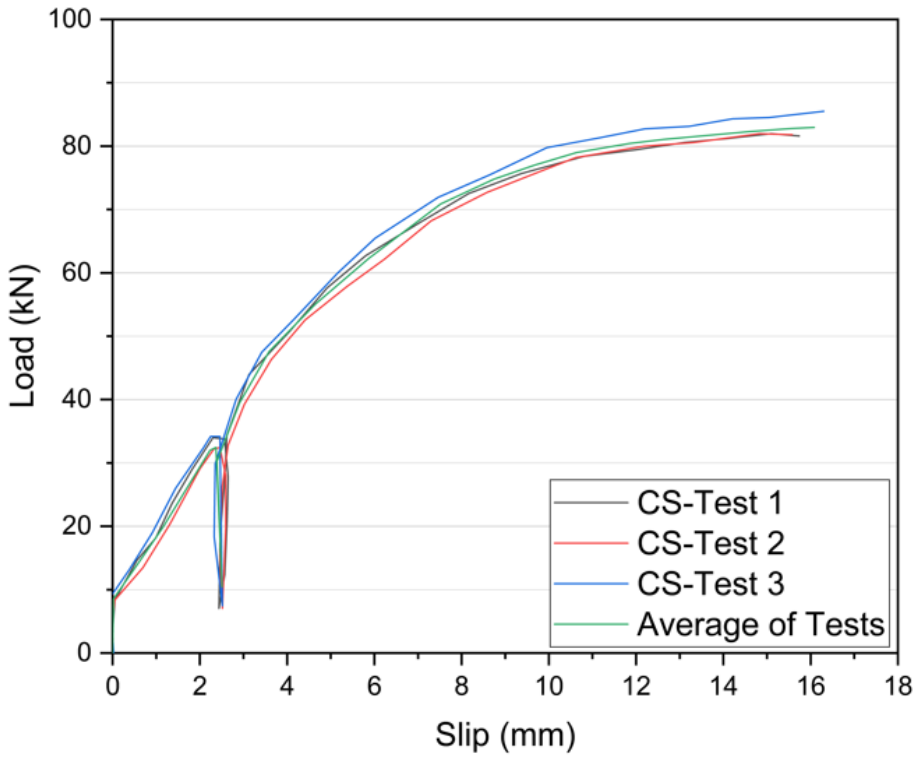

Figure 3.24: Load slip response of specimens with coach screws (CS)

The initial stiffness ($K_{0.4}$) and the pre-peak stiffness ($K_{0.6}$) of these connection types were nearly similar. Unlike SDS connections, which do not require pre-drilling, CS connections were pre-drilled in plywood panels and CFS joists. It could be the reason for having nearly similar stiffness, as there was no pre-

tension or post-tension force to increase the friction between the material while loading.

3.3.2.3 Connections with M12 nuts and bolts (Test series: P-NB12 and P-NBW12)

The load-slip response of the CFS and plywood connections using M12 nut and bolt connectors without and with washers is shown in Figures 3.25 and 3.26, respectively.

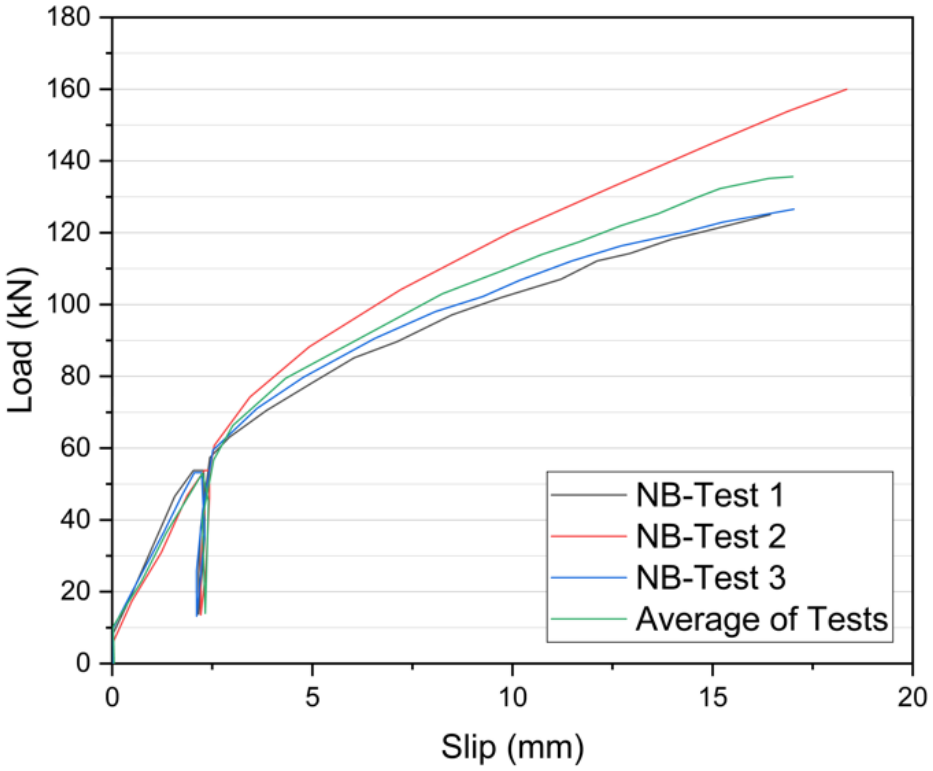

Figure 3.25: Load slip response of specimens with M12 nut and bolt without washer (NB12)

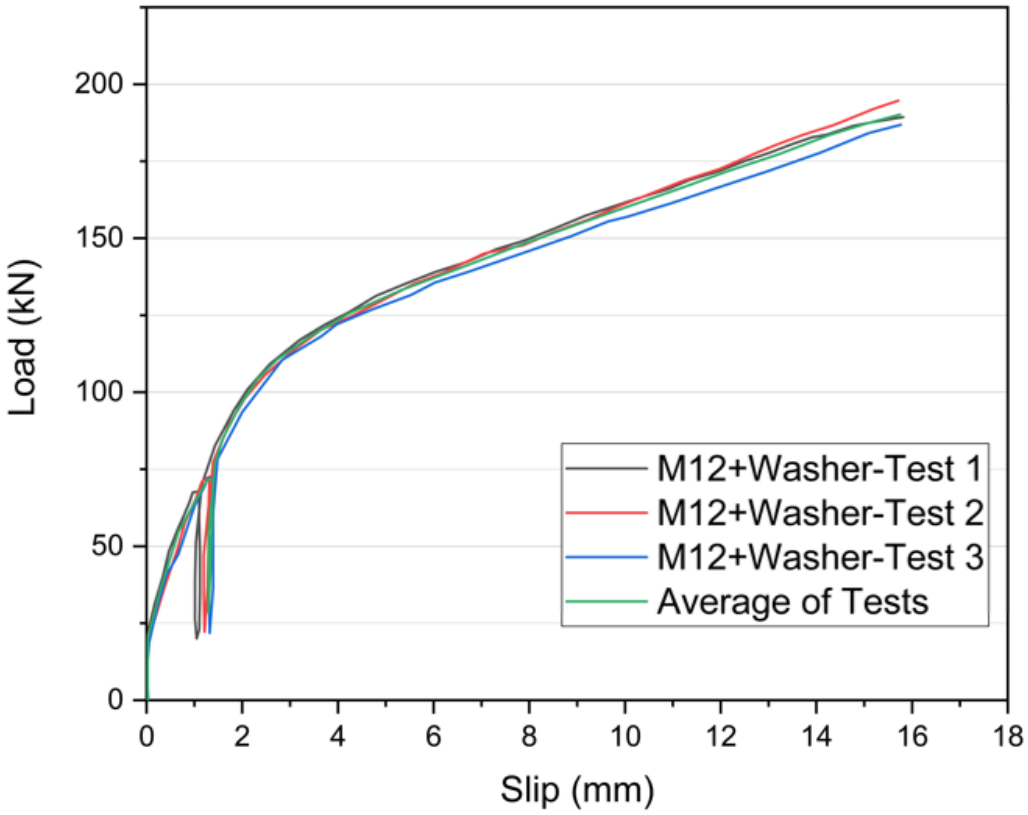

Figure 3.26: Load slip response of specimens with M12 nut and bolt with washer (NBW12)

The initial stage, which is also the no-slip stage, was due to the pre-tensioning of bolts. Bolt pre-tensioning leads to significant friction between the plywood panel and CFS joist and hence negligible relative slip at the shear interface. With the increasing load, slip increased proportionally up to 60% of the loading for the connectors without washers. While for the connectors with washers, the slip was relatively lower with increased loading. The load-slip behaviour was non-linear until the 6 mm joint slipped for the washer connections. As expected, connections that used nuts and bolts with washers demonstrated higher stiffness than those without washers. The load-carrying capacity P_u, stiffness $K_{0.4}$, and $K_{0.6}$ of the

connections without and with washers are provided in Tables 3.7 and 3.8, respectively.

Table 3.7: Load-carrying capacity and slip modulus of M12 nut and bolt (without washer)

Nut and bolt (NB)	Load at failure, P_u (kN)	$K_{s,\,0.4}$ (kN/mm)	$K_{s,\,0.6}$ (kN/mm)
Test 1	121	22.91	16.5
Test 2	145	22.18	20.6
Test 3	123	21.85	17.2
Average of tests	132	21.96	18.26

Table 3.8: Load-carrying capacity and slip modulus of M12 nut and bolt (with washer)

Nut and bolt (NB)	Load at failure, P_u (kN)	$K_{s,\,0.4}$ (kN/mm)	$K_{s,\,0.6}$ (kN/mm)
Test 1	186.5	51.4	40
Test 2	188	46.95	38.94
Test 3	180	44.77	36.14
Average of tests	183.5	44.4	36.8

3.3.2.4 Connections with M8 nut and bolt (Test series: P-NBW8)

Figure 3.27 depicts the load-slip curves for specimens that used M8 nuts and bolts with washers. There was a very minimal slip until the load reached 4 kN, and this initial resistance was due to the tightness of the composite joints due to the pre-tensioning of bolts. Almost all the specimens failed due to fracture of bolts, and hence a sudden drop in the load can be seen in Figure 3.27. The key values measured from the testing of three identical specimens are presented in Table

3.9. The fracture of bolts, as shown in Figure 3.21(b), is consistent with the sudden drop of load in the curve below a 15 mm slip value.

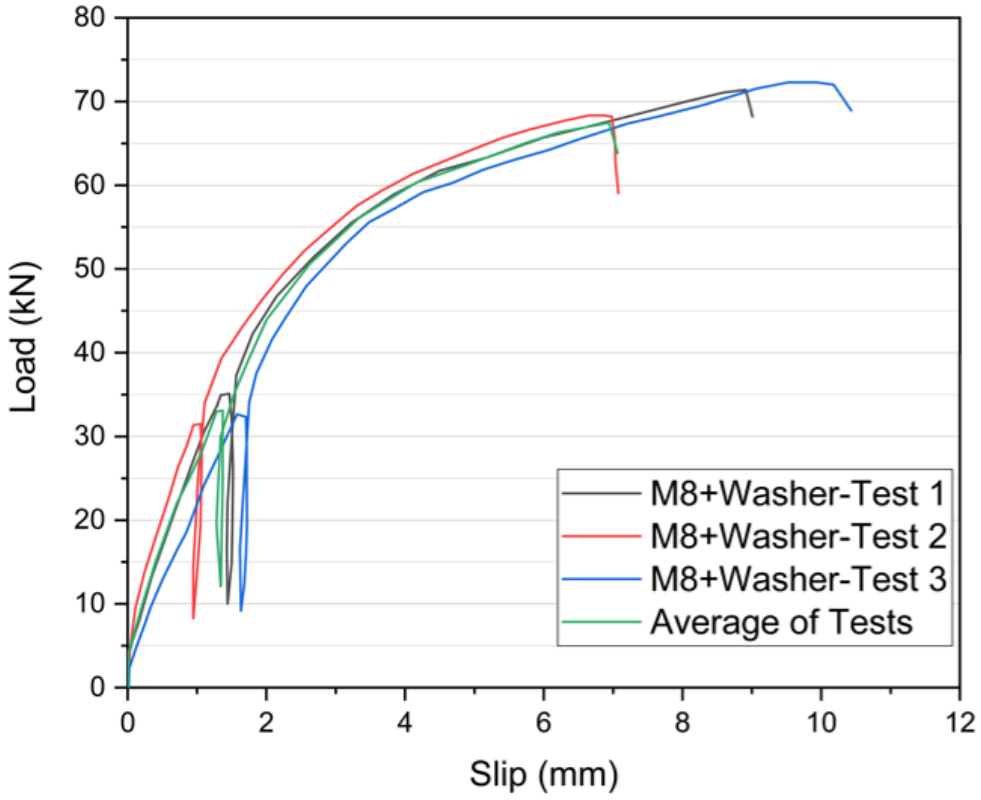

Figure 3.27: Load slip response of specimens with M8 nut and bolt with washer (NBW8)

Table 3.9: Load-carrying capacity and slip modulus of M8 nut and bolt (with washer)

Nut and bolt (NB)	Load at failure, P_u (kN)	$K_{s,\,0.4}$ (kN/mm)	$K_{s,\,0.6}$ (kN/mm)
Test 1	71.4	23.7	23.3
Test 2	68.2	26.7	22.35
Test 3	72	18.35	19.95
Average of tests	67.6	20.2	20

3.3.2.5 Connections with fasteners + adhesives (Test series: P-SDSa, P-CSa, and P-NB12a)

The purpose of using adhesives at the shear interface of plywood and CFS joists with fasteners was to increase the composite behaviour so that the connection joints behaved as full composite sections with no slip. Furthermore, with the use of structural adhesive/glue, the initial stiffness of the connections was found to be significantly increased. There was no slip until 5 kN load for the specimens with SDS and glue and 9 kN load for the specimens with CS and glue. However, the minimal slip was recorded for the specimens with nut, bolt, and glue. The load versus slip response of the test series P-SDSa, P-CSa, and P-NB12a is shown in Figure 3.28, Figure 3.29, and Figure 3.30, respectively.

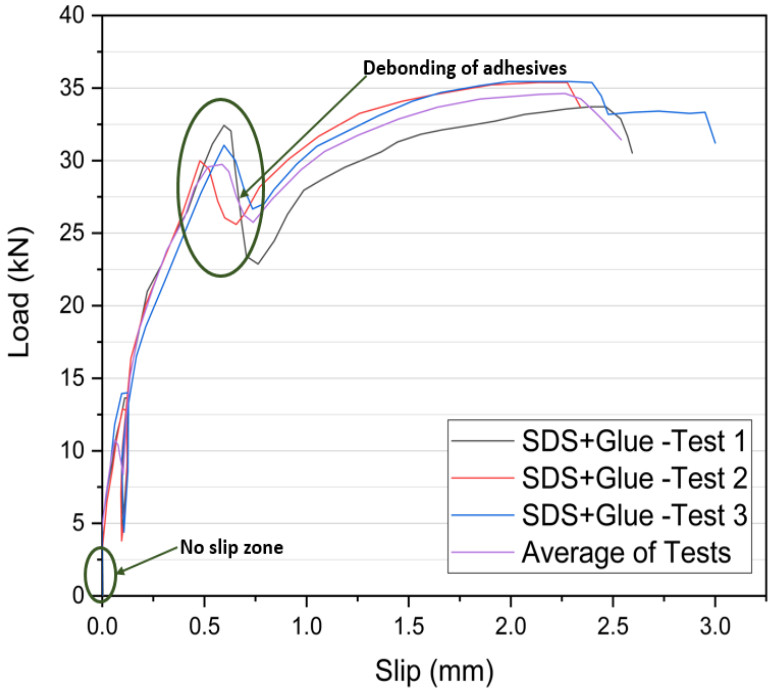

Figure 3.28: Load slip response of specimens with SDS + Glue

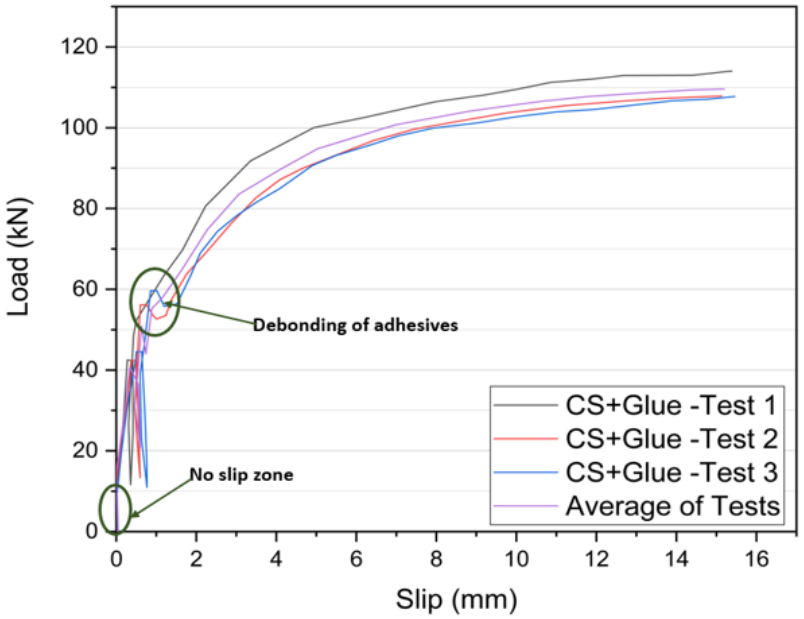

Figure 3.29: Load slip response of specimens with CS + Glue

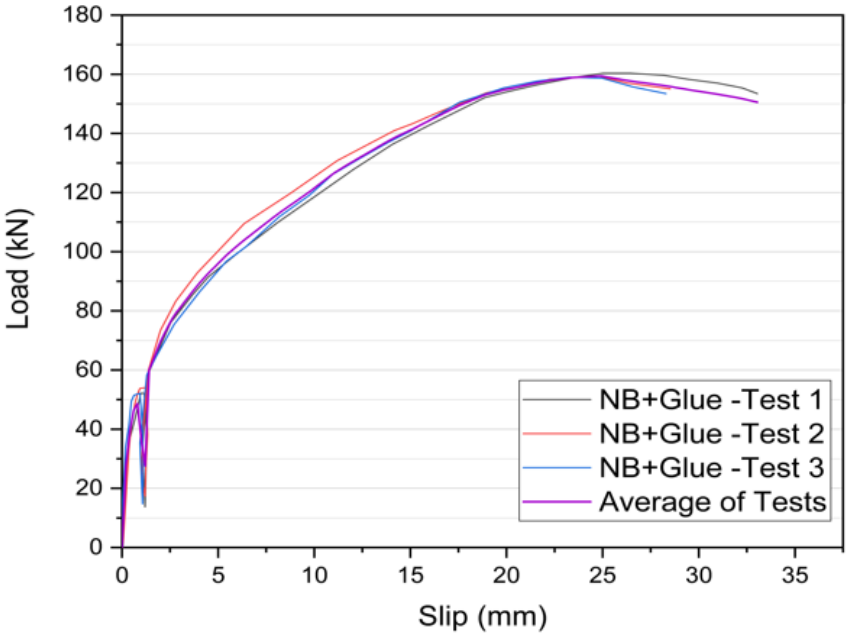

Figure 3.30: Load slip response of specimens with NB + Glue

A sudden drop in the load after 40% of the loading was observed for the test series P-SDSa, and P-CSa, which was due to the delamination of the glue from the shear interface and resulted in brittle failure. Nevertheless, no such phenomenon was observed in the P-NB12 test series. After this brief process of glue failure, the specimens started to take higher loads which can be attributed to the fact that the strength of composite joints relied on the fastener alone. The summary of the test results for P-SDSa, P-CSa, and P-NB12a are provided in Tables 3.10, 3.11, and 3.12, respectively.

Table 3.10: Load-carrying capacity and slip modulus of SDS + Glue (Test series P-SDSa)

SDS + Glue	Load at failure, P_u (kN)	$K_{s,\,0.4}$ (kN/mm)	$K_{s,\,0.6}$ (kN/mm)
Test 1	33.7	84	84.1
Test 2	35.3	90.5	83.1
Test 3	35	82	68
Average of tests	34.6	90.5	73.7

Table 3.11: Load-carrying capacity and slip modulus of CS + Glue (Test series P-CSa)

CS + Glue	Load at failure, P_u (kN)	$K_{s,\,0.4}$ (kN/mm)	$K_{s,\,0.6}$ (kN/mm)
Test 1	113	60.4	39.25
Test 2	107.2	52.2	25.4
Test 3	106.7	48.6	24.3
Average of tests	110	52	29.4

Table 3.12: Load-carrying capacity and slip modulus of M12 NB + Glue (Test series P-NB12a)

NB + Glue	Load at failure, P_u (kN)	$K_{s,\ 0.4}$ (kN/mm)	$K_{s,\ 0.6}$ (kN/mm)
Test 1	137.5	45.2	26.4
Test 2	142.4	47.67	30.4
Test 3	141	70.46	30.16
Average of tests	140.8	55.7	31.5

3.4 Overview of Push-Out Test Findings

As shown in Table 3.3, eight test series and each test series with three identical specimens were tested. The above sections discussed the load-slip behaviour and failure mode of individual tests. An average of tests was also calculated for each test series, as shown in Figure 3.23 to Figure 3.30 and Table 3.5 to Table 3.12, by running a mathematical analysis in a graphing and analysing tool called Origin Pro (OriginPro, 2021). However, a distinctive comparative summary of the results obtained from all the test series is presented in this section. Table 3.13 summarises the key results of all the push-out test series regarding their mean values.

Table 3.13: Summary of key test results (mean values) for different shear connections

Test series	Load at failure, P_u (kN)	$K_{s,0.4}$ (kN/mm)	$K_{s,0.6}$ (kN/mm)	Ductility, D	Normalised stiffness	
					$K_{s,0.4}$ (kN/mm)	$K_{s,0.6}$ (kN/mm)
P-SDS	32.2	17.59	16.99	4.8	2.19	2.12
P-SDSa	34.6	90.5	73.7	23.4	11.31	9.21
P-CS	82.8	10.89	10.66	5.3	1.36	1.33
P-CSa	110	52	29.4	15.7	6.5	3.6
P-NB12	132	21.96	18.26	7.1	2.75	2.28
P-NB12a	140.8	55.7	31.5	19	6.96	3.93
P-NBW12	183.5	44.4	36.8	11.2	5.55	4.6
P-NBW8	67.6	20.2	20	6.1	2.52	2.5

The slip modulus at 40% (initial stiffness) and 60% (pre-peak stiffness) of the loading is calculated per shear connector, which is the normalised stiffness as tabulated in Table 3.13. The ductility of the connections, which is the ability to undergo large slip without reducing strength, is also determined by Equation (3.1) in accordance with BS EN 12512 (CEN, 2005).

$$D = \frac{V_u}{V_y} \tag{3.1}$$

Where V_u and V_y are the ultimate slips and yield slips, respectively, as defined in BS EN 12512. It was found that the use of structural adhesives along with fasteners significantly increased the stiffness and ductility of the connections. Test series, P-SDSa, which utilises self-drilling screws and adhesive at the shear interface between two materials, produced stiffer and more ductile connections

than any other test series. There was no pre-drilling required for the specimens that use SDS. Even though SDS is smaller in diameter and lesser in strength than CS and bolts, the threads of the screws firmly clamped with CFS flange and plywood after drilling, which produced post-tensioning force. As a result, very high friction exists between CFS and plywood panels due to the influence of glue and post-tensioning force. Hence, the composite joints act as a perfect composite section with minimal slip and higher stiffness. Connection joints with CS only (P-CS) were demonstrated to be less stiff and relatively low ductile than others. However, with the use of adhesive at the shear interface along with CS (P-CSa), the ductility and average stiffness of the connections were increased by 196% and 255%, respectively. Similarly, for the M12 nut and bolt connections, the use of adhesives enhanced the stiffness by 270% and ductility by 167%. Comparing the specimens, P-NB12 and P-NBW12, the stiffness and ductility were found to be increased by 100% and 58%, respectively, for M12 nut and bolt connections with washers. The stiffness and ductility of the M12 nut and bolt connection without washers (P-NB12) were 9% and 16% higher than the connections with M8 nut and bolt with washer (P-NBW8). The reason is that using washers, a more pre-tension force was applied to the bolts with lesser local damage on the plywood itself. Higher pre-tension force, which was developed while tightening the bolts, created a compressive force on the connection joints, which ultimately increased the rigidity of the joints.

3.5 Analytical Load-Slip Model of Connections

In this section, a non-linear regression analysis of the load-slip behaviour of the tested connection joints is carried out to develop an analytical relationship of load

versus slip. An equation developed by Foschi (Foschi, 1977) is used in this study to predict the load slip relationship of the connections. A slight modification of the Foschi formula is made in this study to capture the no-slip response and non-linear behaviour of the connection joints. Foschi formula is widely used to simulate the load-slip relationship of mechanical connections like nails and bolts (Kalkert and Dolan, 1997; Yang et al., 2020). The expression for the Foschi curve is given by Equation (3.2).

$$P(s) = (P_O + K_1.S).\left(1 - e^{\left(\frac{-k_o.S}{P_O}\right)}\right) \tag{3.2}$$

A four-parameter model based on the Foschi formula is used in this study to predict the load-slip relationship, which is given by Equation (3.3).

$$P(s) = P_i + (P_{max} - P_i).\left(1 - e^{\left(\frac{-k_o.S}{P_O}\right)}\right) \tag{3.3}$$

Where *P(s)* is the load for a slip *S* (mm), K_o (kN/mm) is the initial stiffness of connection, K_1 (kN/mm) is the stiffness for large slip values, P_i (kN) is the intercept of asymptote with slope K_o, P_o (kN) is the intercept of asymptote with the slope K_1, P_{max} (kN) is the maximum load recorded for the failure of the test. These parameters are obtained by the non-linear curve fitting of the experimental test results, as shown in Figure 3.31. In Figure 3.31, P_i and P_o are the intercepts of the asymptote on the y-axis before and after yield, respectively. P_i corresponds to an initial load after no slip and P_o corresponds to 50% to 60% of the failure load. Origin pro software (OriginPro, 2021) was used for the non-linear regression based on the exponential CDF to determine input parameter values.

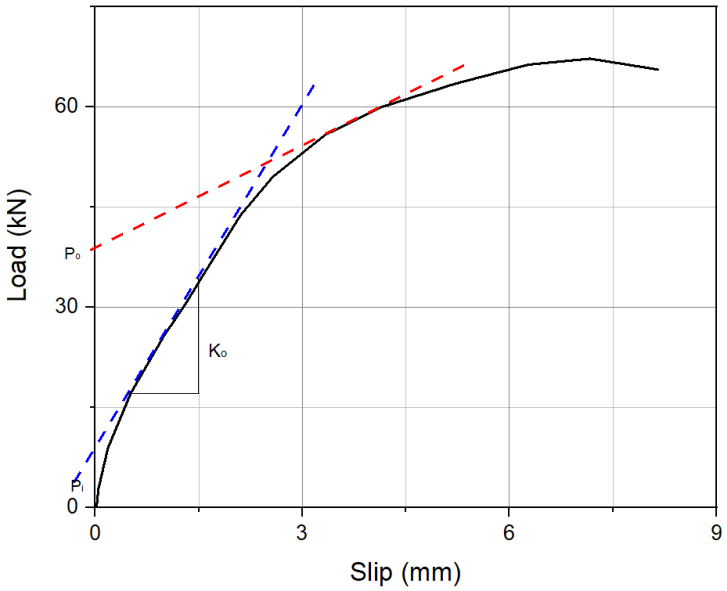

Figure 3.31: Stiffness parameters for load slip behaviour for modified Foschi formula

The calculated parameters from the average results of all the test series are presented in Table 3.14, and the predicted load-slip graphs using the modified Foschi formula are shown in Figure 3.32. As can be seen, the load-slip curves from the analytical equation have a good correlation with the mean of experimental results. The analytical prediction was capable of predicting the initial response and the non-linear behaviour after yielding the experimental load-slip curves. In table 3.14, P(s) from the modified Foschi curve is calculated as per Equation (3) and compared with corresponding P(s) values obtained from the tests. The accuracy of the predicted formula is more clearly seen from the comparison of actual failure load and predicted ultimate/failure load values. R-square values for the modified Foschi curve are also provided in Table 3.14. The values are greater than 0.91, meaning the predicted curves are more than 91% accurate, demonstrating a close agreement between the curve fit models and experimental results.

Table 3.14: Key parameters of modified Foschi formula for the tested CFS and plywood connections

Test series	P_i (kN)	P_o (kN)	P_{max} - P_i (kN)	K_0 (kN/mm)	P(s) test (kN)	P(s) formula (kN)	R^2
P-SDS	0	15	36	8.4	32.2	30.9	0.91
P-SDSa	2.4	22	30.4	80	34.6	32.8	0.95
P-CS	0	42.5	82	10	82.8	79.5	0.95
P-CSa	13	38	91	18	110	104	0.95
P-NB12	7	90	132	16	132	129	0.91
P-NB12a	10	110	145	19	140.8	144	0.93
P-NBW12	16	114	165	26	183.5	175	0.95
P-NBW8	2	30	65.9	9.5	67.6	65.2	0.93

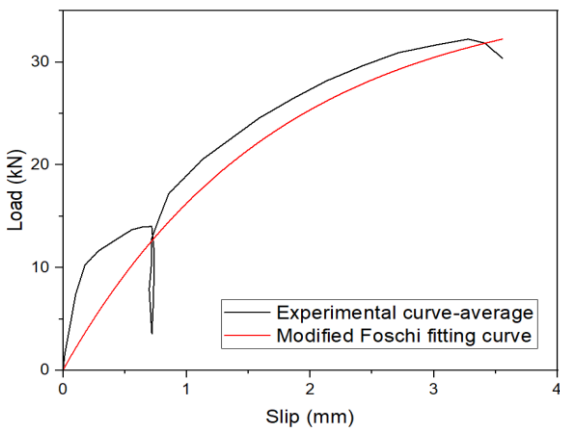

(a) Test series P-SDS

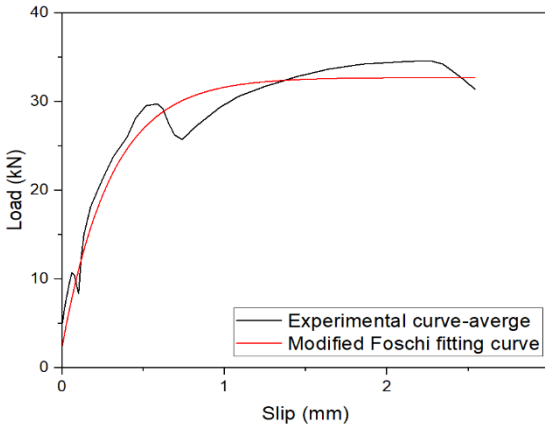

(b) Test series P-SDSa

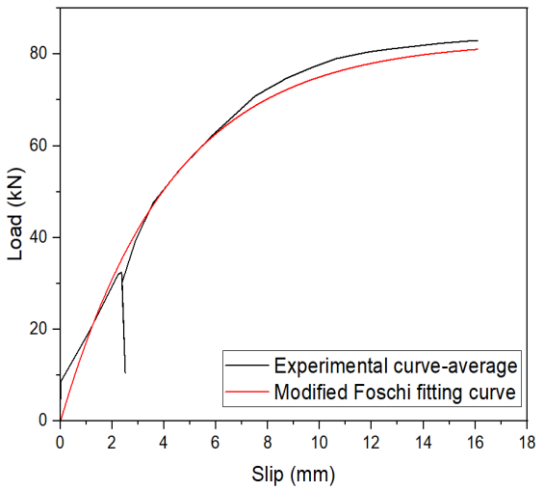

(c)Test series P-CS

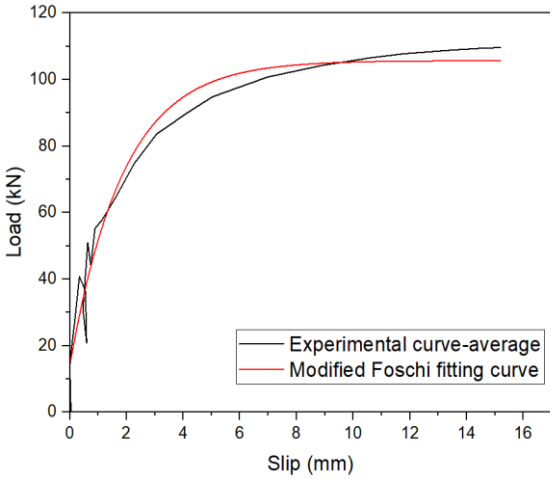

(d)Test series P-CSa

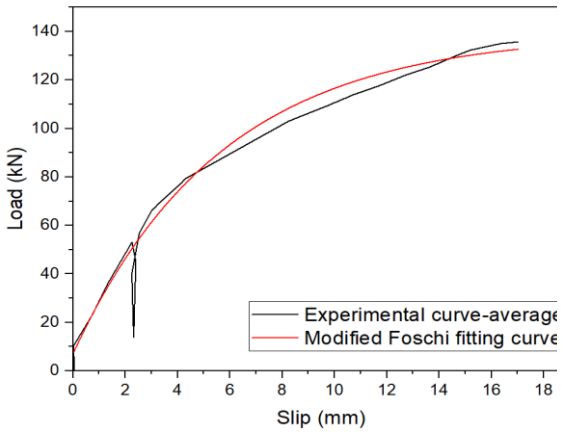

(e) Test series P-NB12

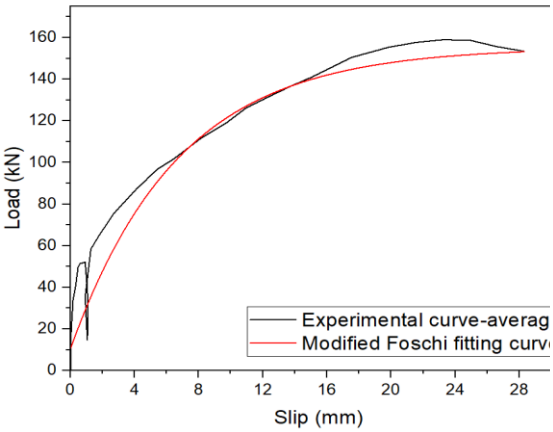

(f) Test series P-NB12a

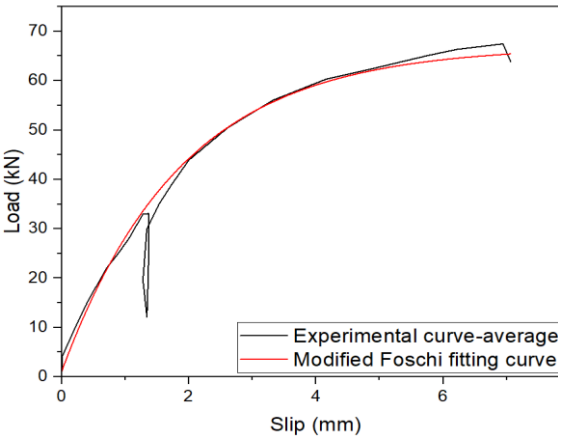

(g) Test series P-NBW8

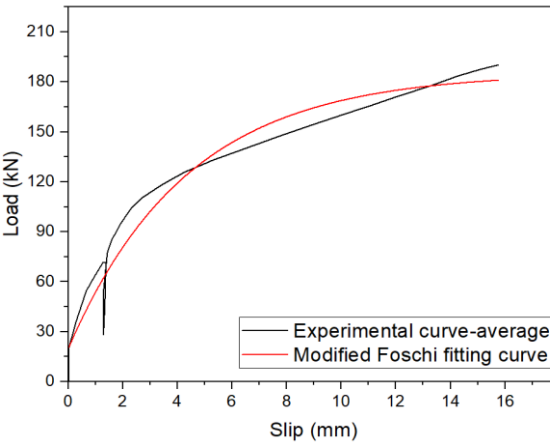

(h) Test series P-NBW12

Figure 3.32: Comparison between the analytical model and mean of experimental load-slip curves for CFS and plywood composite connections

3.6 Concluding Remarks

The ductility and stiffness of the shear connection play a crucial role in the load-carrying capacity of composite floors. As a result, static push-out tests on CFS and plywood connections were carried out on 24 specimens in this study. This chapter investigates and evaluates the load-slip behaviour and failure mode of CFS and plywood composite connections on eight different connection types. The effect of different fastener types (Self-drilling screw, coach screw, nut and bolt) with and without structural adhesives were investigated in terms of their load-slip response and ductility. As expected, composite connections with fasteners alongside adhesives performed better than the fastener alone. Among them, self-drilling screws with adhesive at the interface of the CFS joist and plywood panel (Test series: P-SDSa) demonstrated the highest serviceability, ultimate stiffness, and ductility. However, the load-carrying capacity of these connections was much lower than other connection types. Regarding the connection without adhesives, the M12 nut and bolt with washers (Test series: P-NBW12) had superior ductility and stiffness, among others. The load-carrying capacity of these connections was also higher than any other connection type. It was seen that using washers with bolts helped to take higher pre-tension force, which ultimately helped to improve the strength and stiffness of the fastener. M8 nut and bolt with washer (Test series: P-NBW8) and M12 nuts and bolts without washers (Test series: P-NB12) had similar results in terms of stiffness and ductility. The stiffness and ductility of M12 coach screw connections (Test series: P-CS) were the lowest among other connections, but the load-carrying capacity was higher than SDS and adhesive connections. And lastly, an analytical equation was formulated based on the Foschi formula to predict the load-slip

behaviour of the tested connections. The load-slip curves obtained from the analytical formula agreed with the response obtained from the physical tests.

Fasteners play a vital role in an efficient and economical design for the construction of lightweight composite flooring systems using cold-formed steel and plywood. The design of such flooring systems is governed by the ultimate limit state and serviceability limit state requirements. Just because large mechanical fasteners like M12 have higher stiffness and ductility does not mean they are the best choice as shear connections for composite CFS and plywood flooring systems. From the push-out tests carried out in this study, it was observed that the structural behaviour of the CFS-plywood joints with large mechanical fasteners (e.g. M12 nut and bolt, M12 coach screw) is primarily governed by the material yielding (e.g. plywood crushing, deformed CFS joist) rather than the strength and stiffness of fasteners. Hence based on the observation made on push-out test results, self-drilling screws and M8 nuts and bolts would make an ideal fit as mechanical fasteners for designing composite cold-formed steel and timber flooring systems. Moreover, using structural adhesives along with fasteners can enhance the strength and stiffness of the system.

4 Flexural Behaviour of Cold-Formed Steel and Timber Flooring System

4.1 Introduction

As discussed in the previous chapter, it has become apparent from the existing literature that only self-drilling screw was used as shear connectors in composite cold-formed steel and timber-based flooring systems. Hence to overcome the current knowledge gaps, there is a need to investigate the performance of different types of mechanical fasteners with higher ductility as shear connectors for this type of flooring system.

This experimental study aims to investigate the structural performance of a novel composite cold-formed steel and timber (CFST) floor module comprising a CFS C-section joist and structural plywood panel as floor sheathing. As discussed in the previous chapter, four types of shear connectors are used to fabricate the modular floor components by combining CFS C-section and structural plywood panels. The main advantage of these modular floor components is that they can be fabricated off-site and easily and quickly assembled on-site, which reduces the construction time that will effectively address the current housing demand. CFST flooring systems offer the advantage of a high strength-to-weight ratio and lead to less seismic and gravity load on the foundation of the buildings. CFST floor module can be easily and quickly fixed to the main structural steel beams using only bolts or screws with cleat brackets at the end of the joists. A typical reference construction system and assembly method of the CFST prefabricated floor components is shown in Figure 4.1. In this chapter, the flexural behaviour of the composite CFS C-section and structural plywood flooring system is

experimentally investigated. Four-point bending tests were conducted on thirteen composite beam specimens and one bare CFS system (used as a benchmark study for comparative purposes) as part of an experimental study. The main variables in the four-point bending tests was the shear connection between the CFS joists and plywood sheathing. The key results of the experimental testing are summarised herein this chapter. The ultimate loading capacity, flexural stiffness, cross-sectional strain distribution and failure mode of the composite beam is examined and discussed. The bending capacity and flexural stiffness of the considered composite CFST beams were theoretically calculated based on the plastic analysis approach to summarise the findings of the four-point bending tests.

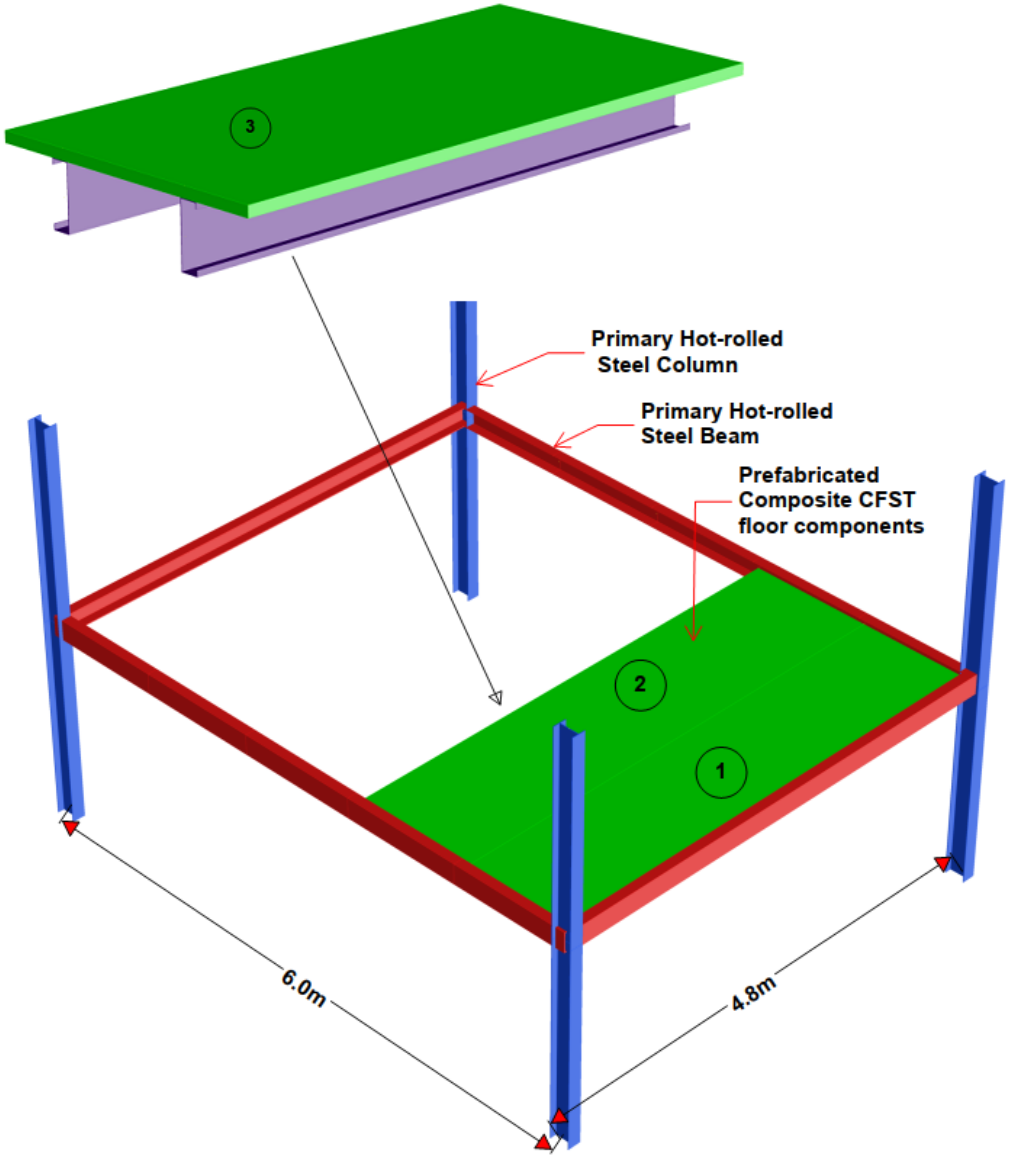

Figure 4.1: Typical reference construction system and sequence of assembly for prefabricated composite floor components

4.2 Experimental Investigation

4.2.1 Specimen Details

Thirteen 4-point bending tests were conducted on composite CFS and structural plywood flooring systems. Table 4.1 summarises tested composite systems with

different means of shear connections. 254mm deep and 2.4mm thick CFS C-sections were employed as floor joists with 45mm thick F11 grade structural plywood panels as sheathing. The reason for choosing 254mm deep, 2.4mm thick CFS C-section as a joist and 45mm thick plywood panel as floor sheathing for the construction of prefabriacated flooring system in this research study is considering the case of medium span floor in a residential building to satisfy the ULS and SLS requirements and the availability of the off-the-shelf product in the market for faster fabrications. CFS C-section and plywood panel material tests were conducted as per AS 1391:2007 (Standard Australia, 2007) and AS/NZS 2269.1:2012 (Standard Australia, 2012), respectively and the detailed description of the tests is provided in Chapter 3.

Table 4.1: Summary of full-scale specimen for four-point bending tests

Specimen	Web hole in joist	Type of shear connection	Spacing of shear connection	Structural adhesive at the beam-board interface
SP-1[a]	No	NA	NA	NA
SP-2	No	Self-drilling screw	400	No
SP-3	No	Self-drilling screw	200	No
SP-4	No	Self-drilling screw	400	Yes
SP-5	No	M 12 Coach screw	400	No
SP-6	No	M 12 Coach screw	200	No
SP-7	No	M12 nut and Bolt	400	No
SP-8	No	M12 nut and Bolt	800	No
SP-9	No	M12 nut and Bolt	800	Yes
SP-10	No	M8 nut and Bolt	200	No
SP-11	No	M8 nut and Bolt	400	No
SP-12	Yes	M12 nut and Bolt	800	No
SP-13	Yes	M 12 Coach screw	200	No

SP-14	No	M12 Coach screw	400	Yes

A bare CFS system was also tested to provide a benchmark response for which the remaining composite systems could be compared. For all the specimens, adhesives were applied at the joints between adjacent plywood panels, as shown in Figure 4.2.

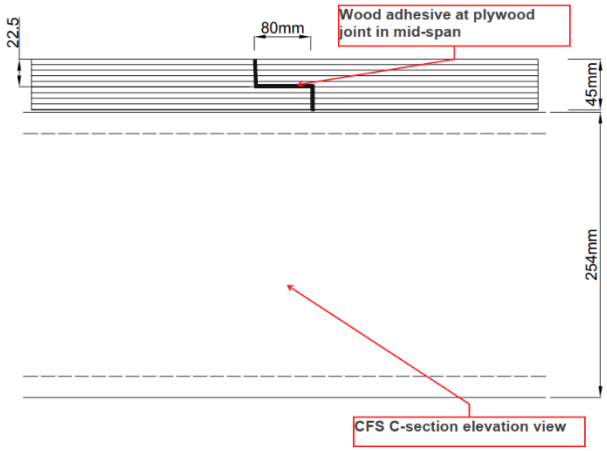

Figure 4.2: Typical plywood joint details

4.2.2 Test Setup and Procedure

The overall test layout for all beam tests is shown in Figure 4.3. All the tested composite beams consist of two CFS joists, back to back faced 600mm apart, and were connected to plywood floor sheathing with different means of shear connection and various spacings. For the bare CFS system, 50x50x3 mm equal steel angles were used to restrain the top flanges of the two joists, as depicted in Figure 4.4. The beams were supported simply on pin and roller across a 4.5m span with a 100mm overhang from each support. A spreader beam was used to transfer the load from the loading jack through load-bearing spherical to two loading beams running across the width of the plywood. The spherical bearings

have a concave spherical surface in the housing washer that matches a convex surface on the shaft washer. They can primarily withstand axial and combined axial and radial loads; therefore, no axial force would be applied to the beam. Longitudinal slips at the ends of the beams were measured using four LVDTs at each end, whereas the vertical deflection at the midspan of the beam was recorded using string potentiometers beneath each CFS joist. Strain gauges were fixed along the height and width of the midspan cross-section to take the readings of strain distribution during the testing and, ultimately, to locate the position of neutral axes through the depth of composite sections. Figures 4.5 and 4.6 illustrate the employed instrumentation for all the bending tests. The CFS joist's webs were stiffened locally at supports and loading points using 12mm thick (Grade 350) steel plates on either side, held in place by M16 (Grade 8.8) through rods. This was done to avoid the localised failure of the CFS web and to assist in equal loading distribution by preventing any possible twisting.

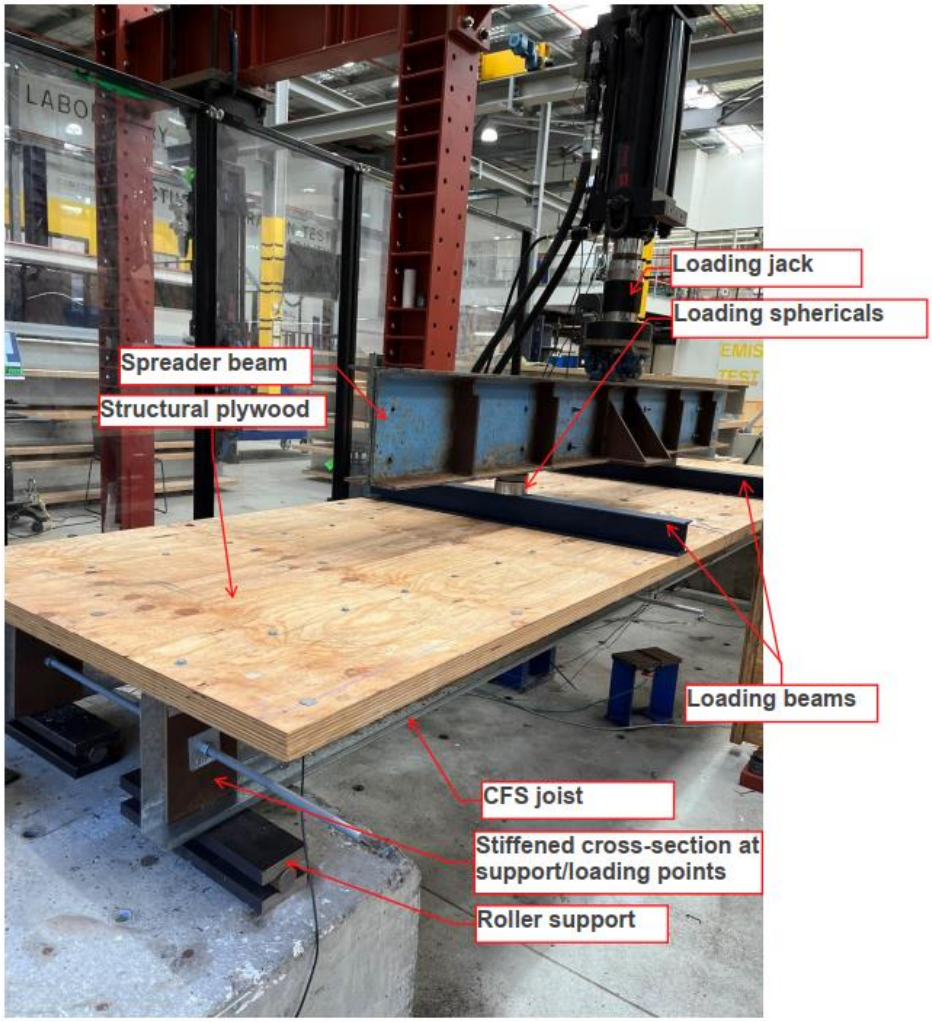

Figure 4.3: Four-point bending test layout of composite beam tests

The load was applied using a single hydraulic actuator (MTS 201.35) connected in a closed loop PID control system (MTS FlexTest 60), utilising a customisable portal load frame and concrete support blocks. The single actuator utilised suitably stiff spreader beams with suitable connections to apply two line loads across the deck at 1/3rd and 2/3rd spans of equal loads. Data were acquired utilising a NI PXIe-1083 chassis with PXIe-4330 modules and a single PXIe-4302 module. Flexlogger was used for acquiring the test data at a rate of 100Hz. All sensors were internally calibrated before testing. All the tests were conducted in the displacement control condition and statically loaded to obtain the ultimate

bending load. Each specimen was loaded up to 10% of the estimated ultimate load to ensure the correct functioning of the instrumentation and settling of the specimen. Afterwards, the load was gradually applied to failure at a 1mm/min displacement rate.

Figure 4.4: Overall test layout of bare CFS beam tests

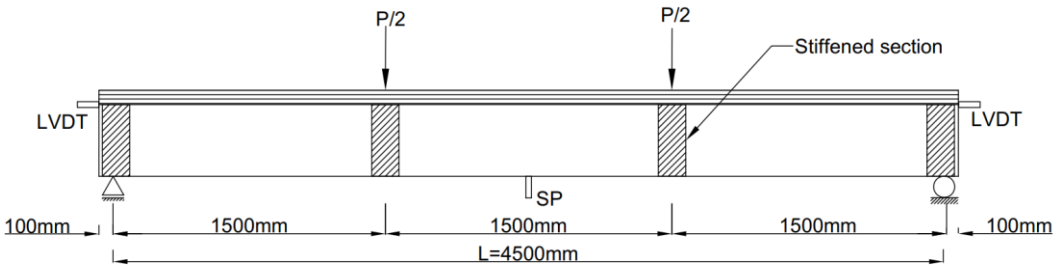

Figure 4.5: Arrangement of instrumentation for composite beam tests

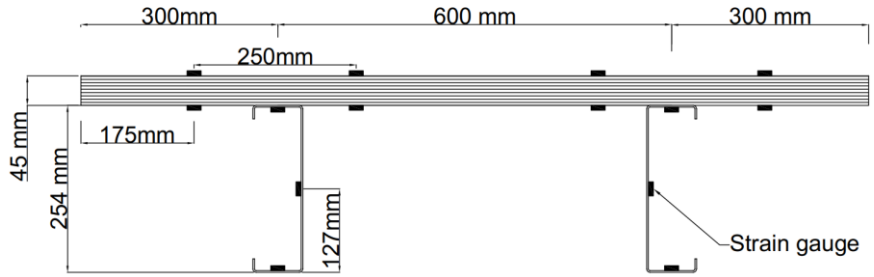

Figure 4.6: Arrangement of instrumentation for composite beam tests

4.2.3 Test Results

A total of thirteen,1.2m x 4.5m, prefabricated composite cold-formed steel and plywood flooring systems were tested in bending to investigate the flexural strength and stiffness resulting from composite action that arises between the interface of CFS joist and plywood due to the use of various fasteners. Two distinctive failure characteristics were observed in the tests. The specimens with 400mm and 800mm fastener spacing exhibited distortional buckling of the top flange of the CFS joist between the fixings in the constant moment region, as shown in Figure 4.7. In contrast, the specimens with 200mm spacing (namely

SP-3, SP-6, and SP-10) exhibited bending due to the rotation in the bottom flange of the CFS joist near the supports. This failure mode is depicted in Figure 4.8.

Figure 4.7: Distortional buckling between fixings in the constant moment span (Specimen SP-11)

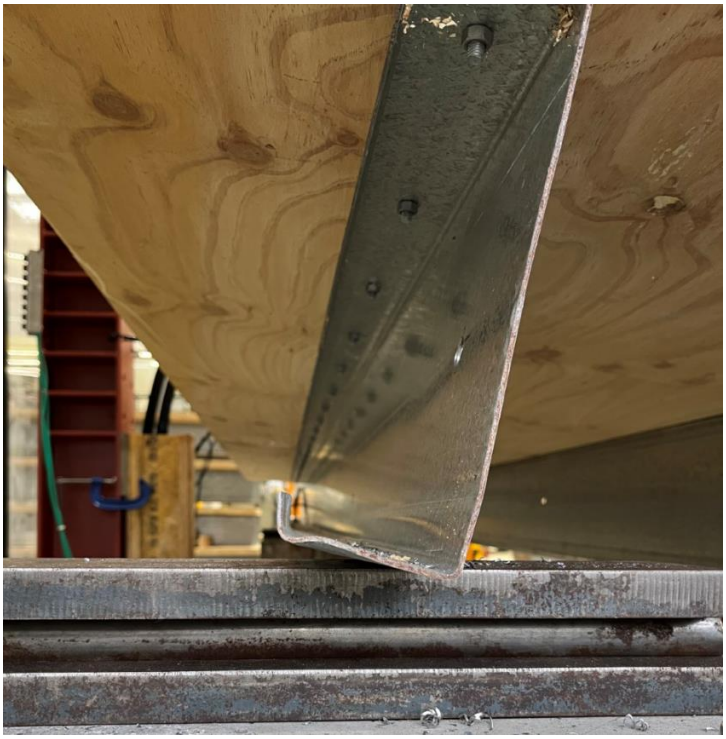

Figure 4.8: Bottom flange rotation and bending near the supports (Specimen SP-10)

It is obvious that the specimens with 200mm fastener spacing are stronger and stiffer than their 400mm spacing counterparts; hence the specimens with 200 mm spacing demonstrated the tensile yielding of the bottom flange near the supports, concluding that the yield strength of the CFS joist governed the ultimate capacity of SP-3, SP-6, and SP-10. It was observed in almost all the specimens that by reducing the fastener spacing, the position of the neutral axis moved toward the top of the section due to the increasing degree of shear connection. The key results of the specimens with different shear connectors are tabulated in the below sub-sections, in which M_u is the moment capacity, δ_u is the average vertical midspan deflection at ultimate load, S_u is the average slips at the ends of the beam at ultimate load, and EI is the flexural stiffness of the composite beam.

4.2.3.1 Connection with Self-Drilling Screws

The key results of composite beam tests with SDS as shear connectors are provided in Table 4.2. Figure 4.9 depicts the load-deflection responses of the specimens with 6mm diameter self-drilling screws. SDS at 400 mm centres and glue at the interface exhibited 10% higher moment capacity and flexural stiffness than SDS at 400 mm centres only. However, SDS at 200 mm centres has a 20% higher moment capacity than 400 mm centre screws. The cross-section strain distribution through the depth of specimens SP-3 and SP-4 at the mid-span is illustrated in Figure 4.10.

Table 4.2: Key results of four-point bending tests of a composite beam with self-drilling screws as shear connectors

Specimen	M_u (kN.m)	EI (N.m^2)	δ_u (mm)	S_u (mm)
SDS at 200	52.5	2.65x10^6	43.6	2.6
SDS at 400	42.9	2.5x10^6	36.5	2.4
SDS at 400+glue	47	2.83x10^6	36.6	1.9

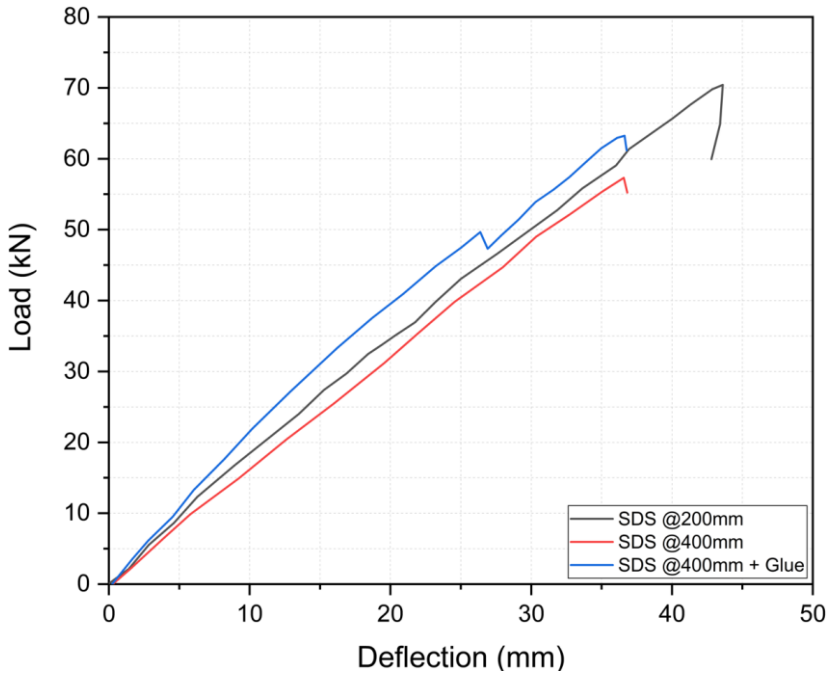

Figure 4.9: Load deflection curves of the full-scale specimens with self-drilling screws (SDS)

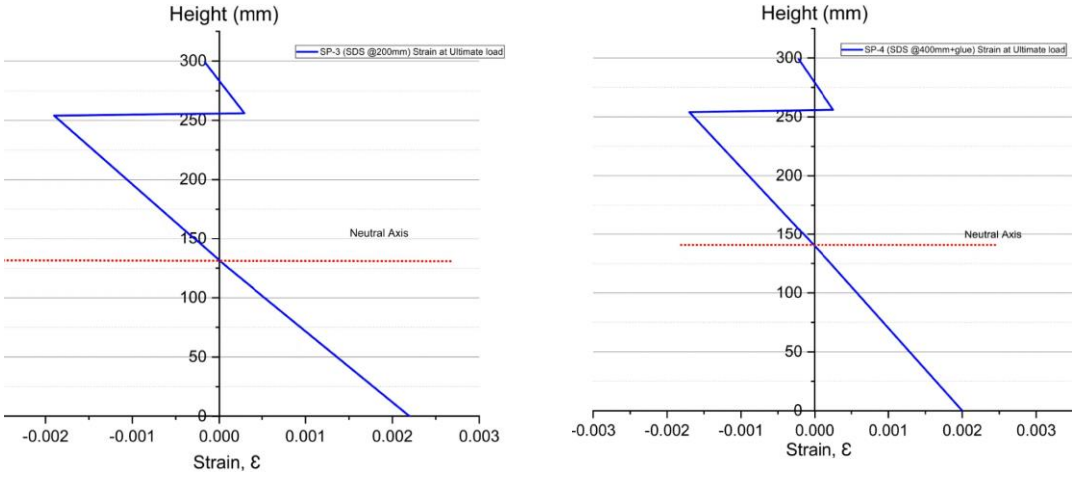

(a) (b)

Figure 4.10:Strain distribution at mid-span section of specimens: (a) SP-3 (SDS @200mm) ; (b) SP-4 (SDS @400+Glue)

4.2.3.2 Connection with Coach Screws

The load-deflection curves of the composite beam specimens with 12mm diameter coach screws are shown in Figure 4.11. As can be seen, four specimens with different spacings and arrangements were tested. The key results of the specimens with M12 coach screws as shear connectors are tabulated in Table 4.3. Failure of all specimens ultimately was governed by the yield strength of the CFS joist. Connections with coach screws at 400 mm centres with and without glue have similar loading capacities. The specimen with glue at the interface demonstrated 15% higher stiffness up to serviceability load, and after that, the stiffness of both specimens was similar. The sudden drop in the load-deflection response of the glued sample is because of the brittle failure of the adhesive bond on each joist and plywood interface, and afterwards, the coach screw started to take the flexural load. The specimen with coach screws at 200mm centres showed only 4% higher moment capacity but 15% higher flexural stiffness than

those with coach screws at 400 mm spacing. The distribution of strain through the depth of specimens at the mid-span is shown in Figure 4.12.

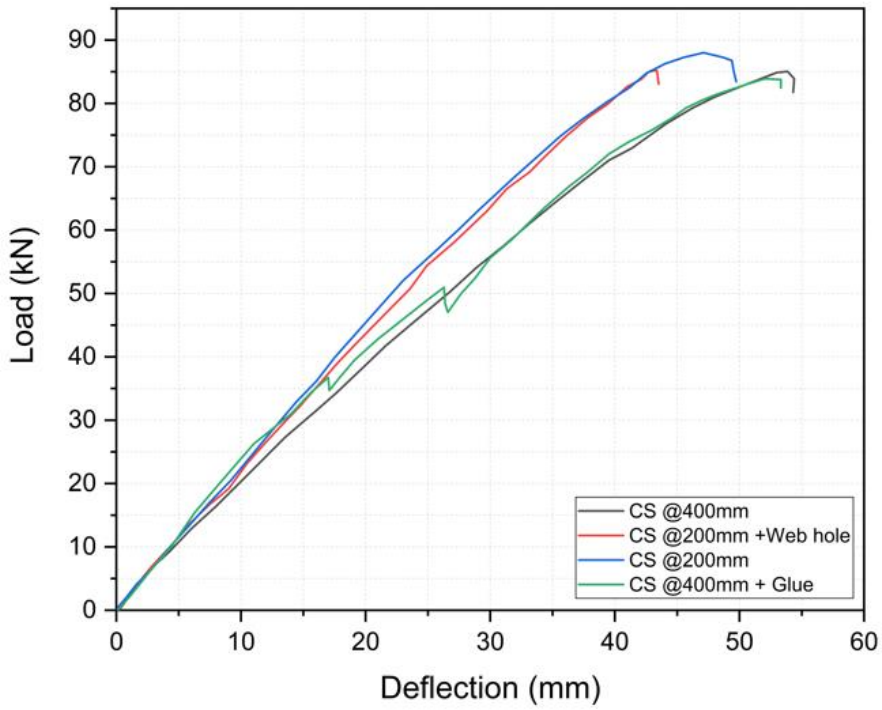

Figure 4.11: Load deflection curves of the full scale specimens with M12 coach screws (CS)

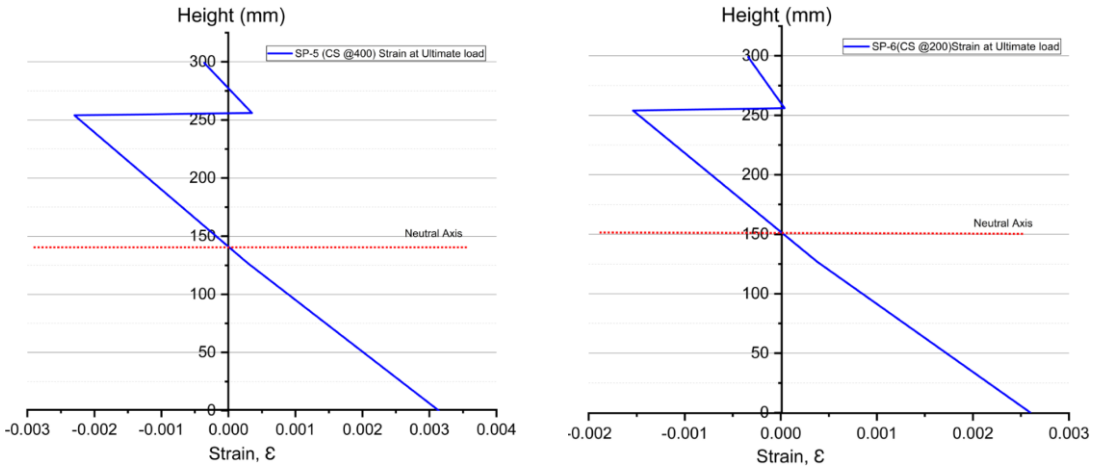

(a) (b)

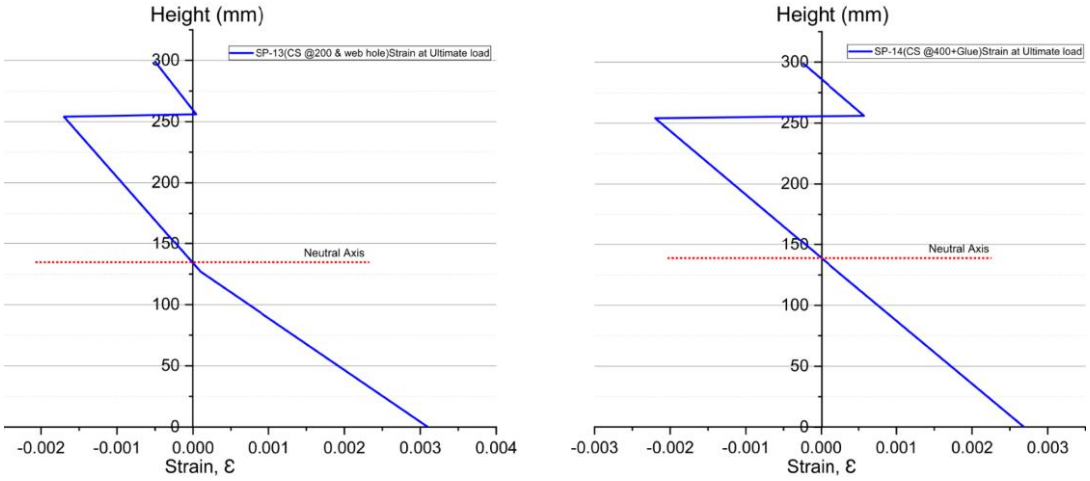

(c) (d)

Figure 4.12: Strain distribution at midspan section of specimens: (a) SP-5 (CS @400mm) ; (b) SP-6(CS @200); (c) SP-13 (CS @200+webhole); (d) SP-14 (CS @400+Glue)

Table 4.3: Key Results of Four-point Bending Tests of a composite beam with coach screws as shear connectors

Specimen	M_u (kN.m)	EI (N.m^2)	δ_u (mm)	S_u (mm)
CS at 200	66	3.23x10^6	47.11	2.05
CS at 400	63.6	2.78x10^6	53.86	3.6
CS at 400+glue	62.9	2.83x10^6	52	2.2
CS at 200, and web holes in CFS joist	64.5	3.2x10^6	44	1.99

4.2.3.3 Connection with M8 Nuts and Bolts

The load-deflection responses of the composite beam specimens with M8 nuts and bolts are shown in Figure 4.13. The specimen with 200 mm spacing

demonstrated minimal enhancement in the ultimate strength and stiffness, which is only 6 % and 5 % higher than 400 mm spacing. The moment capacity Mu, average vertical mid-span deflection δ_u, average slip S_u, and flexural stiffness EI are presented in Table 4.4. It can be observed that with an increasing degree of shear connection, the neutral axis position in the CFS joist moved toward the top of the section, as can be seen in Figure 4.14.

Table 4.4: Key Results of Four-point Bending Tests of a composite beam with m8 nut and bolts as shear connectors

Specimen	M_u (kN.m)	EI ($N.m^2$)	δ_u (mm)	S_u (mm)
M8-NB at 200	64.35	$2.99x10^6$	53	3.2
M8-NB at 400	60.75	$2.82x10^6$	52.2	3.9

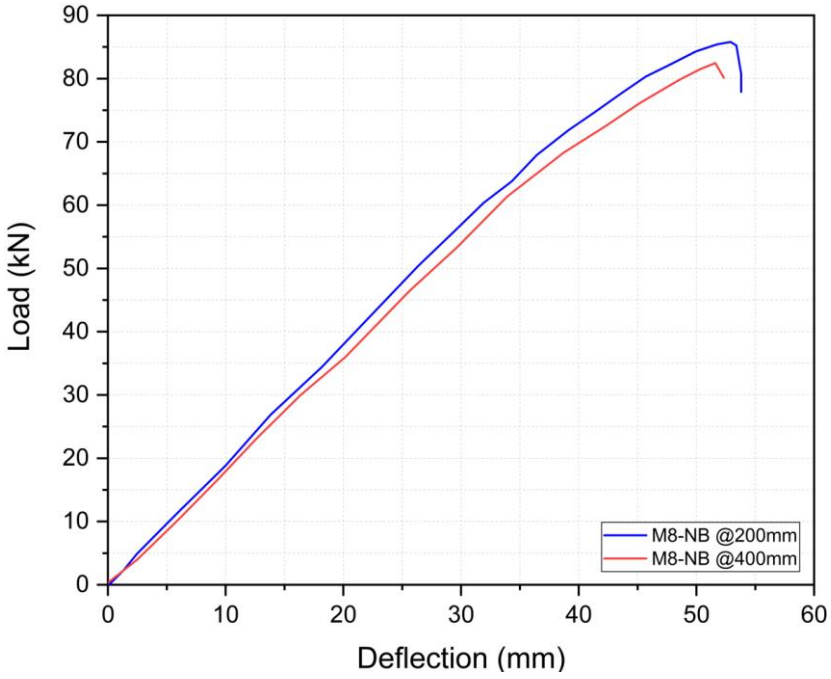

Figure 4.13: Load deflection curves of the full scale specimens with M8 nuts and bolts

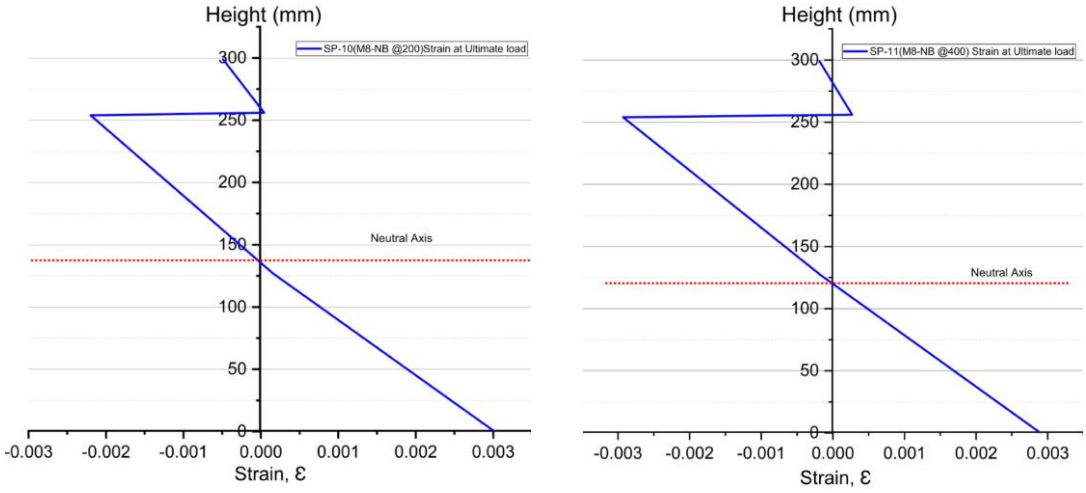

(a) (b)

Figure 4.14:Strain distribution at mid-span section of specimens: (a) SP-10 (M8-NB @200mm) ; (b) SP-11 (M8-NB @400)

4.2.3.4 Connection with M12 Nuts and Bolts

Four specimens with different shear connection arrangements were tested, and the load-deflection histories and cross-section strain distribution of all the tested specimens are presented in Figures 4.15 and 4.16, respectively. From the push-out tests described in Chapter 3, it was understood that M12 nuts and bolts provide the most ductile and stiffest shear connections compared to other fasteners; hence 400 mm and 800mm fastener spacing was chosen for this composite floor assembly. 400 mm nuts and bolts spacing achieves 20% higher moment capacity and 11% higher stiffness than 800 mm spacing. The influence of structural adhesives for the 800 mm spacing on the stiffness was only 5%, but the strength capacity was enhanced by 10%. The key results of the specimens with M12 nuts and bolts as shear connectors are given in Table 4.5.

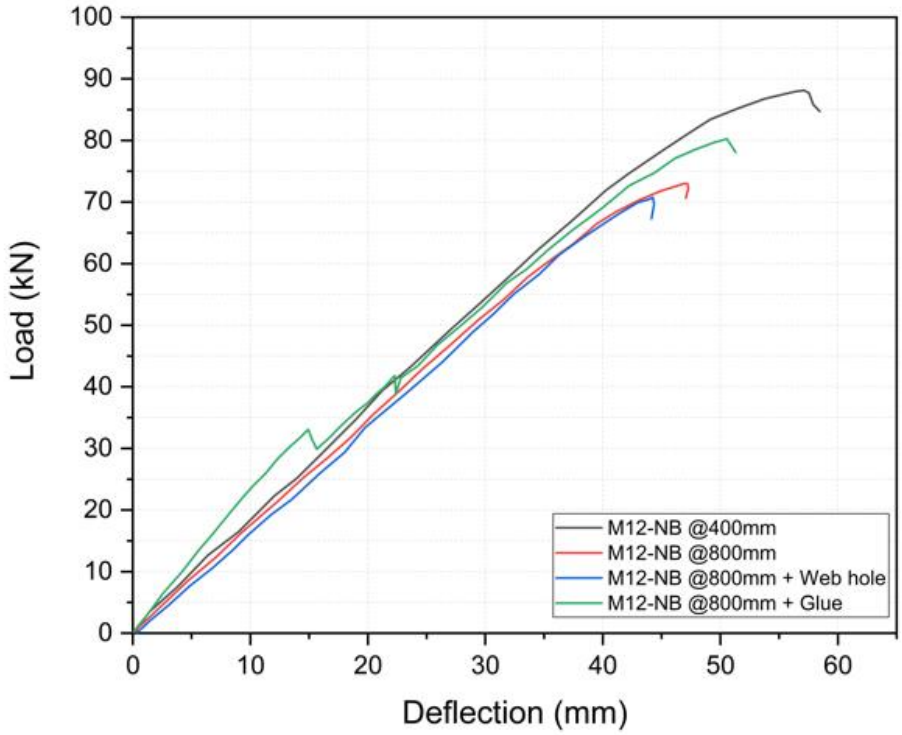

Figure 4.15: Load deflection curves of the full-scale specimens with M12 nuts and bolts

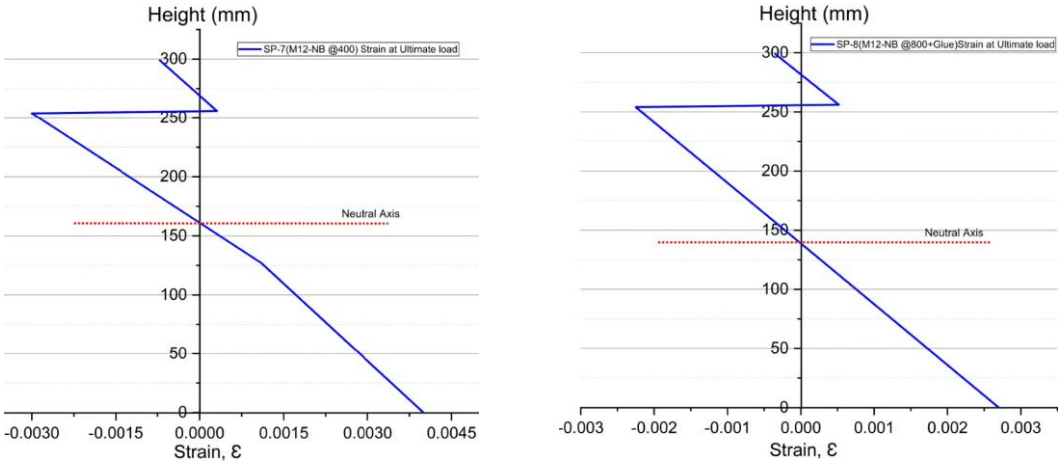

(a) (b)

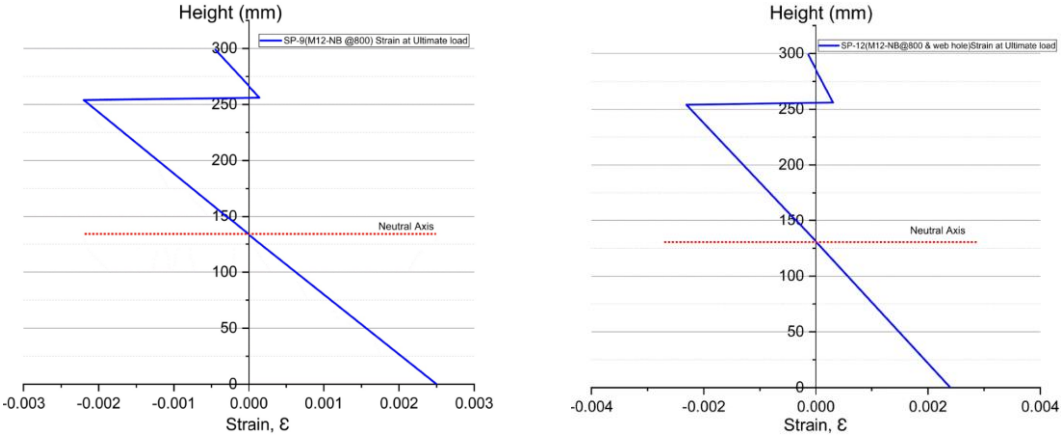

(c) (d)

Figure 4.16: Strain distribution at the mid-span section of specimens: (a) SP-7 (M12-NB @400mm) ; (b) SP-8(M12-NB @800+Glue); (c) SP-9 (M12-NB @800); (d) SP-12 (M12-NB @400+webhole)

Table 4.5: Key results of four-point bending tests of a composite beam with M12 nut and bolts as shear connectors

Specimen	M_u (kN.m)	EI (N.m^2)	δ_u (mm)	S_u (mm)
M12-NB at 400	66.05	2.87x10^6	57.1	4
M12-NB at 800	54.1	2.62x10^6	46.8	4.79
M12-NB at 800 + web hole in CFS joist	53.25	2.65x10^6	44.2	4.35
M12-NB at 800+Glue	60	2.7x10^6	50.5	4.15

4.3 Summary of Experimental Findings

One of the main purposes of this study was to experimentally investigate the shear connector's performance of different fastener types on the structural behaviour of composite cold-formed steel and timber flooring systems. Hence in this section, more comparative findings are discussed. Figure 4.17 shows the

load-deflection histories of composite specimens that utilise self-drilling screws, M12 coach screws, M8 nuts and bolts, and M12 nuts and bolts as shear connectors at 400 mm spacings compared with bare CFS beam. The moment capacity was increased by 7%, 60%, 56%, and 58% for the composite specimens with SDS, M12-CS, M8-NB, and M12-NB, respectively, compared to the bare CFS joist alone. Figures 4.18 and 4.19 display the maximum moment capacity and flexural stiffness of each specimen, normalised by the moment capacity, M, and flexural stiffness, EI, of the corresponding CFS beam. As expected, all the tested specimens exhibited composite action phenomena and improved strength and stiffness capacities. As seen from the bar charts in Figure 4.18 and Figure 4.19, the spacing of the fasteners and the application of structural adhesives at the CFS joist and plywood interface were found to have improved performance at the moment capacity and flexural stiffness of these lightweight flooring systems. It was also observed that the presence of unstiffened web holes does not have any influence on the flexural performance of these flooring systems.

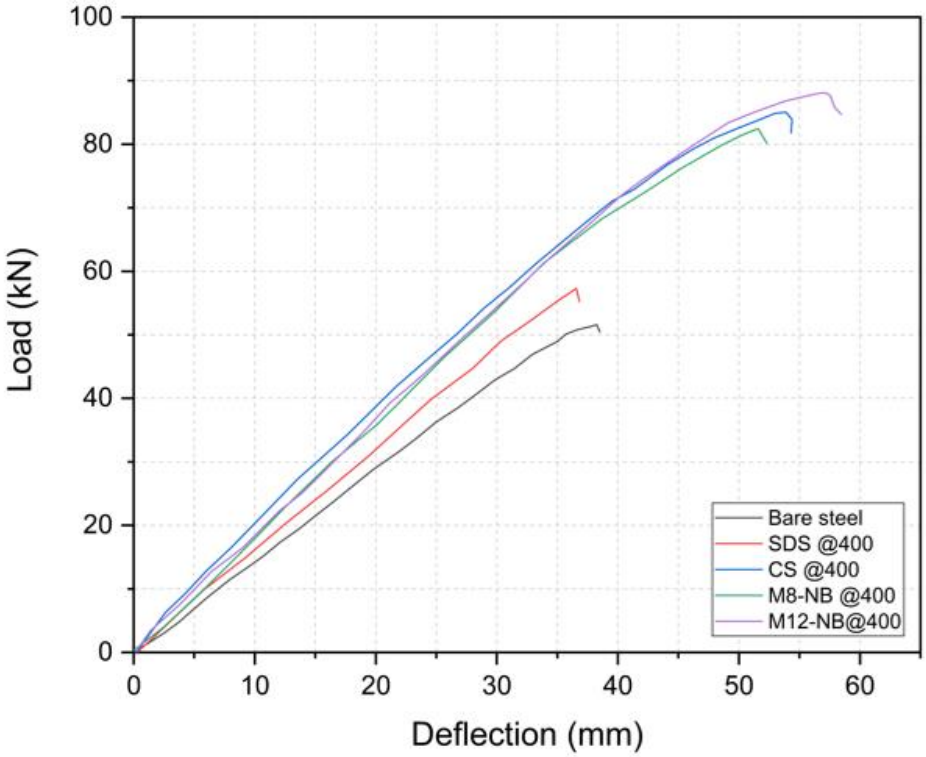

Figure 4.17: Load deflection curves comparison of bare CFS with composite beams

For ductile connections like the M12 coach screws and M12 nuts and bolts at 400mm spacing, the moment capacity was significantly enhanced (by more than 50%), and flexural stiffness was improved by 19% and 22% only. However, for the M12 coach screw at 200 mm spacing, the flexural stiffness was found to be increased by 40%, but the moment capacity was similar to that of 400 mm spacing. Hence from this observation, it has become clear that there is a trade-off between the ductility and spacing of shear connectors with the yield strength of the CFS joist in these flooring systems.

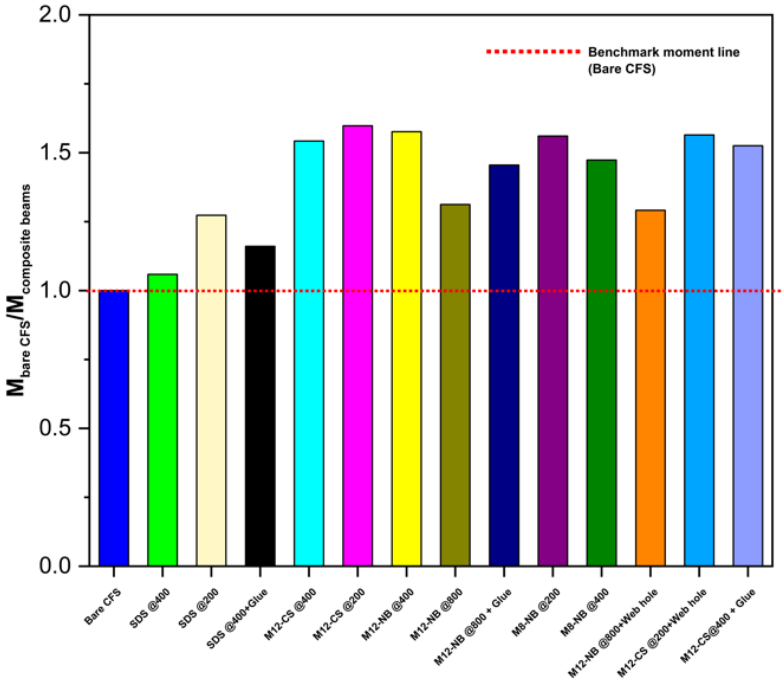

Figure 4.18: Enhancement in moment capacity of the composite systems in comparison with bare CFS system

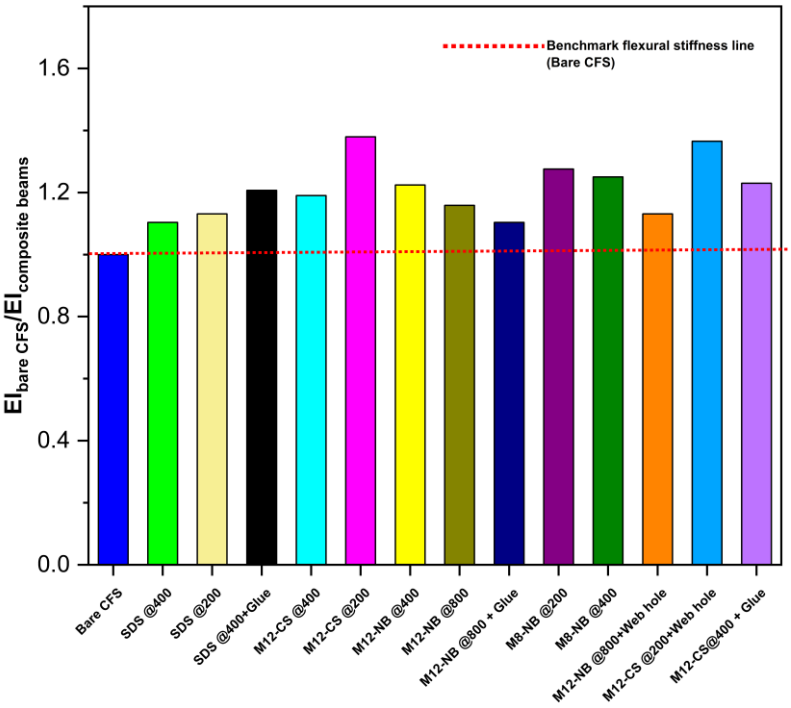

Figure 4.19: Enhancement in flexural stiffness of the composite systems in comparison with bare CFS system

4.4 Plastic Analysis of Results

Following the fundamental principle as per Clause 3.5.8 of AS/NZS 2327 (Standard Australia, 2017), to provide composite action phenomenon, shear connectors shall be capable of transmitting the longitudinal shear force between the floorboard sheathing and the CFS joist without causing crushing or any damage to the plywood and without allowing excessive slip or vertical separation between plywood and CFS joist. It is crucial to consider the slip between the two members to predict the ultimate moment capacity and deflection of the composite cold-formed steel and timber flooring system. To achieve the full shear interaction, the number of shear connectors provided should be such that the full plastic bending resistance can be achieved with the material strengths exploited to their greatest extent (Couchman, 2016; Kyvelou et al., 2017a).

4.4.1 Theoretical Plastic Bending Resistance and Flexural Stiffness Assuming Full Shear Interaction

The theoretical plastic bending resistance of the composite section can be determined considering full composite action between the plywood panel and CFS joist with the plastic distribution of stresses. Two possible scenarios are considered; Figure 4.20 illustrates the case where the plastic neutral axis (PNA) lies within the plywood panel, and Figure 4.21 illustrates the case where PNA lies within the steel section.

For the scenario shown in Figure 4.20, the force equilibrium can be expressed as:

$$N_S + N_{p,t} = N_{p,c} \tag{4.1}$$

$$A_S F_y + A_{pt} F_{tp} = A_{pc} F_{cp} = b_{eff} t_a F_{cp} \tag{4.2}$$

Where A_s is the area of the CFS section, F_y is the yield strength of CFS, F_{tp} and $F_{cp}$are the tensile and compressive strength of the plywood, respectively, b_{eff} is the effective width of plywood sheathing (taken as 600 mm). The plastic moment capacity of the composite section (about the axis of the compressive force $N_{p,c}$) can be calculated as:

$$M_{pl} = N_s Z + N_{p,t}\frac{t_p}{2} \quad (4.3)$$

In which $$Z = h - t_a/2 - y_c \quad (4.4)$$

Where h is the height of the composite section, and y_c is the distance from the bottom flange to the centroid of the steel section.

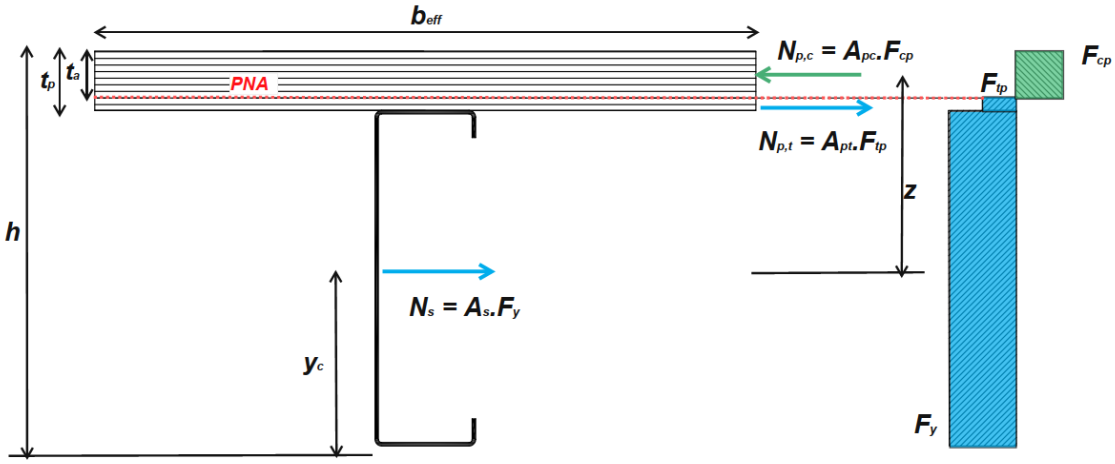

Figure 4.20: Distribution of plastic stress with the neutral axis in the floorboard sheathing

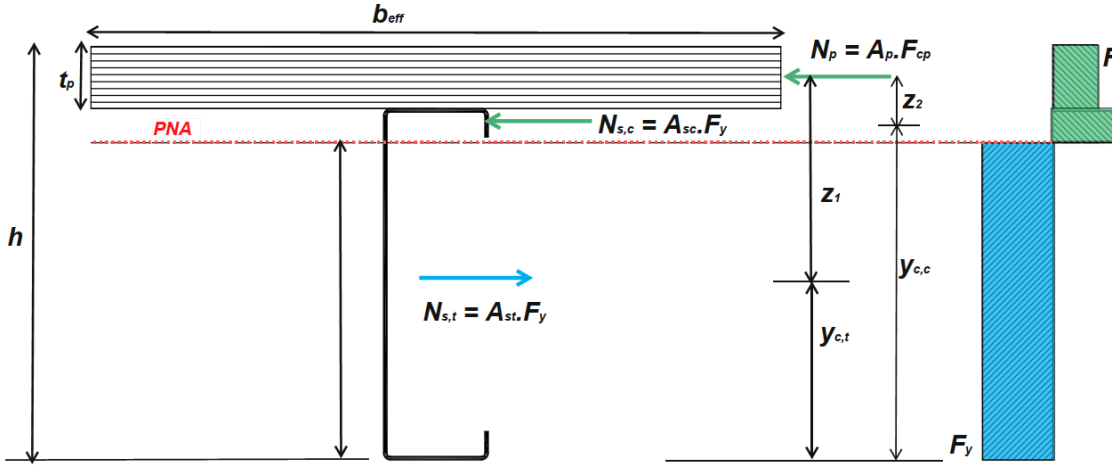

Figure 4.21: Distribution of plastic stress with the neutral axis in the CFS joist

For the scenario illustrated in Figure 4.21, the force equilibrium can be expressed as:

$$N_{st} = N_{sc} + N_p \tag{4.5}$$

$$A_{st}F_y = A_{sc}F_y + A_pF_{cp} \tag{4.6}$$

Where A_{st} and A_{sc} are the areas of the steel section in tension and compression respectively, A_p is the area of the plywood sheathing. The plastic moment capacity of the composite section (about the axis of the compressive force $N_{p,c}$) can be calculated as:

$$M_{pl} = N_{s,t}z_1 - N_{s,c}z_2 \tag{4.7}$$

$$z_1 = h - y_{c,t} - t_p/2 \tag{4.8}$$

$$z_2 = h - y_{c,c} - t_p/2 \tag{4.9}$$

Where z_1 is the distance between the centroid of the steel section to the centroid of plywood, z_2 is the distance between the bottom fibre of the plywood to the centroid of the plywood, $y_{c,t}$ and $y_{c,c}$ are the distances from the lower extreme

fibre of the steel section to the centroids of the portions of the steel section in tension and compression, respectively.

Hence, assuming a full shear connection for the tested composite system, the plastic compressive force in the plywood sheathing was calculated to be N_p = 756 kN. Since the compressive force of plywood (756 kN) is greater than the tensile force in steel beam (A_{st} x F_y = 550 kN); hence theoretical plastic neutral axis lies in the plywood sheathing. The plastic moment capacity of the tested composite system was calculated as M_{pl}= 81.46 kN.m using the force equilibrium expression as shown in Figure 4.20 and Equation (4.1) to (4.4).

The stiffness of the composite system is determined by transforming the area of plywood sheathing into an equivalent area of steel, as demonstrated in Figure 4.22.

$$I_{comp} = I_s + \frac{b_{eff} t_p^3}{12n} + A_s(y_{el} - y_c)^2 + \frac{A_p}{n}\left(y_{el} - h - \frac{t_p}{2}\right)^2 \qquad (4.10)$$

Where, $I_s$and A_s are the second moment of area and area of the steel section, A_p is the area of plywood, and n is the ratio of elastic moduli of steel to plywood. y_{el} is the distance from the bottom flange of the steel to the centroid of the composite section and is determined from Equation (11).

$$y_{el} = \frac{y_c A_s + \frac{A_p}{n}\left(h_s + \frac{t_p}{2}\right)}{A_s + \frac{A_p}{n}} \qquad (4.11)$$

For the composite beam examined in this project, using Equations (10) and (11), the second moment of area I_{comp} is determined to be 22.9x10^6 mm^4.

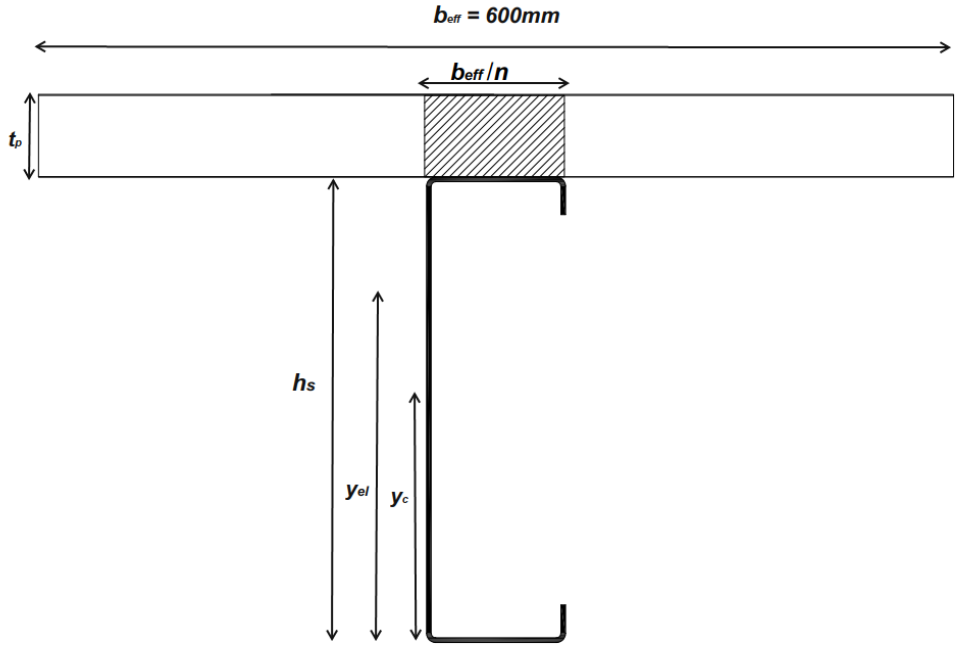

Figure 4.22: Transformed section for the determination of stiffness of the composite system

4.4.2 Comparison of Experimental Results With Full Composite Plastic Bending Capacity and Flexural Stiffness

The ultimate moment capacity $M_{u,exp}$ and flexural stiffness $(EI)_{exp}$ of each of the examined composite beams normalised by theoretical plastic moment capacity $M_{pl,r}$ and flexural stiffness $(EI)_{comp}$ of the fully composite system are presented in Figures 4.23 and 4.24, respectively. The specimen with superior ductile connections like the M12 coach screw or M12 nut and bolt demonstrated higher strength and stiffness than others by attaining around 80% of the plastic moment capacity and 70% of the flexural stiffness of the fully composite system.

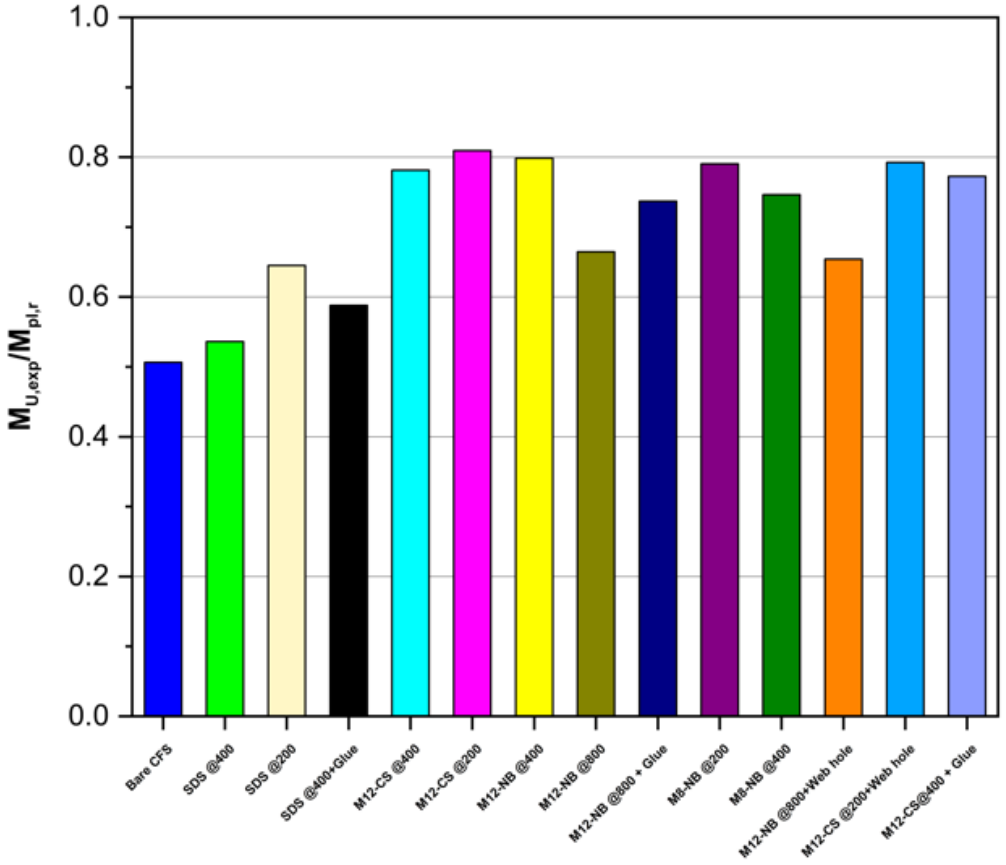

Figure 4.23: Moment capacity of the composite systems relative to the corresponding theoretically fully composite system

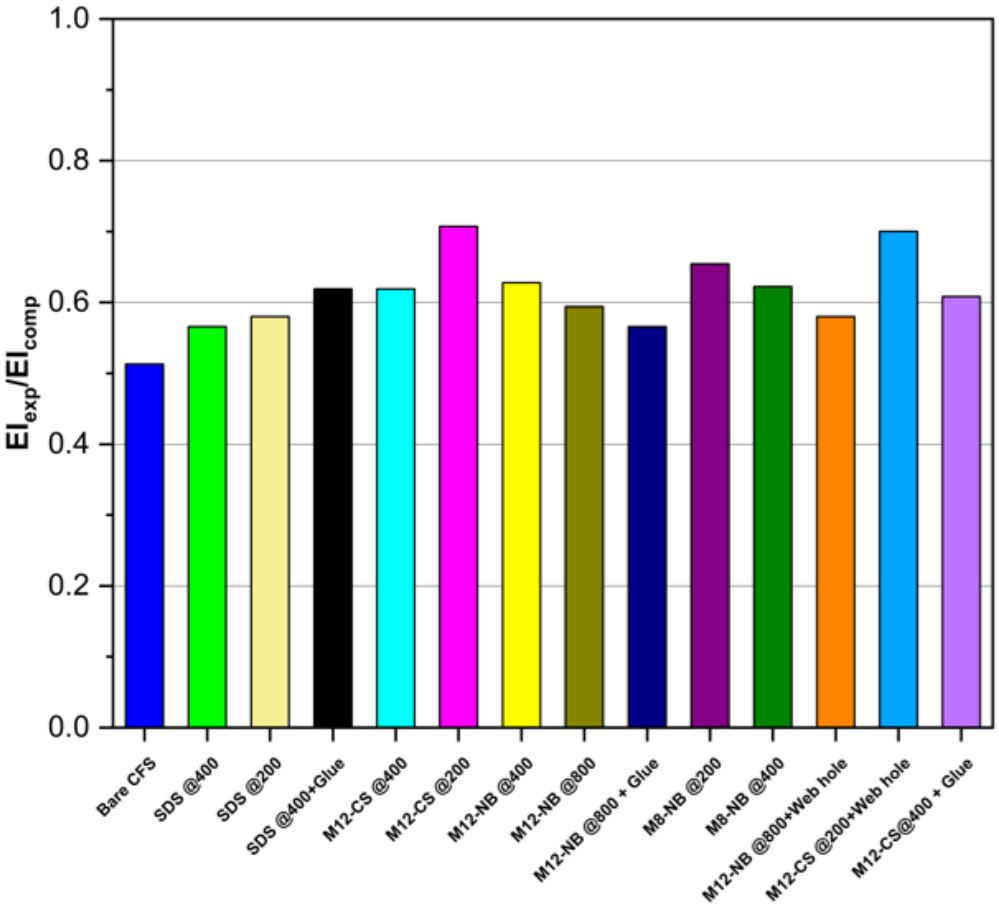

Figure 4.24: Flexural stiffness of the composite systems relative to the corresponding theoretically fully composite system

4.5 Concluding Remarks

The experimental results of 13 full-scale composite CFST beams using cold-formed steel C-section sheathed with structural plywood panels are presented in this chapter. This investigation aimed to explore the feasibility of composite action using four types of shear connectors with cold-formed steel flooring systems and to quantify the benefits derived from composite action. This study found significant improvements in the structural performance of cold-formed steel flooring systems by utilising the shear interaction between the steel section and

timber-based floor sheathing. The ductility of fasteners and their spacing were found to have a substantial impact on the moment capacity and flexural stiffness of these systems. Up to a 40% increase in flexural stiffness was observed in the composite system compared to the bare steel system.

In comparison to the bare CFS joist alone, the moment capacity for the composite CFST systems with 400mm fastener spacing was found to be increased by 6%, 47%, 54%, and 58% with SDS, M8 nuts and bolts, M12 coach screws and M12 nuts and bolts, respectively. Similarly, for the composite CFST system with 200mm fastener spacing, the moment capacity was enhanced by 27%, 56% and 60% for SDS, M8 nuts and bolts, and M12 coach screws. For stiffer connections like nuts and bolts and coach screws, the influence of fastener spacing on the moment capacity and flexural stiffness was not of too much difference as, in such cases, the capacity was found to be governed by the material strength of CFS or timber sheathing in comparison with the ductility of shear connectors.

Modular and prefabricated construction systems are a potential substitute for the fast construction of multi-story residential buildings. Pursuing a more sustainable built environment has recently prompted the construction industry to develop energy-efficient systems. Buildings should substantially decrease the amount of energy consumed throughout their life cycle, as well as the associated emissions of CO_2 into the environment. This chapter has highlighted that using innovative construction techniques can assist with sustainability goals and is a good potential way to build green buildings.

5 Numerical Model Validation and Parametric Studies

5.1 Introduction

In the previous chapter, the experimental program was described, and it was concluded that the development of composite action that arises due to the interaction of the top flange of cold-formed steel joist and the bottom surface of plywood as a result of mobilising the shear connection is feasible, leading to the significant improvements in the structural performance of composite CFST floors.

In this chapter, finite element models of composite CFST flooring systems are presented and validated against the experimental test results reported in Chapter 4. Since laboratory test alone is costly and time-consuming to study all the factors that influence the structural behaviour of the composite cold-formed steel flooring system, validated numerical models are then employed for parametric studies to investigate the influence of key parameters.

5.2 Development of Finite Element Models

The finite element software package ANSYS (Ansys Inc.), which has been extensively used in the past for the analysis of CFS members (Majdi et al., 2014; Zhou et al., 2019; Wang and Zhang, 2009), was chosen for the performed numerical studies. The developed finite element models were used to simulate full-scale composite beam tests. The experimental testings were conducted with a pair of CFS joists 600mm apart, but in this study, a single joist with an effective width of floor-board sheathing, as shown in Figure 5.1, was modelled with the necessary boundary conditions applied on the axis of symmetry. The key features

of the developed FEMs are discussed in this section, followed by validation and parametric studies.

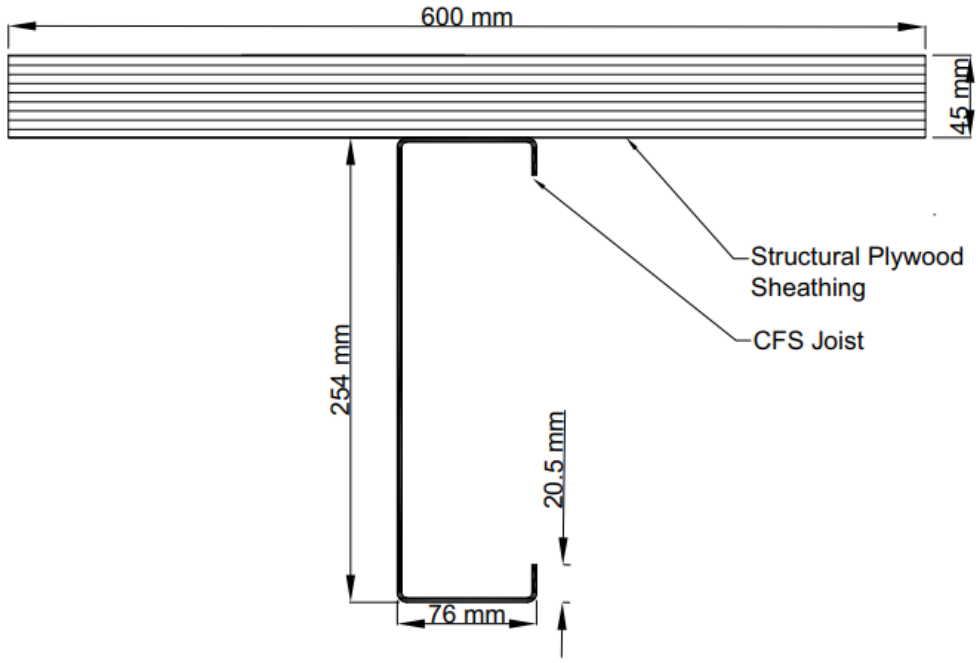

Figure 5.1: Cross-section of composite CFST beam used in finite element analysis for model validation

5.2.1 Material Inputs

The material properties of all the members must be precisely incorporated into the finite element models to simulate the response of a structural system accurately. Based on the material property tests conducted, the mechanical properties of the cold-formed steel and structural plywood panel are included in the numerical simulations.

5.2.1.1 Modeling of Cold-formed Steel Material

Cold-formed steel material exhibited a multi-linear stress-strain curve in uniaxial tension. Figure 5.2 depicts the average stress-strain curve, and Table 5.1

summarises the mechanical properties of CFS obtained from the tensile coupon tests.

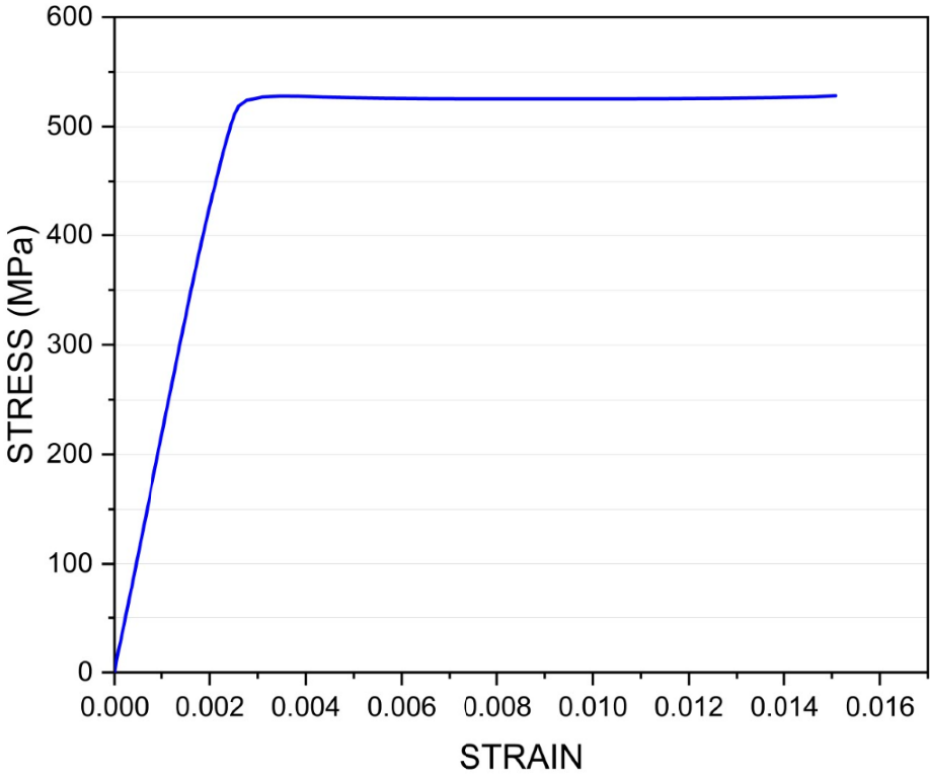

Figure 5.2: Average of stress-strain data obtained from CFS tensile test

In a non-linear analysis with large-strain solutions, all stress-strain inputs and results are in terms of true stress and true (or logarithmic) strain (Ansys Inc.). For input into the developed ANSYS shell elements, the nominal stresses (σ) and nominal strains (Ɛ) obtained from coupon tests have been converted into true stresses and strains by using the well know equations (5.1) and (5.2), respectively.

$$\sigma_{true} = \sigma(1 + \varepsilon) \tag{5.1}$$

$$\varepsilon_{true} = \ln(1 + \varepsilon) - \frac{\sigma_{true}}{E} \tag{5.2}$$

The Von Mises yield criterion is used with the associative flow and isotropic hardening rules to model CFS material in ANSYS. Note that since CFS typically

does not show a clear yield point in its stress-strain curve, the yield stress f_y was obtained by using the 0.2% nominal proof stress (Majdi et al., 2014; Pham and Hancock, 2010). Residual stress of CFS members was not taken into account in FE models as its influence is negligible in the ultimate moment capacity of CFS beams (Kankanamge and Mahendran, 2012; Schafer and Pekoz, 1998a) and since the material property is taken from the coupon tests as the residual stresses are inherently embedded in the member (Standard Australia, 2018; Kyvelou et al., 2018).

Table 5.1: Mechanical and geometrical properties of CFS beam

Thickness, t (mm)	Height,h (mm)	Flange width, b_f (mm)	Elastic modulus (MPa)	Yield strength (MPa)	Tensile strength (MPa)
2.4	254	76	207000	504	567

5.2.1.2 Modelling of Plywood Material

Plywood panel is treated as homogeneous material owing to its small thickness of laminates. The stress-strain relationship of the plywood panel based on constitutive law (Al-Hunaity et al., 2023), as shown in Figure 5.3, is an ideal elastoplastic model. The structural plywood panel sheathing was assumed orthotropic; however, the mechanical properties of the plywood are assumed to be identical in all directions. Material test results on the plywood discussed in Chapter 3 were employed in the current numerical models. As shown in Table 2, the average yield strength and modulus of elasticity in bending plywood sheathing were 17 MPa and 10,000 MPa, respectively. Poissons ratio is adopted as 0.3 (Arriaga-Martitegui et al., 2008) in FE models.

Table 5.2: Average measured mechanical properties of structural plywood (in MPa)

Bending parallel to grain ($f_{b,0}$)	Bending perpendicular to grain ($f_{b,90}$)	Tension parallel to grain ($f_{t,0}$)	Tension perpendicular to grain ($f_{t,90}$)	Compression parallel to grain ($f_{c,0}$)	Compression perpendicular to grain ($f_{c,90}$)	Modulus of Elasticity (E)
40	45.5	22	17	31.5	28	10000

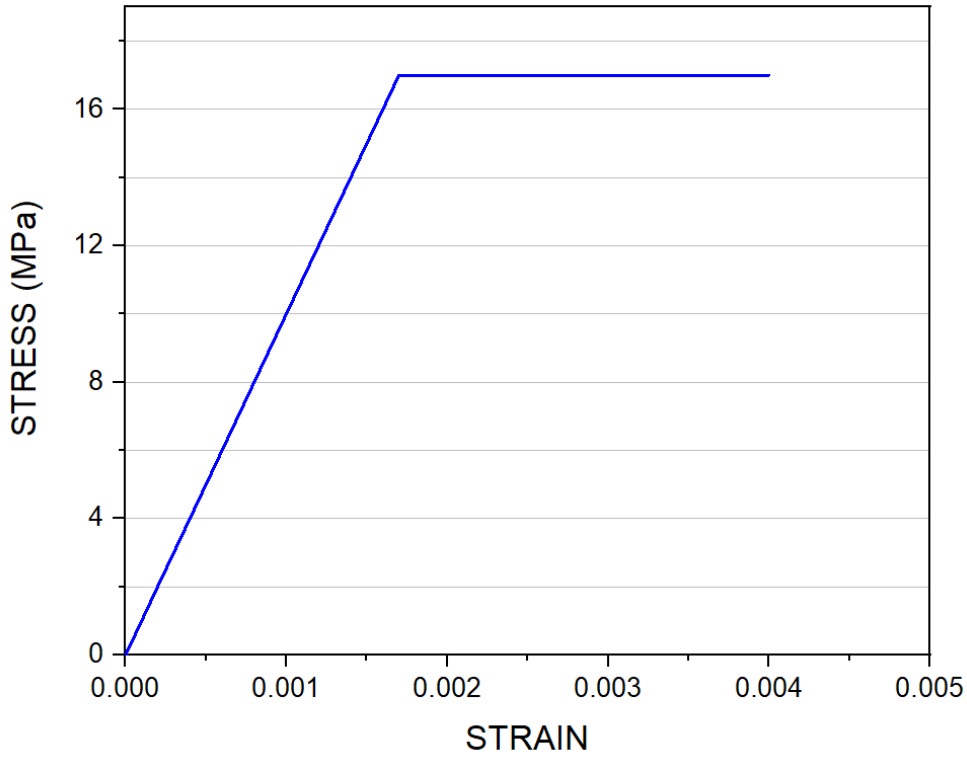

Figure 5.3: Elastoplastic model adopted for plywood in FE model

5.2.2 Element Types and Meshing

CFS joists were simulated using the SHELL181 element. Several studies (Xu et al., 2009; Majdi et al., 2014; Ren et al., 2006) have utilised this element for

modelling cold-formed steel structures, obtaining excellent replication of the physical test behaviour. SHELL81 is a four-node element with six degrees of freedom at each node, i.e., translation and rotation about the x, y, and z axes. This element can capture large plastic deformations and is appropriate for analysing non-linear problems with thin to moderately thick shell constructions. SOLID185, used for 3D modelling of solid structures, is used to simulate structural plywood panels. It is defined by eight nodes with three degrees of freedom at each node: translational in the directions of the nodal x, y, and z. This element has large deflection and large strain capabilities.

The accuracy and effectiveness of the finite element models depend upon selecting an adequate mesh size. Coarser mesh generally has less computational times but might not accurately capture failure modes, while finer mesh may result in longer computational times, although it can capture local instabilities (Kyvelou et al., 2018). Mapped mesh method was used to finely mesh the geometry with regular shape to get a more accurate analysis and efficient computing time. For the finite element analysis conducted within this study, 131 solid elements for plywood and 62 shell elements for CFS were used in cross-section, as represented in Figure 5.4. The model's mesh size was set at 10mm for shell elements and 20mm for solid elements in the longitudinal direction.

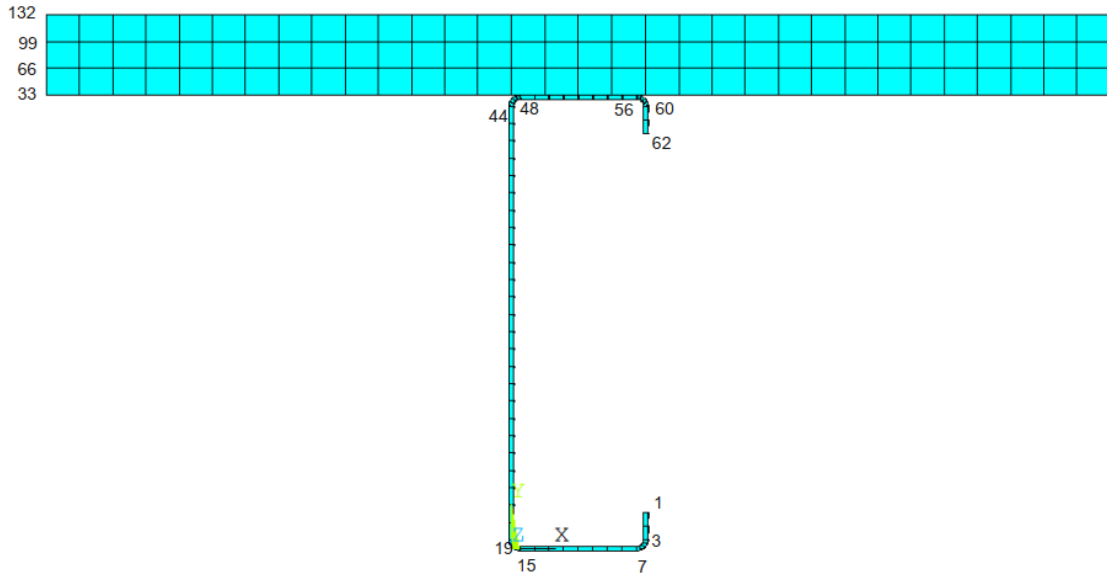

Figure 5.4: Cross-sectional mesh and node numbers for CFS joist and floorboard

5.2.3 Modelling of Fasteners and Contact Surface

Size 14 (6mm diameter) self-drilling screws, M8 nuts and bolts, M12 coach screws, and M12 nuts and bolts were used as the shear connection between the plywood panels and CFS joists. COMBIN39, a unidirectional nonlinear spring element with nonlinear generalised force-deflection capability, was used to replicate the shear connection. The load-slip response of the mechanical fasteners experimentally investigated through a series of push-out tests in Chapter 3 was utilised for the spring behaviour of the COMBIN39 element, as shown in Figure 5.5.

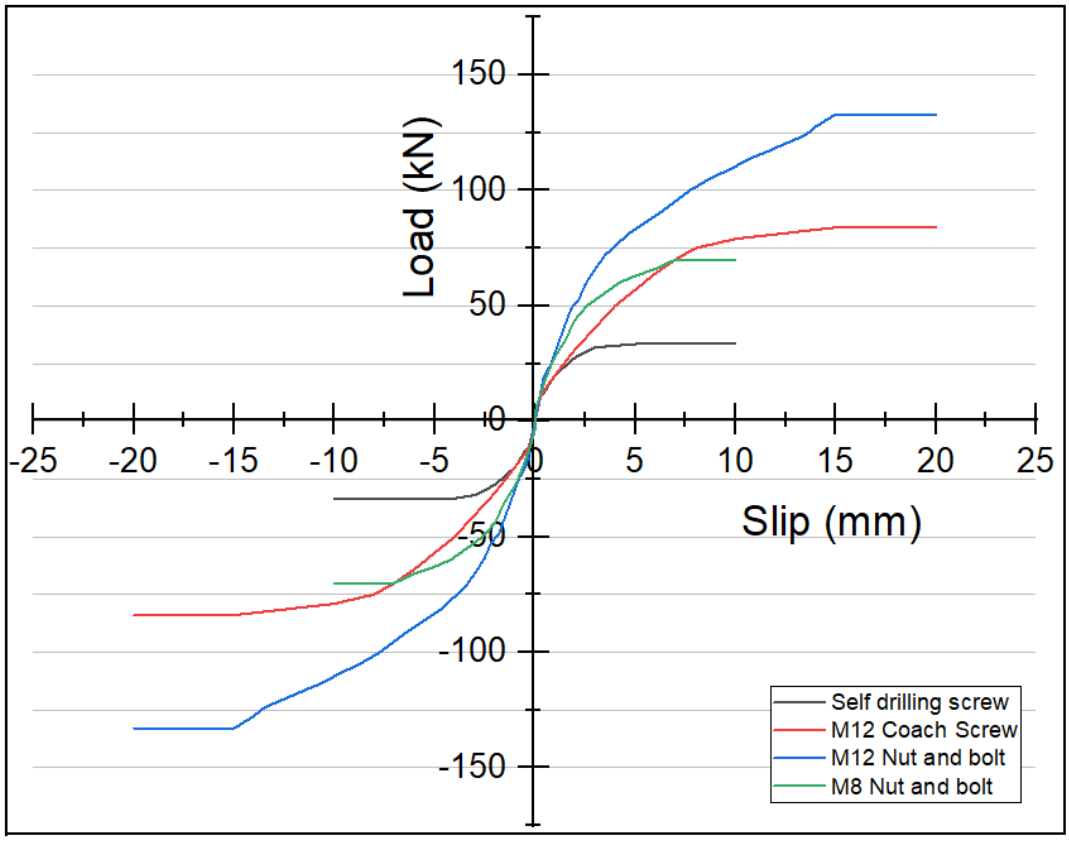

Figure 5.5: Load-slip relationship assigned to non-linear springs for different fastener types

Surface-to-surface pair-based contact and target element were used to simulate the interaction between the top flange of CFS joists and the bottom surface of plywood sheathing. CONTA 174 and TARGE170 were chosen as contact and target elements, respectively. The bottom surface of plywood sheathing was defined as the contact surface, while the top flange of the CFS joist was defined as the target surface, as shown in Figure 5.6. This element has the same geometric characteristics as the solid or shell elements face with which it is connected. The behaviour of the contact surface was assumed to be standard. A Coulomb isotropic friction coefficient of 0.35 was defined between the contact and sliding surfaces of steel and timber (Al-Hunaity et al., 2023).

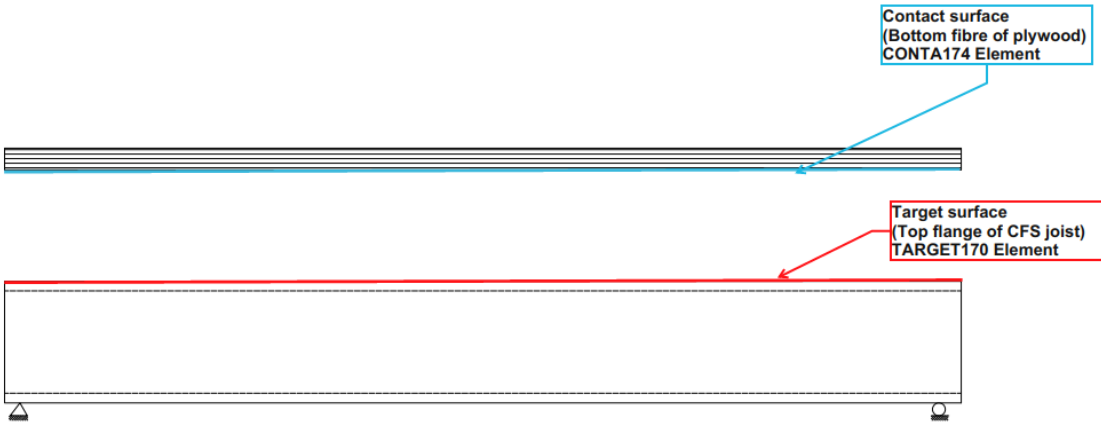

Figure 5.6: Schematic diagram of CFST beam showing contact and target surface for FEM

5.2.4 Loading and Boundary Conditions

In the experimental setup, a 4700mm composite CFST beam was supported across a 4500mm span in a simply supported condition. During four-point bending tests, at the position of loading points and supports, where the beam was subjected to high concentrated forces, it was stiffened locally to prevent any instability and web failure. Hence in this FEA study, rigid plates were connected to CFS joists at those positions. An artificially high elastic modulus (10 x E_{steel}) was considered for the rigid plate. Vertical and out-of-plane deflections were constrained at both supports, while rigid body motion was prevented by constraining the longitudinal translational degree of freedom of one support. Since all the tested specimens were symmetric, only half of the cross-section, as shown in Figure 5.1, was modelled with appropriate boundary conditions applied on the axis of symmetry to reduce computing time. Two concentrated vertical loads (equivalent to P/2) are applied to each model in one-third and two third of the span, as shown in Figure 5.7. Pure bending will result from the applied forces

under this kind of loading. An overview of the model geometry and boundary conditions is illustrated in Figure 5.8.

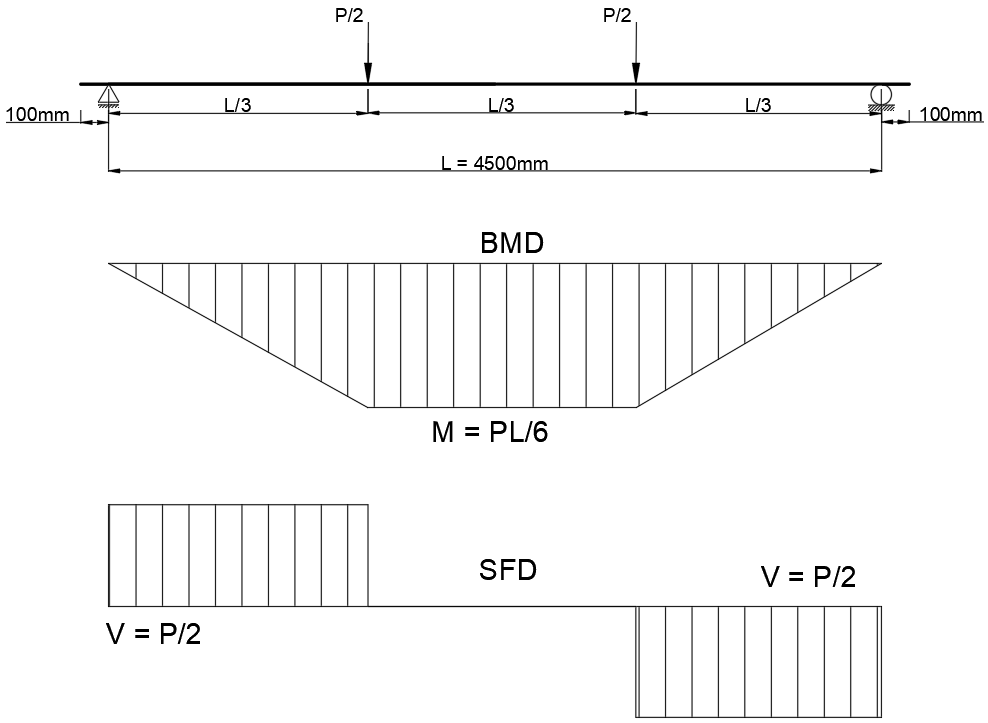

Figure 5.7: Simplified analysis model of four-point bending test

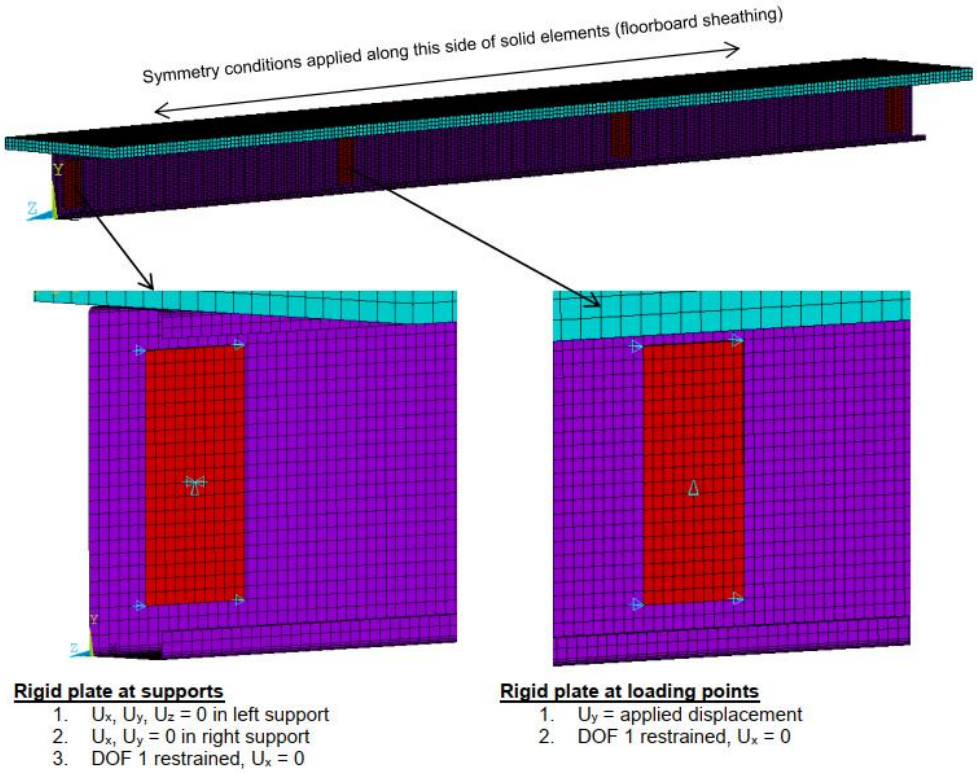

Figure 5.8: Boundary conditions used in finite element model for numerical analysis

5.2.5 Analysis Assumptions

Non-linear analysis was performed using the Newton-Raphson method for all the conducted analyses in this study. Large displacement static analysis, which considers material and geometrical nonlinearities, was used for the analysis. All models were loaded gradually in multiple steps based on the displacement control procedure. Because of nonlinearity in the system due to large deformation, material behaviour, and large contact surface, solution convergence was very difficult to achieve in all the conducted analyses herein. Hence, a non-linear stabilisation technique was employed and activated in a multi-frame restart to overcome the convergence issues.

5.3 Validation of Finite Element Models

The accuracy of the developed finite element models were validated against the results of the experimental four-point bending tests. As discussed in Chapter 4, thirteen composite beam specimens with different means of shear connections and one bare steel system, simply supported at a 4500mm span, were physically tested. Out of the thirteen composite systems, five of them are used for the validation of the numerical models developed in this study. From four shear connection groups, one from each at 400mm spacing was selected for this numerical study. SP-2 (SDS at 400 mm), SP-5 (CS at 400 mm), SP-7 (M12 NB at 400 mm), and SP-11 (M8 NB at 400 mm) are used to check the accuracy of finite element analysis. SP-3 (SDS at 200 mm) is also chosen to simulate the specimen with 200mm shear connection spacing for further validation.

The comparisons between the ultimate moment capacities $M_{u,exp}$ and flexural stiffness $(EI)_{exp}$ obtained from experimental testing, and those predicted by finite element models $M_{u,fea}$ and $(EI)_{fea}$ are presented in Table 5.3. As can be seen from Table 5.3, the mean ratio of the ultimate moment and flexural stiffness are 0.98 and 0.97, respectively.

Table 5.3: Summary of comparisons between finite element analysis and test results

Specimen	$M_{u,fea}$ / $M_{u,exp}$	$(EI)_{fea}$ / $(EI)_{exp}$
SP-2	1.02	0.99
SP-3	1.05	1.02
SP-5	0.96	0.965
SP-7	0.95	0.91
SP-11	1.02	1.01

Mean	0.98	0.97

The finite element models could predict the failure modes, as illustrated in Figures 5.9 and 5.10.

(a) Test

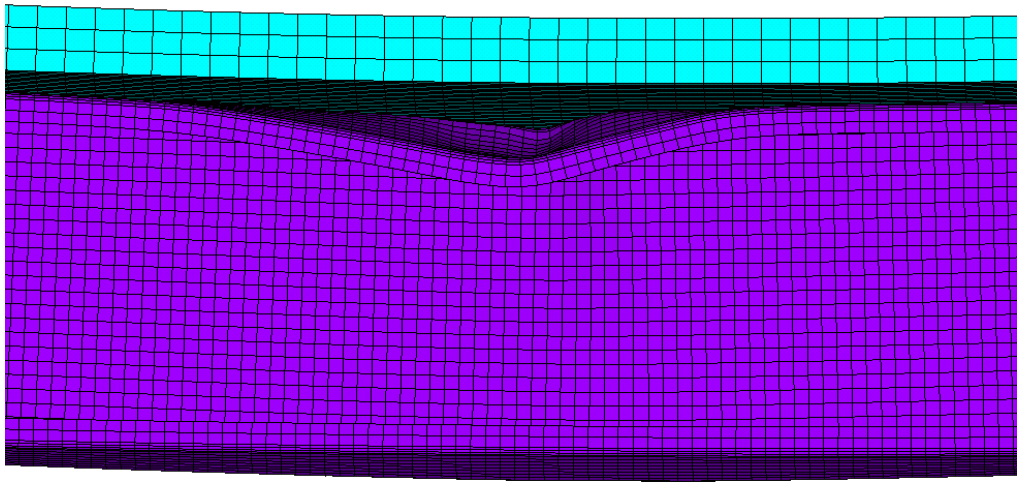

(b) Finite element analysis

Figure 5.9: Typical observed failure mode of specimen SP-11.

(a) Test

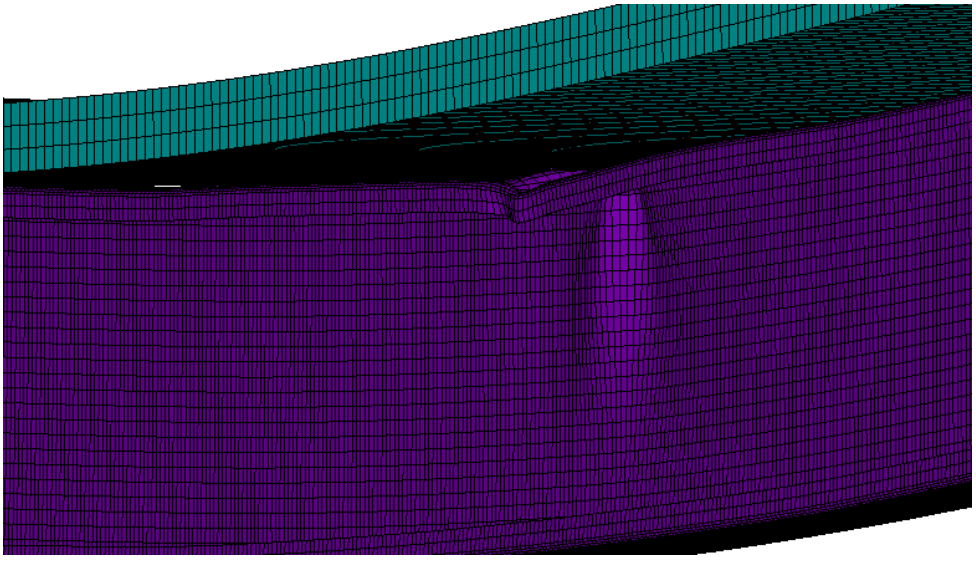

(b) Finite element analysis

Figure 5.10: Typical observed failure mode of specimen SP-7.

The load-deflection responses and strain distribution at the ultimate load obtained from FEA were in good agreement with experimental tests, as shown in Figures 5.11 and 5.12, respectively. All the specimens at 400 mm shear connector spacing failed in-plane at the constant moment region exhibiting distortional buckling of the top flange of the CFS joist between fixings, as illustrated in Figure 5.13.

After successful validation, the developed finite element models are utilised to further investigate the parameters that affect the structural behaviour and capacity of the composite CFST beams.

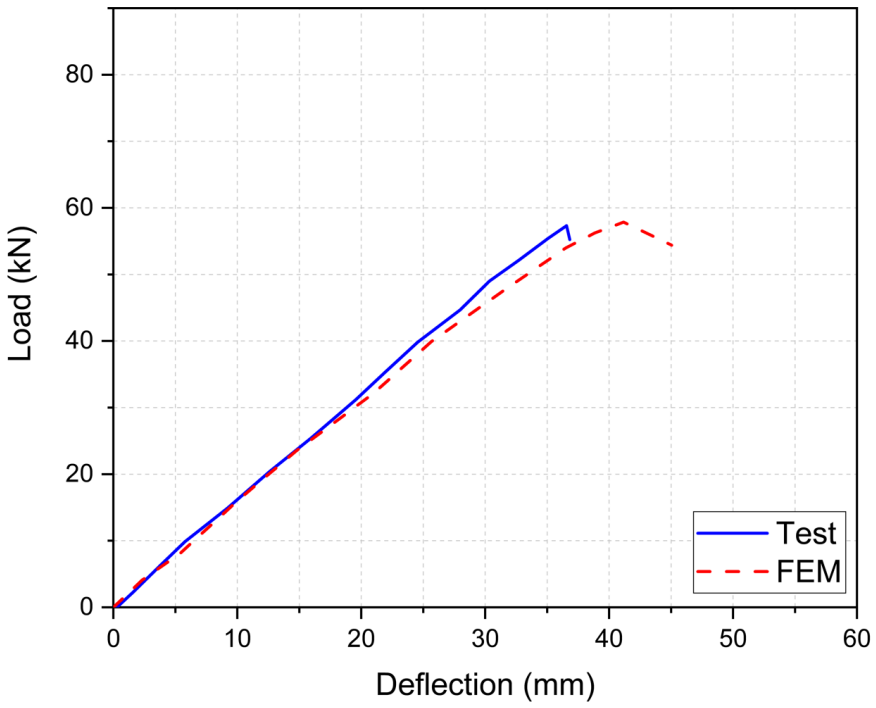

(a) Specimen SP-2 (SDS at 400 mm)

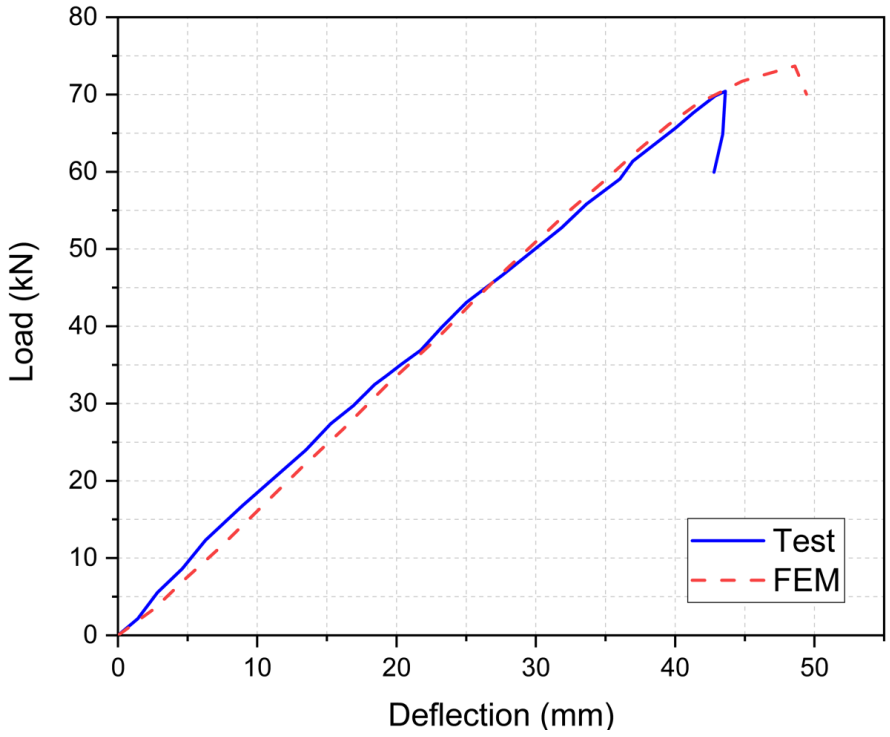

(b) SP-3 (SDS at 200 mm)

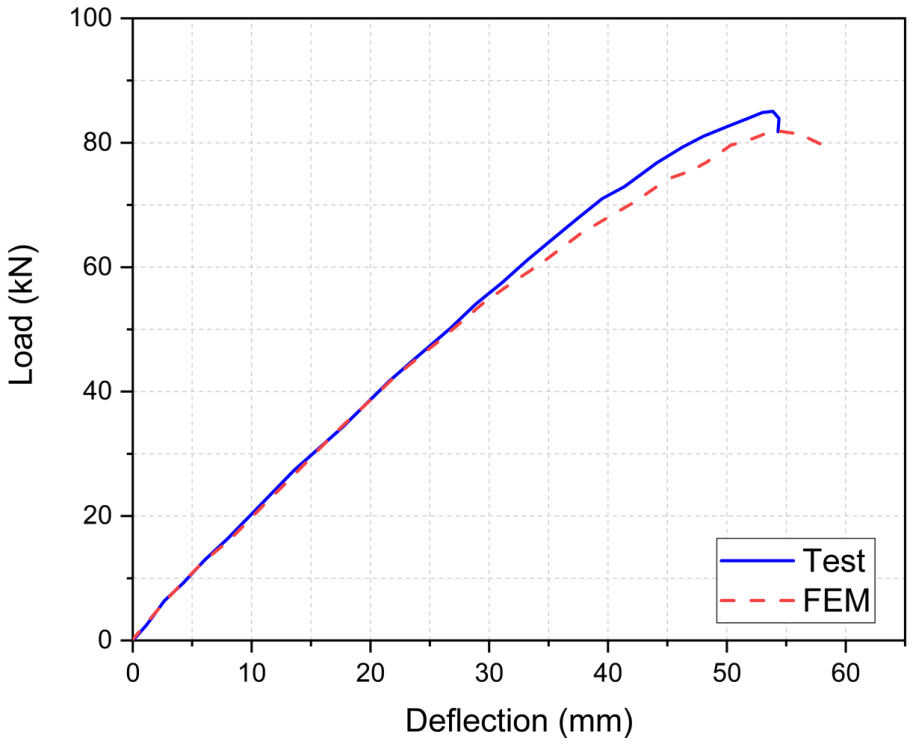

(c) SP-5 (M12 CS at 400 mm)

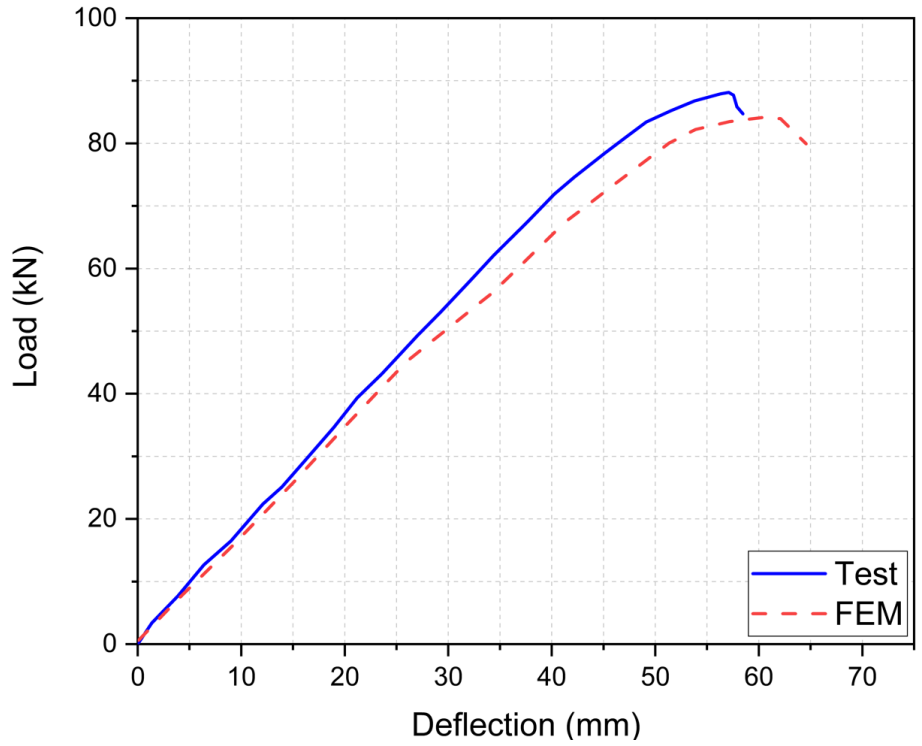

(d) SP-7 (M12 NB at 400 mm)

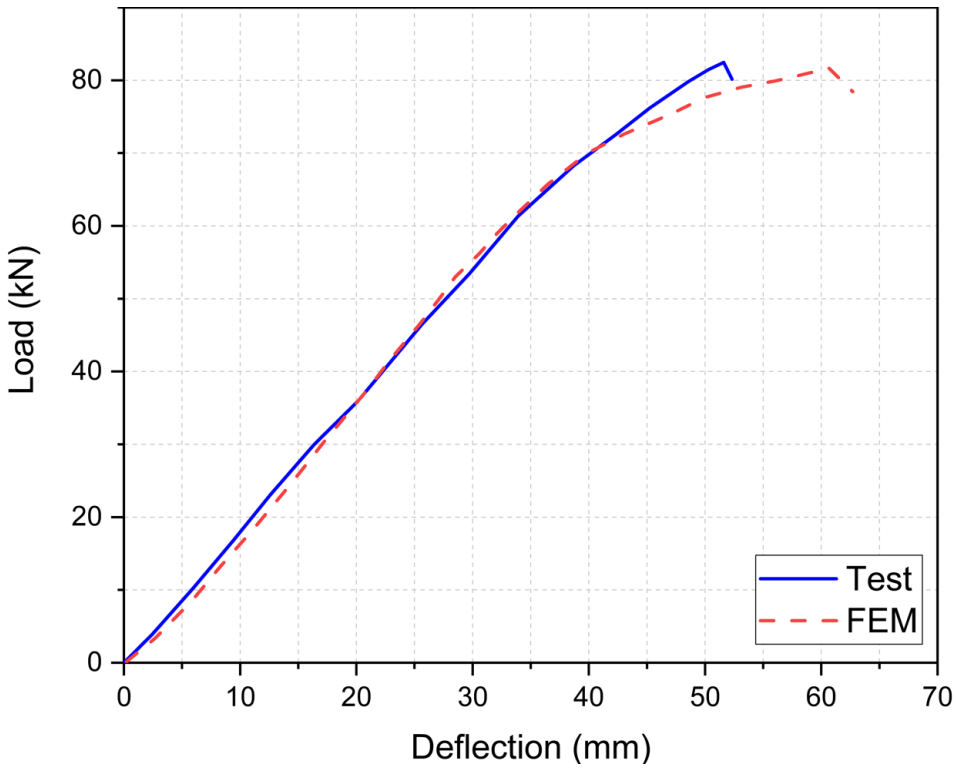

(e) SP-11 (M8 NB at 400 mm)

Figure 5.11: Comparison of load-deflection curves of the specimens from test and finite element model

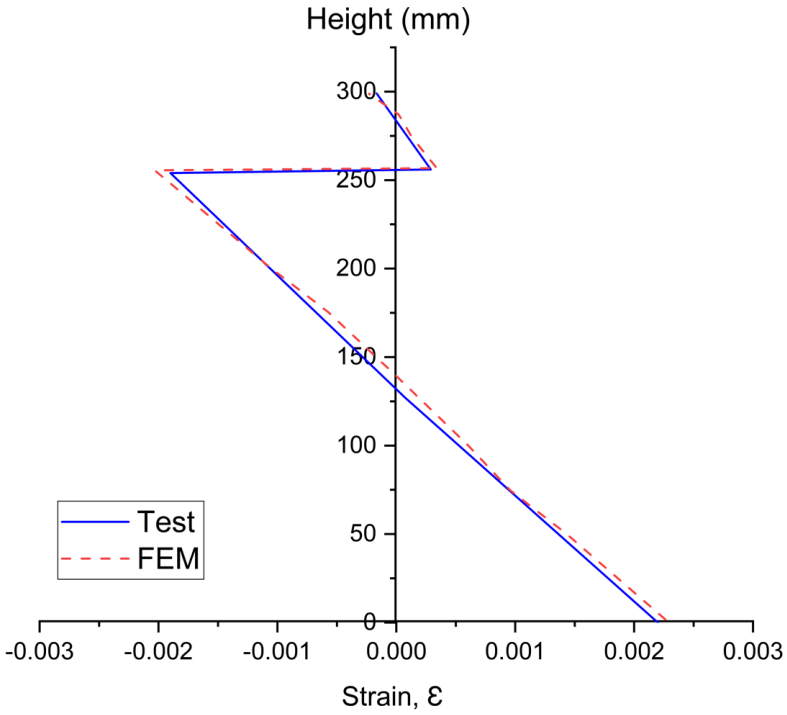

(a) SP-3 (SDS at 200 mm)

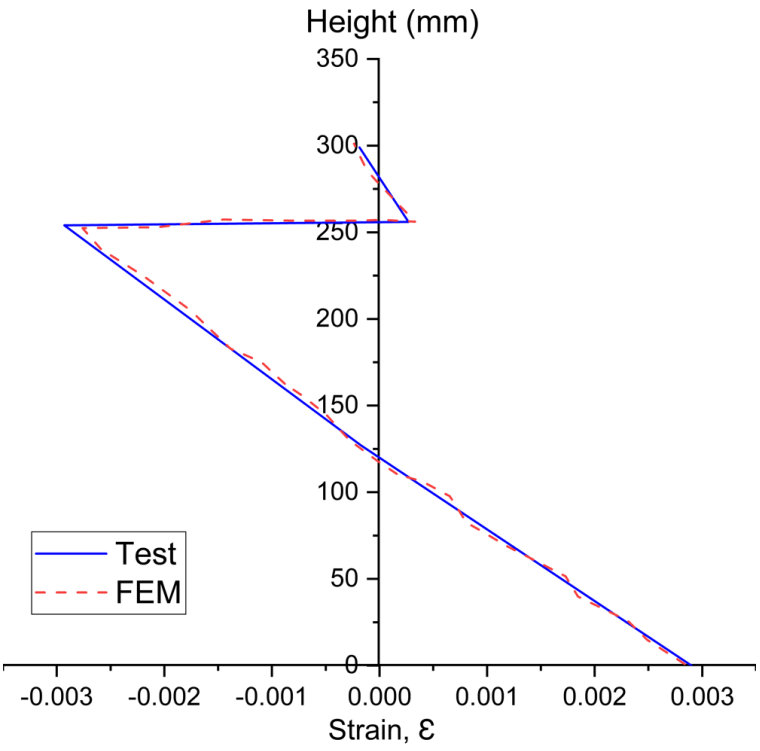

(b) SP-11 (M8 NB at 400 mm)

Figure 5.12: Comparison of cross-sectional strain distribution at ultimate load from test and finite element model

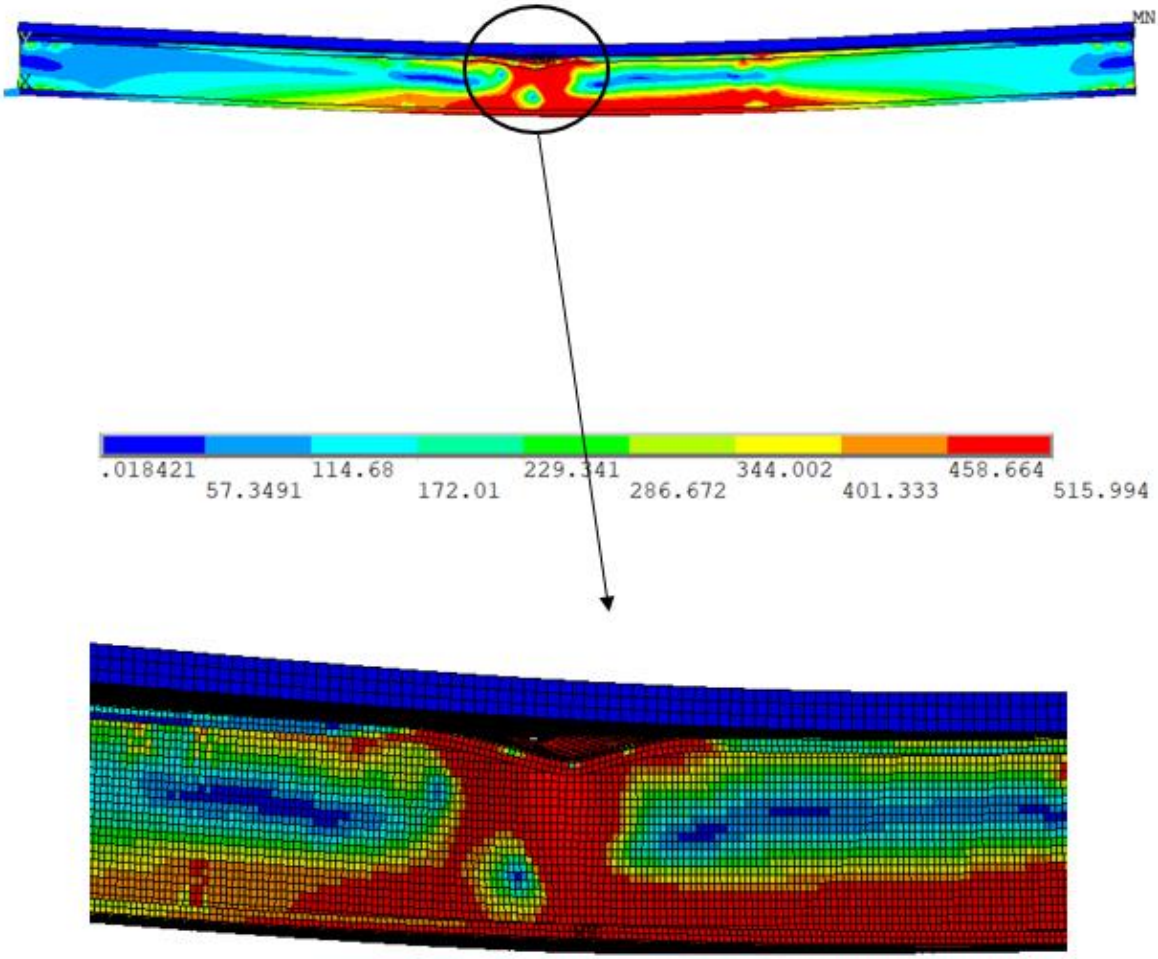

Figure 5.13: Typical bending failure near midspan with distortional buckling between fasteners

5.4 Parametric Studies and Result Discussions

Parametric studies were conducted to investigate the influence of the CFS joist thickness, depth, and fastener spacing on the structural performance of

composite floors comprising cold-formed steel joists and structural plywood sheathing. The results are studied in terms of ultimate bending capacity and stiffness with the degree of composite action achieved. For all the parametric studies herein, the load-deflection response of the M8 bolt is utilised to simulate the shear connector behaviour.

5.4.1 Influence of CFS Joist Thickness

CFS sections with three different thicknesses (1.5 mm, 2.0 mm, and 3.0 mm), which are readily available in the market, have been chosen for the study. Except for thickness, all the geometrical parameters of CFS were similar to the ones used in composite beam tests. The flexural capacities of composite CFST beams associated with the variation of CFS joist thickness, as obtained from FE parametric studies, are presented in Fig. 5.14 and Table 5.4. It can be observed that an increase in section thickness enhanced the loading capacity of composite beams almost in a linear fashion. When the joist thickness increased from 1.5 mm to 2.0mm, 2.0mm to 2.4mm, and 2.4mm to 3.0mm, the corresponding enhancements in the bending capacity of the composite beam were 37%, 20.5%, and 23%, respectively. Similarly, the predicted flexural stiffness of the composite CFST beam was found to be increased by 18%, 7%, and 28%, respectively. An increase in CFS section thickness led to the increase of section modulus and moment of inertia of the composite beam, which resulted in the enhancement of ultimate moment capacity and flexural stiffness of the composite CFST beam. Furthermore, the increased thickness means an improvement in the resistance of cold-formed steel to the flange buckling deformation, which resulted in the load-carrying capacity of the system.

Table 5.4: Influence of CFS joist thickness on the flexural capacity and stiffness of composite CFST beams

Numerical specimens	CFS joist thickness (mm)	Predicted ultimate moment capacity, M_u (kN.m)	Predicted flexural stiffness under service load ($N.m^2$)
C25015	1.5	35.36	2.33×10^6
C25020	2.0	48.45	2.74×10^6
C25024	2.4	58.35	2.9×10^6
C25030	3.0	71.4	3.72×10^6

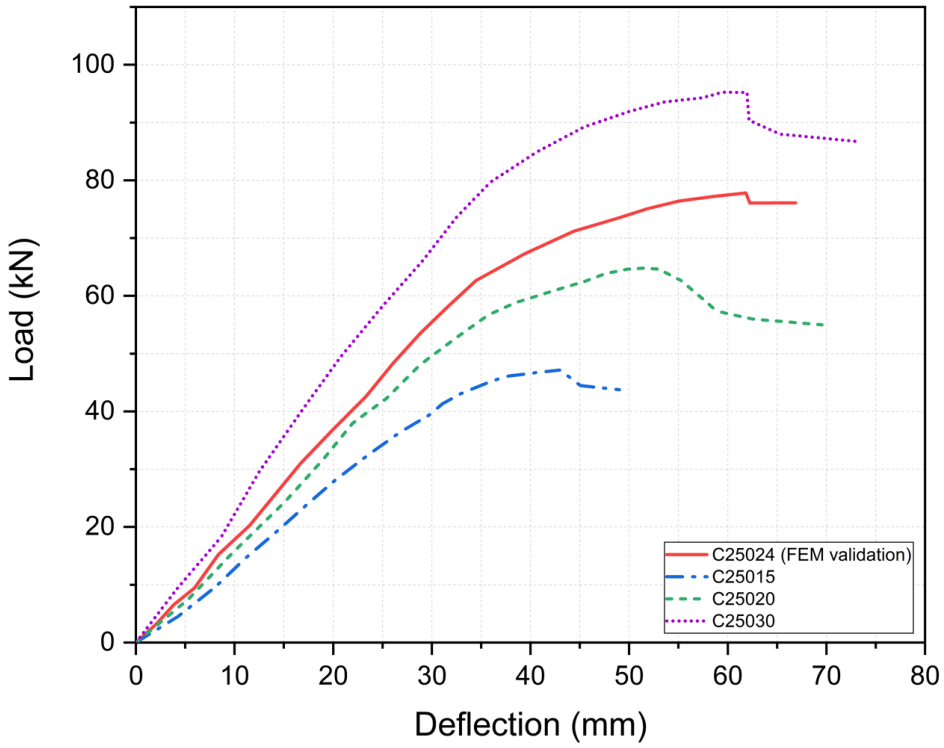

Figure 5.14: Load and deflection response for specimens with different CFS joist thickness

5.4.2 Influence of CFS Web Height

All the CFS parameters were unchanged except the web height in this study. CFS sections with three different web heights (150 mm, 200 mm, and 300 mm) and off-the-shelf products available in the construction industry were chosen to investigate the influence of CFS web height on the structural performance of

composite CFST flooring systems. The predicted moment capacity and flexural stiffness of composite CFST beams obtained from finite element analysis with different CFS web heights are presented in Table 5.5. As expected, increasing the section depth resulted in increased stiffness and strength of the composite system, illustrated in Figure 5.15. For example, increasing the joist height from 150 mm to 250 mm enhanced moment capacity and bending stiffness by 87% and 190%, respectively. It is a well-known strength of material theory that increasing the section depth leads to a higher moment of inertia, resulting in stronger sections and a substantial improvement in the flexural capacity of the composite beam. However, it is worth noting that increasing the depth of the CFS joist means increasing the cost of floor construction and the overall floor depth in a finished building. Therefore in designing such flooring systems, the ultimate limit state (ULS) and serviceability limit state (SLS) requirement should govern the depth of the joist.

Table 5.5: Influence of CFS web height on the flexural capacity and stiffness of composite CFST beams

Numerical specimens	CFS web height (mm)	Predicted ultimate moment capacity, M_u (kN.m)	Predicted flexural stiffness under service load ($N.m^2$)
C15024	150	31.2	0.99×10^6
C20024	200	44.55	1.73×10^6
C25024	250	58.35	2.9×10^6
C30024	300	70.12	2.33×10^6

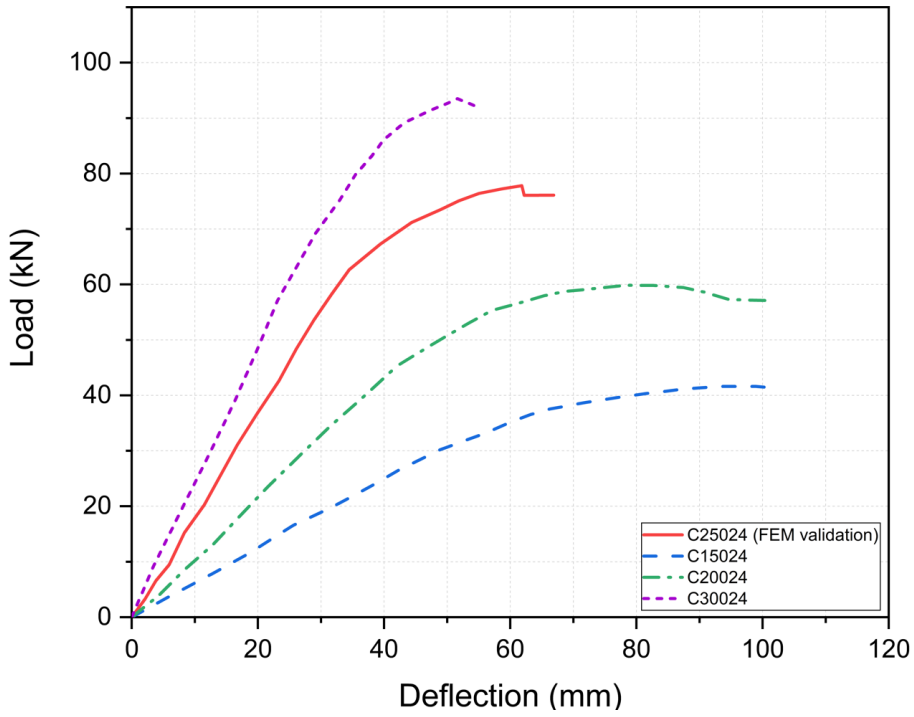

Figure 5.15: Load and deflection response for specimens with different CFS web height

5.4.3 Influence of Fastener Spacing

The effect of 200 mm, 400 mm and 800 mm fastener spacing was experimentally investigated for four types of shear connections. The findings of these experimental investigations are promising to explore the influence of the different types of shear connections and their spacing limitations. From the experimental investigation, it was concluded that for the ductile shear connectors like M12 coach screws and M12 bolts, material yielding of CFS limited the structural behaviour of composite CFST beams making it an inappropriate choice of shear connection for a lightweight cold-formed steel flooring system. Hence, to expand the existing data pool and quantify the benefits, the effect of 100 mm, 200 mm, 300 mm, 400 mm, 500 mm, 600 mm and 700 mm for M8 nut and bolt is carried out numerically. Decreasing the fastener spacing minimises the slip between two components, and hence the shear transfer capability among floorboard sheathing

and CFS section was improved, which consequently enhanced the composite action of the system. The predicted moment capacity and flexural stiffness of composite CFST beams obtained from finite element analysis with different CFS shear connection spacing are illustrated in Figure 5.16 and Table 5.6. The ultimate moment capacity and flexural stiffness were increased by 48% and 43%, respectively, by reducing the spacing from 700 mm to 100 mm. The influence of fastener spacing on the loading capacity of composite CFST beams is depicted in Figure 5.17.

Table 5.6: Influence of fastener spacing on the flexural capacity and stiffness of composite CFST beams

Fastener spacing (mm)	Predicted ultimate moment capacity, M_u (kN.m)	Predicted stiffness under service load ($N.m^2$)
100	73.5	3.3×10^6
200	66.5	3.3×10^6
300	61.2	3.11×10^6
400	58.35	2.9×10^6
500	54.8	2.86×10^6
600	52.2	2.65×10^6
700	50.6	2.3×10^6

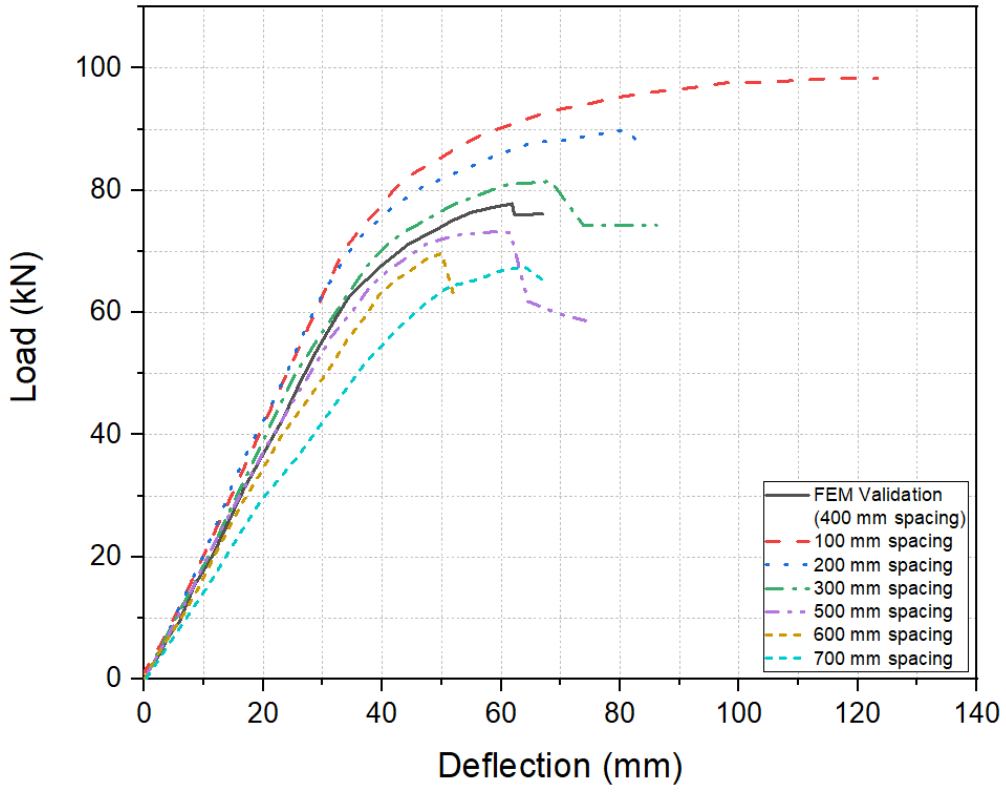

Figure 5.16: Load and deflection response for specimens with different fastener spacing

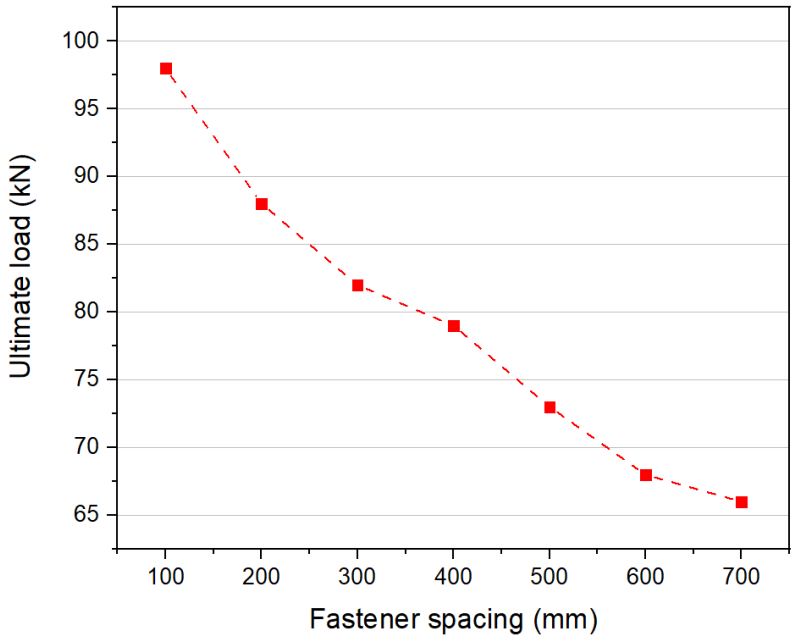

Figure 5.17: Influence of fastener spacing on the capacity of composite CFST beams

The wavelength of the CFS section corresponding to local buckling and distortional buckling as determined by finite strip software THINWALL (CASE, 2006) was 140 mm and 600 mm, respectively. As can be seen from Figure 5.16, higher flexural capacity for the specimen with 100 mm fastener spacing was achieved as the local buckling of the top flange of the CFS joist was restrained at 100 mm spacing less than the local buckling wavelength, which corresponds to the higher load carrying capacity. When the fastener spacing increased from 500 mm to 600 mm and 700 mm, the slope of the load-deflection was significantly reduced; this is because the fastener spacing is greater than the wavelength of distortional buckling. With self-drilling screws as shear connectors, Shi et al. (2020) observed that if the screw spacing was more than the wavelength of the distortional buckling mode, there was a considerable reduction in the flexural capacity of the composite beams. However, in this study, M8 nut and bolt was chosen as a shear connector, which is more ductile than the self-drilling screw; hence moment capacity was not drastically reduced, but the flexural stiffness of the composite beam was considerably lower.

5.5 Concluding Remarks

This chapter presents finite element models to simulate the structural response of composite cold-formed steel and timber flooring systems. The developed 3D finite element models were validated against the relevant experimental test results discussed in Chapter 4. CFS joists 254 mm deep and 2.4 mm thick were sheathed with 45mm thick structural plywood panels using four different fasteners

comprising self-drilling screws, M8 nuts and bolts, M12 coach screws and M12 nuts and bolts in physical testing. Following the successful validation of finite element models for each specimen with different fastening arrangements, parametric studies were conducted to investigate the influence of important parameters like joist thickness, web depth and fastener spacing on the load-carrying capacity and stiffness of the composite system. Results from the parametric studies have demonstrated that increasing the cross-section thickness or depth of CFS joists can improve the flexural capacity of composite floors. The influence of fastener spacing on the strength and stiffness of the system is highlighted. By reducing the fastener spacing (M8 nut and bolt) from 700 mm to 100 mm, the predicted flexural capacity and stiffness were enhanced by 43% and 48%, respectively. From the outcomes of this numerical study, it has become apparent that there is ample proof to consider the composite behaviour in the composite CFST flooring system and the benefits to be gained in terms of strength and stiffness.

6 Design of Cold-Formed Steel and Timber Flooring Systems

6.1 Introduction

When a composite cold-formed steel and timber floorboard assembly is loaded, the load is transferred from the timber sheathing through the connectors into the framing beneath the sheathing. The amount of load shared depends on the amount of slip that arises between two members or materials. The load-slip response of each connection type obtained from push-out tests is described in Chapter 3. Mechanical fasteners, which act as the shear connection between the composite system components, prevent the relative slip at the interface and enhance the mobilisation of composite action. It is nearly impossible for the composite cross-section to act monolithically without slipping at the beam-board interface (full shear interaction) because all fasteners will deform with increasing load (Ellobody and Young, 2006; Nie and Cai, 2003). Since slip develops at the interface, and the failure of the shear connection or material yielding affects load-carrying capacity in all the tested composite systems; the shear interaction is assumed to be partial.

Numerous research works have been done on composite steel-concrete, and timber-concrete floors in the past, and many investigations have been done to develop shear connections. In comparison, the benefit of composite construction, e.g., hot-rolled steel and concrete (Ellobody and Young, 2006; Rackham et al., 2009), timber and concrete (Deam et al., 2008; Lukaszewska et al., 2010), and hot-rolled steel and timber (Hassanieh et al., 2016a, 2017a) are well established and understood with few recent types of research on lightweight floors with CFS joists and timber (Kyvelou et al., 2017b; Zhou et al., 2019). Consequently, the

beneficial interaction between cold-formed steel joists and timber floorboards is mostly unsubstantiated, resulting in conservative designs of CFS joists alone.

This chapter proposes analytical equations for the design of composite cold-formed steel and timber (CFST) flooring systems. A relationship is presented to determine the spacing of shear connectors to attain complete shear connection. Design equations are provided for calculating the moment capacity and flexural stiffness of CFST beams considering the attained degree of shear connection. The accuracy of the design expressions is compared with the results obtained from the experimental testing and numerical analyses reported in Chapters 4 and 5, respectively.

6.2 Design of Shear Connectors for Complete Shear Connection

The design of shear connectors requires consideration of the ability of the mechanical fasteners to transmit the shear force between the timber sheathing and CFS joist without either the fastener shearing off or the failure of the two material components. Hence, for a composite CFST floor to achieve complete shear connection, the number of fasteners in the system should be such that material strengths are exploited to their greatest extent for achieving the full plastic bending resistance. If the number of fasteners in the composite system is inadequate for complete shear connection, then the fasteners' capacity is limited to transfer the shear force and thus results in what is known as partial shear design giving a reduced ultimate flexural strength. A free-body diagram of the composite beam and floor sheathing only to the left of the midspan is depicted in Figure 6.1 to better understand the shear transfer concept.

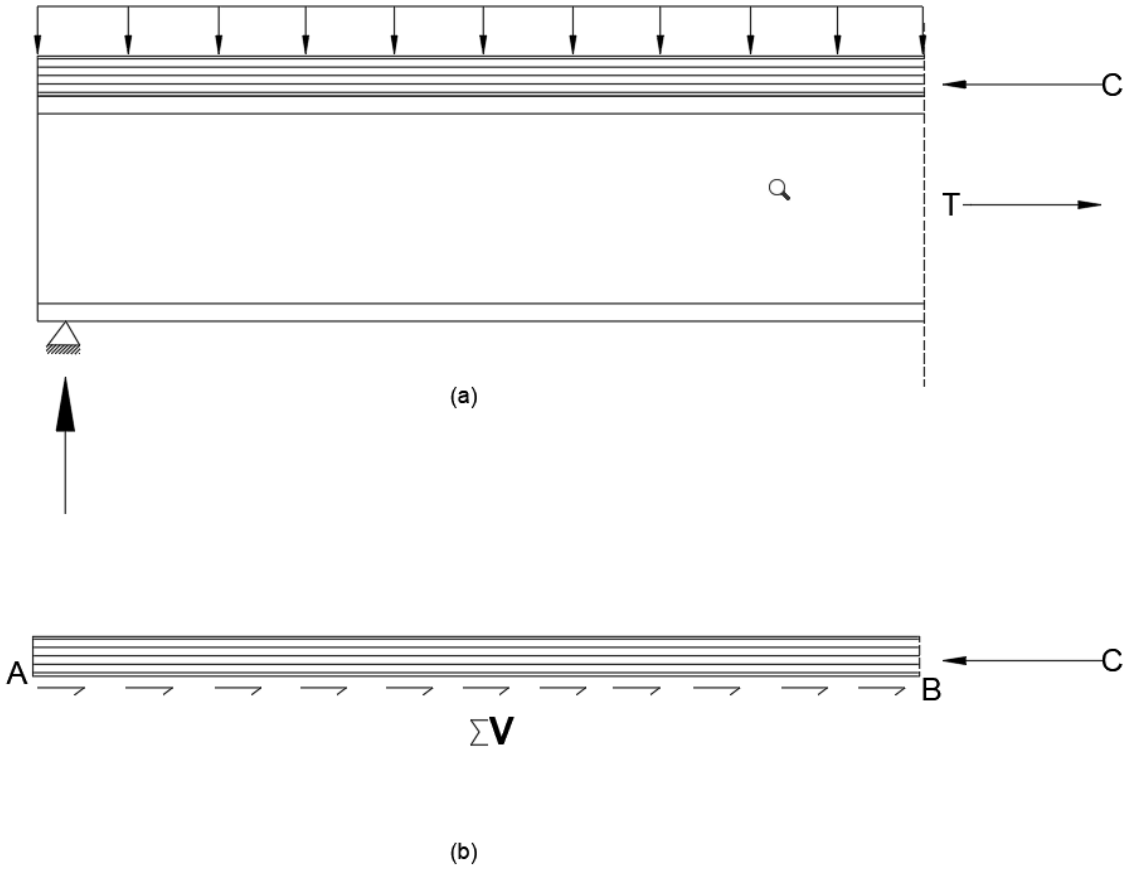

Figure 6.1: (a) Free-body diagram of the entire composite beam to the left of mid-span; (b) free-body diagram of the floor sheathing to the left of the mid-span

Considering a horizontal equilibrium of the composite system, from Figure 6.1 (a) and (b), C = T, and ΣV = C, respectively. This equation can be rewritten as C = ΣV = T. As broadly discussed in Chapter 4, the tensile force, T, on the CFS joist or compression force, C, on the floorboard sheathing can be calculated as per Equations (6.1) and (6.2), respectively.

$$T = A_{st} \times f_y \quad (6.1)$$

$$C = A_b \times f_{cb} \quad (6.2)$$

Hence, if the shear connection between the timber sheathing and CFS joist can transfer the full 'ΣV', a complete shear connection is achieved, and the full tension 'T' and compression 'C' can be developed. And, if the number of fasteners is less than that required, then ΣV < T or C results in a partial shear connection controlled by the shear connectors' resistance.

Adopting the simplified principles of AS2327.1 Composite Structures-Part 1: Simply supported beams (Standard Australia, 2017), the longitudinal shear force Q that can be resisted by the shear connectors of a composite beam is limited by the shear capacity of the fastener V_f or by the bearing resistance of the timber board V_b. The design shear capacity of an individual fastener can be calculated as per Equation (6.3) and Equation (6.4) or from the push-out tests for the fastener utilised in this thesis. Equation (6.3) is in accordance with clause 5.3 of AS/NZS 4600: Cold-formed steel structures for the design of connections in shear.

$$V_f = \phi \text{ x } 0.62 \text{ x } f_{uf} \text{ x } n_s \text{ x } A_f \quad (6.3)$$

Where f_{uf} is the ultimate strength of the fastener, n_s is the number of the shear plane, and A_f is the cross-sectional area of the fastener. Similarly, the bearing resistance of the timber board for each loaded fastener can be determined from Equation (6.4).

$$V_b = \phi \text{ x } d_f \text{ x } t_b \text{ x } f_{cb} \quad (6.4)$$

Where, $\phi = 0.8$ is the capacity reduction factor, d_f is the nominal diameter of the fastener, t_b is the thickness of the floorboard, and f_{cb} is the compressive strength of the floorboard.

Hence, the magnitude of longitudinal shear force Q is the minimum of V_f or V_b. For a complete shear connection, the number of shear connectors n_f required along each critical length of the beam (from mid-span to left or right support) is:

$$n_f = \Sigma V \text{ or } T/Q \quad (6.5)$$

Since there are two critical spans requiring the number of shear connectors, n_f, on either side from mid-span, the total number of shear connectors N_f required along the full length of the beam is:

$$N_f = 2\, n_f \quad (6.6)$$

Hence, for a flooring system with n connectors in total span, the attained degree of shear connection η_s is determined as:

$$\eta_s = n/N_f \leq 1 \quad (6.7)$$

For all the conducted experimental and parametric studies to study the influence of fastener spacing herein, the attained degree of shear connection is calculated and summarised in Table 6.1

Table 6.1: Attained degree of shear connection for various fasteners and their spacings

Fastener spacing (mm)	Attained degree of shear connection, η			
	Self-drilling screw	M8 nut and bolt	M12 coach screw	M12 nut and bolt
100	0.26	0.35		
200	0.13	0.175	0.26	
300	0.09	0.13		
400	0.075	0.08	0.14	0.15
500	0.057	0.07		
600	0.05	0.062		
700	0.04	0.05		
800				0.07

6.3 Elastic Analysis of Test Results

The elastic moment resistance of the composite system with the partial shear connection is assumed to vary between the elastic moment capacity of the bare CFS beam and the elastic moment capacity of the fully composite beam. Note that cold-formed steel sections are thin-walled, and their section moment capacity is limited due to their susceptibility to local instabilities like distortional or local buckling (Hancock, 1998; Yu and Schafer, 2003); hence calculation is done following the direct strength method (DSM) of AS/NZS 4600:2018 (Standard Australia, 2018). THIN WALL-2 (CASE, 2006) is used in this study to develop the signature curve of the buckling stress versus buckling half-wavelength for the C-section. Figures 6.2 and 6.3 depict the signature curve of the buckling load factor versus buckling half wavelengths for local and distortional buckling, respectively. The local and distortional buckling stress was 509 MPa and 430 MPa, respectively.

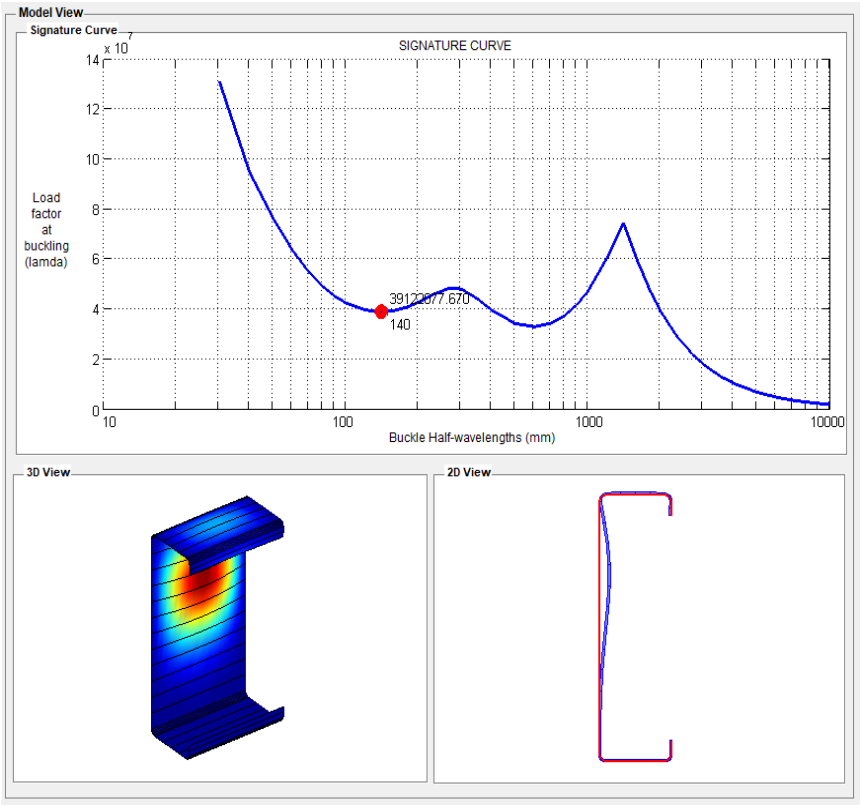

Figure 6.2: Signature curve obtained from THIN WALL-2 for examined cold-formed steel C-section showing local buckling mode and half-wavelength

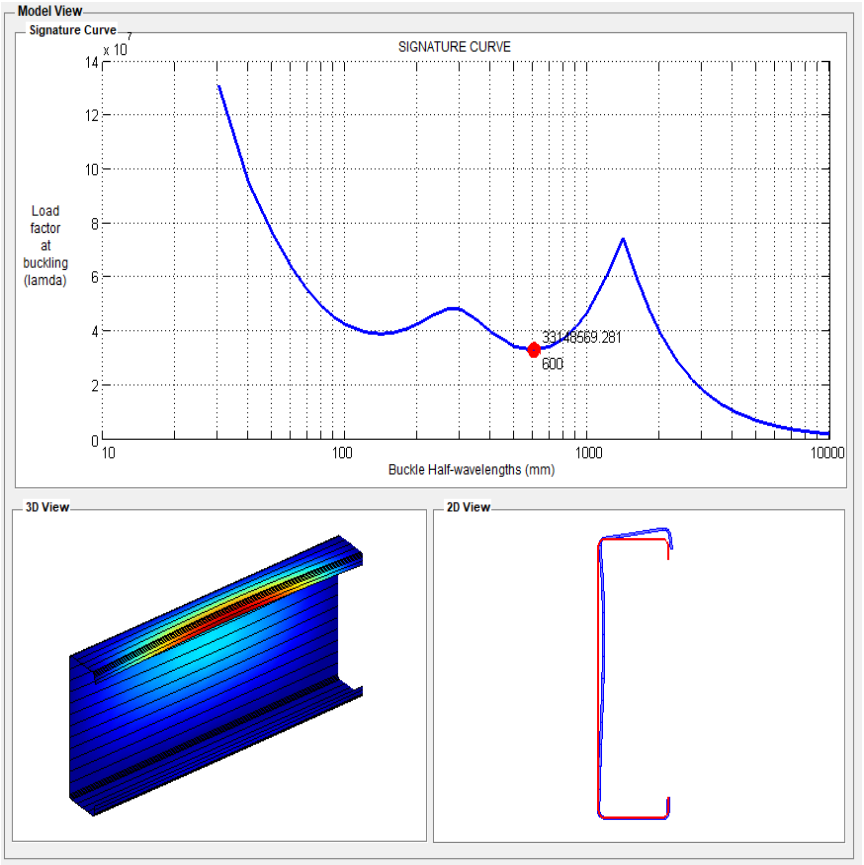

Figure 6.3: Signature curve obtained from THIN WALL-2 for examined cold-formed steel C-section showing distortional buckling mode and half-wavelength

Table 6.2 summarises the four-point bending tests of the CFS C-section, including the ultimate peak loads (P_u) and the tested bending moments (M_t). The elastic local buckling moment (M_{ol}), elastic distortional buckling moment (M_{od}), the yield moment (M_y) based on tensile coupon test results, and plastic moment (M_p) are also presented in Table 6.1. M_{ol} and M_{od} are calculated by multiplying elastic section modulus (Z) with the local buckling stress (F_{ol}) and distortional buckling stress (F_{od}), respectively. As can be seen from the values summarised in Table 6.2, the tested moment capacity of the C-section is slightly larger than the yielding moment or local buckling moment capacity, which is relatable to the inelastic reserve capacity of cold-formed thin-walled steel sections (Pham and

Hancock, 2013). Hence, the yield strength of CFS is reasonable to be used to compute the elastic ultimate bending moment of CFST beams.

Table 6.2: Four-point bending test results, elastic and plastic bending capacities of CFS C-section used in the study

P_u (kN)	M_t (kN.m)	F_{ol} (mPa)	F_{od} (mPa)	Z (mm^3)	S_x (mm^3)	M_{ol} (kN.m)	M_{od} (kN.m)	M_y (kN.m)	M_p (kN.m)
52.5	39.37	509	430	75651	83530	39.1	32.5	38.12	43

6.3.1 Theoretical Elastic Bending Moment Capacity of CFST Beams

Based on the research conducted by Hsu et al. (2014) and Liu et al. (2022) on the performance of CFS-concrete and steel timber composite beams, respectively, similar assumptions and methodology is adopted in this study to investigate the elastic bending moment capacity of composite CFST beams. Under serviceability load conditions, the CFS and plywood panel are in the elastic stage. To calculate the elastic bending capacity of CFST beams following assumptions are made:

- Under the flexure assumption, plywood sheathing and cold-formed steel joists that comply with the plane section remain plane;
- Both steel and timber are ideal linear elastic bodies;
- When the slip occurs at the interface, the curvature of plywood sheathing and cold-formed steel remains the same, and the lifting effect may be ignored.

If the plywood sheathing of CFST beams were damaged first, the elastic bending capacity M_{el} with the full shear connection could be calculated according to Equation (6.7). When the failure in CFST beams is initiated by yielding cold-formed steel, M_e can be computed as per Equation (6.8). The ultimate elastic bending moment of the CFST beam with the full shear interaction may be taken as the smaller value of Equation (6.7) or (6.8).

$$M_{el} = f_{yp} I_T n / z \tag{6.7}$$

$$M_{el} = f_{ys} I_T / z \tag{6.8}$$

Where f_{yp} denotes parallel to grain compression strength of plywood panel (MPa), f_{ys} denotes the yield strength of cold-formed steel (MPa), I_T (mm^4) is the transformed section moment of inertia which is calculated as per Equation (10), n is the ratio of elastic moduli of steel to plywood (E_s/E_p), z is the centroidal position of transformed section (mm) and determined from Equation (6.9)

$$z = \frac{A_s Z_1 + A_t z_2 / n}{A_s + A_t / n} \tag{6.9}$$

Considering the slip between the CFS and plywood interface, the actual bending capacity of composite CFST beams with a partial shear connection can be calculated according to Equation (6.10).

$$M = M_{el} - \Delta M \tag{6.10}$$

Where, M_{el} is the elastic bending capacity of CFST beams with full shear interaction, ΔM is the moment due to slip strain. It is assumed that when the slip occurs at the interface, the curvature of plywood sheathing and cold-formed steel remains the same at a given section, and the lifting effect may be ignored. Hence,

the additional curvature (ΔΦ) due to slip strain ($\varepsilon_{s'}$) of CFST beams with partial shear interaction can be calculated according to Equations (6.11) and (6.12). The strain distribution in composite CFST beams under elastic bending is represented in Figure 6.3.

$$\Delta\Phi = \frac{\varepsilon_{s't}}{h_t} = \frac{\varepsilon_{s's}}{h_s} = \frac{\varepsilon_{s't} + \varepsilon_{s's}}{h_t + h_s} = \frac{\varepsilon_{s'}}{h} \tag{6.11}$$

$$\varepsilon_{s'} = h\Delta\Phi \tag{6.12}$$

Where $\varepsilon_{s't}$ and $\varepsilon_{s's}$ are the strains at the bottom of the plywood and top of cold-formed steel due to the stiffness of connections, $\varepsilon_{s'}$ denotes the slip strain at the CFS and plywood interface.

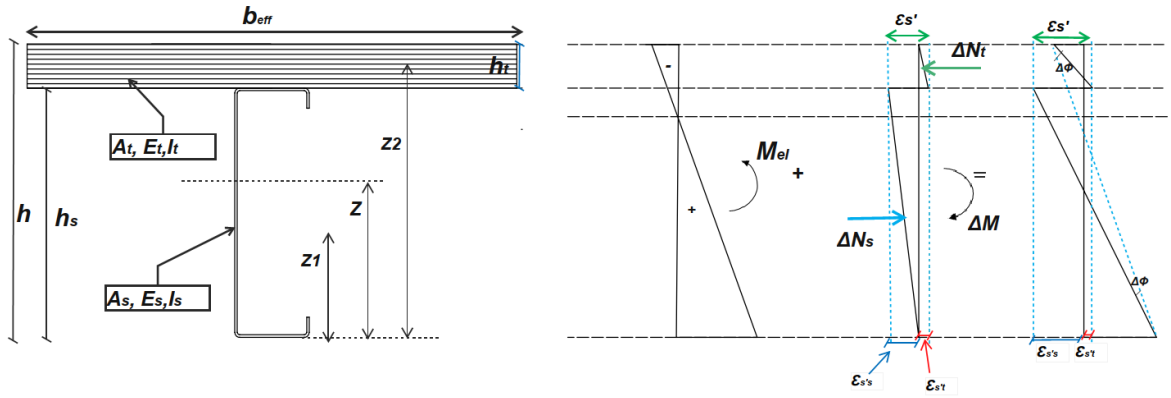

Figure 6.4: Strain distribution in CFST beams under elastic bending

The strain at the top of CFS ($\varepsilon_{s's}$) can be found by rearranging Equation (6.11)

$$\varepsilon_{s's} = \frac{h_s}{h}\varepsilon_{s'} \tag{6.13}$$

The tensile force variation in the CFS section due to slip (ΔN_S) can be computed according to Equation (6.14).

$$\Delta N_S = \sigma A = \varepsilon_{s's} E_s \left(A_{sf} + \frac{1}{2} A_{sw} \right) = \frac{E_s \varepsilon_{s's} h_s A_s}{2h} \quad (6.14)$$

A_{sf} (mm^2) is the area of the top flange, A_{sw} (mm^2) is the area of the web. The force equilibrium equation can be obtained from Equation (6.15).

$$\Delta N_S = \Delta N_t \quad (6.15)$$

Where ΔN_t denotes the resultant compressive force of additional stress for the plywood section. The moment ΔM due to slip strain can be computed according to Equation (6.16).

$$\Delta M = \frac{h_s}{6} E_s \varepsilon_{s'} A_s = \frac{M_{el} h h_s A_s (E_s I_T - EI_{eff})}{6 EI_{eff} I_T + h h_s E_s A_s I_T} \quad (6.16)$$

6.3.2 Effective Bending Stiffness of CFST Beams

The importance of determining effective bending stiffness for constructing timber-concrete composite floors was underlined in previous studies (Ceccotti, 2002; Steinberg et al., 2003), and a similar methodology is employed in this study. Previous studies (Loss and Davison, 2017; Yang et al., 2021) estimated the deformation of steel and timber beams using Gamma (γ) method and found the experimental results close to the theoretical values. Most recently, Kyvelou et al. (2017a) proposed an equivalent formula based on the Gamma method to calculate the effective bending stiffness of cold-formed steel and particleboard flooring system. Hence, the effective bending stiffness for CFST beams in this study is calculated based on Appendix B of Eurocode 5 (CEN, 2004). The obtained slip modulus values discussed in Chapter 3 and Karki et al. (2022) are used to calculate the effective bending stiffness of a cold-formed steel and timber

composite assembly. Shear bond coefficient, γ, is calculated first to obtain the effective bending stiffness value of a composite assembly using Equation (6.17).

$$\gamma = \frac{1}{1 + \frac{\pi^2 S E_t A_t}{K L^2}} \tag{6.17}$$

In Equation (17), γ is shear bond coefficient, S is the spacing of shear connections (mm), E_t is the modulus of elasticity of timber floorboard (MPa), A_t is the area of timber floorboard (mm^2), K is the slip modulus (N/mm), and L is the length of the member (mm). The effective stiffness $(EI)_{eff}$ of the cold-formed steel and timber composite assembly can be determined using Equation (6.18).

$$(EI)_{eff} = E_t I_t + \gamma E_t A_t a1^2 + E_s I_s + E_s A_s a2^2 \tag{6.18}$$

Where I_t is the moment of inertia of timber floorboard, a1 is the distance between the centroid of timber and centroid of composite assembly, E_s is the modulus of elasticity of CFS, I_s is the moment of inertia of CFS, A_s is the area of CFS, a2 is the distance between the centroid of CFS and composite assembly. The distance between the CFS joist centroid and the centroid of the composite assembly can be determined from Equations (6.19) and (6.20).

$$a2 = \frac{\gamma E_t A_t (h_s + h_t)}{2(\gamma E_t A_t + E_s A_s)} \tag{6.19}$$

$$a1 = \frac{1}{2}(h_s + h_t) - a2 \tag{6.20}$$

The mid-span deflection of a simply supported beam loaded at its third point with two equal concentrated loads P can be calculated using Equation (6.21) in accordance with the theory of elasticity.

$$\delta = 23PL^3/648EI_{eff} \tag{6.21}$$

6.3.3 Comparison of Experimental and Theoretical Elastic Calculations

Tables 6.3 and 6.4 compare the ultimate theoretical elastic bending moment values and mid-span deflection values, respectively, according to the proposed analytical methods discussed and the physical test values. In Table 6.3, $M_{u,exp}$ is the moment capacity obtained from the experiments, M_{el} is the elastic bending moment with full-shear interaction calculated in accordance with Equation (6.8), and M is the ultimate elastic bending moment capacity with partial shear interaction of the CFST beams obtained using Equation (6.10).

Table 6.3: Comparison of elastic ultimate theoretical bending moment values with test values

Specimen	$M_{u,exp}$ (kN.m)	M_{el} (kN.m)	ΔM (kN.m)	M (kN.m)	$M_{u,exp}/M$
SP-2	43.65	59.8	14.3	45.5	0.96
SP-3	51.5	59.8	10	49.8	1.05
SP-4	47.85	59.8	9.6	50.2	0.95
SP-5	63.6	59.8	10	49.8	1.28
SP-6	65.89	59.8	7.24	52.56	1.25
SP-7	65	59.8	8.5	51.3	1.27
SP-8	54.1	59.8	14.2	45.6	1.19
SP-9	60	59.8	10.25	49.55	1.21
SP-10	64.35	59.8	8.5	51.3	1.25
SP-11	60.75	59.8	10.65	49.15	1.24
SP-12	53.25	59.8	10	49.8	1.07
SP-13	64.5	59.8	5.4	54.4	1.19
SP-14	62.9	59.8	9	50.8	1.24

Similarly, in Table 6.4, δ_{exp} is the deflection of the composite CFST beam obtained from the experiments, and $\delta_{analytical}$ is calculated using Equation (6.21) by considering the effective bending stiffness.

As seen from Tables 6.3 and 6.4, the results calculated by the elastic analysis approach based on the composite coefficient method were in good agreement with the test values. The tested bending capacities of the composite beam utilising ductile shear connectors (M8 and M12 nuts and bolts and M12 coach screws) were found to be 20 to 28% higher than the capacities proposed by the elastic design approach. This approach produced slightly conservative results compared to the plastic analysis method, but this approach is believed to produce a safer design of such flooring systems in actual construction in the lack of extensive experimental data. The effective bending stiffness values of the composite CFST beams obtained experimentally and using the γ method were close. Therefore, the calculated deflection of the composite beams in the elastic stage demonstrated good results with the test observations. Hence, the proposed analytical methods can reliably be used to calculate the ultimate elastic bending capacity and mid-span deflection of composite CFST beams.

Table 6.4: Comparison of elastic limit theoretical deflection values with test values

Specimen	δ_{exp} (mm)	$\delta_{analytical}$ (mm)	Relative Error (%)
SP-2	36.5	37.7	-3.2
SP-3	43.6	40.11	8.7
SP-4	36.6	36.55	0.13
SP-5	53.86	46.33	16.2
SP-6	47.11	41.35	13.9
SP-7	57.1	49.37	15.65

SP-8	46.8	46.53	0.58
SP-9	50.5	48.5	4
SP-10	53	47.8	10.8
SP-11	52.2	51.4	1.56
SP-12	44.2	38.79	13.9
SP-13	44	40.48	8.7
SP-14	52	45.2	15

There are well-developed design guidelines for hot-rolled steel beams and reinforced concrete slabs, and timber concrete composite floors, but unfortunately, no adequate design methods exist for lightweight CFST floors except for some preliminary research in this field with promising findings(Kyvelou et al., 2017a). In the next section, a simplified design example is presented with the purpose of demonstrating the beneficial effect of composite action on the flexural capacity of cold-formed steel and timber flooring systems.

6.4 Worked Example

Design a 6.0m long-span flooring system comprising G450 CFS joists at 600mm centres sheathed with timber floorboard panels as shown in Figure 6.5 to satisfy ultimate limit state (ULS) and serviceability limit state (SLS) requirements. The floor is subjected to uniform loading of 2.0 kPa and 3.0 kPa dead and live load, respectively. The shear connectors for this flooring to be M8 nuts and bolts at the spacing of 300mm. The mechanical properties and geometrical characteristics of the steel sections, timber floorboards and shear connectors are presented below.

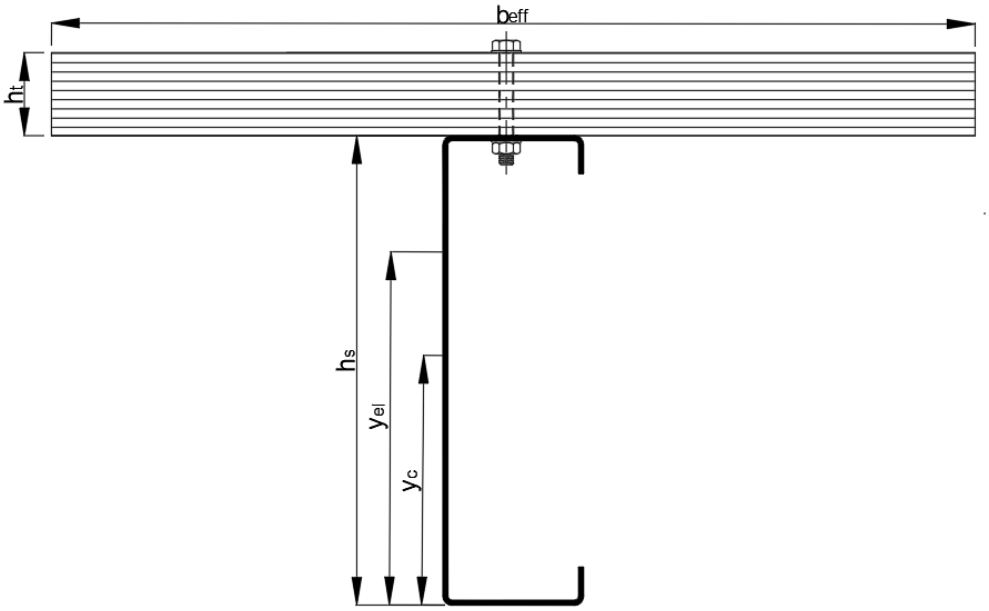

Figure 6.5: Cross-section of examined CFST beam for worked example

CFS joist description:

Yield strength, Fy = 450 MPa; Elastic modulus, Es = 200,000 MPa

Height, h_s = 200mm; Thickness, t_s = 2.4 mm; Area A_s = 900 mm^2; Second moment of area, I_s = 5.68x10^6 mm^4 ; Z_x = 56.62x10^3 mm^3

Timber floorboard:

Timber type = F11 grade structural plywood panel; Bending yield strength, F_{by} = 20 MPa; Compressive strength, F_{cb} = 28 MPa; Elastic modulus in bending, E_b = 10,000 MPa; Thickness, t_b = 45mm; Effective width, b_{eff} = 600mm; Second moment of area, Ib = 4556250 mm^4

6.4.1 Design Loads

Uniformly distributed dead load as line load on each beam, DL = 2.0 x 0.6 = 1.2 kN/m

Uniformly distributed live load as line load on each beam, LL = 3.0 x 0.6 = 1.8 kN/m

For ULS design, the design load is: q* = 1.2DL + 1.5LL = 1.2 x 1.2 + 1.5 x 1.8 = 4.14 kN/m

For SLS design, the design load is: q_s = 1.0DL + 1.0LL = 1.0 x 1.2 + 1.0 x 1.8 = 3 kN/m

Design bending moment, $M_d = q^*L^2/8$ = 18.63 kN.m

Design shear force, $V_d = q^*L/2$ = 12.42 kN

6.4.2 Attained Degree of Shear Connection

The design shear capacity of the individual fastener and bearing resistance of the timber sheathing are calculated from Equations (6.3) and (6.4), respectively:

$V_f = \phi$ x 0.62 x f_{uf} x n_s x A_f = 9.9 kN

$V_b = \phi$ x d_f x t_b x f_{cb} = 8 kN

The magnitude of longitudinal shear force Q is the minimum of V_f or V_b = 8 kN

The longitudinally transferred shear force is limited by the tensile strength of steel, T or compressive strength of the timber sheathing, C, as determined in Equations (6.1) and (6.2), respectively;

T = 900 × 450 = 405 kN

C = 600 × 45 × 28 = 756 kN

Hence, according to Equations (6.5) and (6.6), the required number of fasteners to achieve a complete shear connection is:

N_f = 2 × 405/8 = 101

The number of the employed fastener in the examined system is; n = 6000/300 = 20

Therefore, attained degree of shear connection η is: η = 20/101 = 0.2 ≤ 1

6.4.3 Calculation of Shear Bond Coefficient and Effective Flexural Stiffness

$$\gamma = \frac{1}{1 + \frac{\pi^2 S E_t A_t}{K L^2}}$$

Where γ is shear bond coefficient,

S (spacing of shear connections) = 300 mm,

E_t (modulus of elasticity of timber floorboard) = 10,000 MPa,

A_t (area of timber floorboard) = 600 x 45 = 27000 (mm^2),

K (slip modulus) = 10000 N/mm,

L (length of member) = 6000 mm

From the above equation, γ = 0.31

The effective stiffness $(EI)_{eff}$ of the cold-formed steel and timber composite assembly can be determined as below.

$$(EI)_{eff} = E_t I_t + \gamma E_t A_t a1^2 + E_s I_s + E_s A_s a2^2$$

a1 is the distance between the centroid of timber and centroid of composite assembly, and a2 is the distance between the centroid of CFS and composite assembly.

$$a2 = \frac{\gamma E_t A_t (h_s + h_t)}{2(\gamma E_t A_t + E_s A_s)} = 39.4\ mm$$

$$a1 = \frac{1}{2}(h_s + h_t) - a2 = 84.6\ mm$$

Hence, $(EI)_{eff}$ = 2.06 x 10^{12} = N.mm^2

6.4.4 Calculation of Bending Moment Capacity

Considering the slip between the CFS and plywood interface, the actual bending capacity (M) of composite CFST beams with a partial shear connection can be calculated according to Equation below.

$$M = M_{el} - \Delta M$$

M_{el} is the elastic bending capacity of CFST beams with full shear interaction, ΔM is the moment due to slip strain

The ultimate elastic bending moment of the CFST beam with the full shear interaction may be taken as the smaller value of the following.

If the failure in the CFST beam is initiated by damage to plywood, $M_{el} = f_{yp} I_T n / y_{el}$

If the failure in the CFST beam is initiated by the yielding of CFS, $M_{el} = f_{ys} I_T / y_{el}$

Where, y_{el} is the centroid of the composite assembly.To calculate the elastic bending moment capacity, first I_T (transformed section moment of inertia), n (ratio of elastic moduli of steel to plywood (E_s/E_p)) is to be calculated

$$n = \frac{210000}{10000} = 21$$

Centroid of the composite assembly can be calculated as below;

$$y_{el} = \frac{y_c A_s + \frac{A_t}{n}\left(h_s + \frac{h_t}{2}\right)}{A_s + \frac{A_t}{n}} = 184.9 \text{ mm}$$

Transformed moment of area is calculated as

$$I_T = I_s + \frac{b_{eff} t_t^3}{12n} + A_s(y_{el} - y_c)^2 + \frac{A_t}{n}\left(y_{el} - h - \frac{h_t}{2}\right)^2 = 11.1 \text{ x } 10^6 \text{ mm}^4$$

Hence, the elastic ultimate bending moment of CFST beam is, M_{el} = 450x11.1x10^6 / 184.9 = 27.1 kN.m

Moment due to slip strain,

$$\Delta M = \frac{M_{el} h h_s A_s (E_s I_T - E I_{eff})}{6 E I_{eff} I_T + h h_s E_s A_s I_T} = 1.3\ kN.m$$

Actual bending moment capacity of composite CFST beam with partial shear connection,

M = 27.1-1.3 = 25.6 kN.m > M_d Ok #

6.4.5 Calculation of Shear Resistance

The mobilisation of composite action behaviour within the investigated flooring system can significantly impact cross-sectional moment capacity, but the shear buckling resistance relies purely on the bare steel joist.

Hence, according to Appendix D of AS/NZS 4600: Cold-formed steel structures, the elastic buckling shear force of the web (Vcr) of CFS members in shear shall be determined as follows;

$$V_{cr} = \frac{\pi^2 E A_w k_v}{12(1 - v^2)\left(\frac{d_1}{t}\right)^2}$$

Where, $K_v = K_{ss} + K_n (K_{sf} - K_{ss})$

Since, a/d1 = 5000/250 = 20 > 1

K_{ss} = 5.34 + 4/(a/d_1) = 5.54, K_n = 0.23

K_{sf} = 8.98+5.61/(a/d_1)^2 – 1.99/(a/d_1)^3 = 8.99

Hence, K_v = 5.54 + 0.23x(8.99-5.54) = 6.33 and $A_w = d_1.t$ = 250x2.4 = 600mm^2

V_{cr} = 63270 N = 63.27 kN

As per the clasue 7.2.3 of AS 4600, the nominal member shear capacity (Vv) of CFS beams shall be calculated as follows

Since, $\lambda_v = \sqrt{\frac{V_y}{V_{cr}}}$

V_y = 0.6xA_wxf_y = 0.6x600x450 = 162 kN

λ_v = (162/63.27)^0.5 = 1.6> 1.227, $V_v = V_{cr}$ = 63.27 kN

V_{cr} = 63.27 kN > V_d Ok#

6.4.6 Calculation of Deflection

The midspan deflection of simply supported beam under uniformly distributed load q_s* is;

$$\delta_{max} = \frac{5q_s L^4}{384EI_{eff}}$$

$\delta_{max} = 24.5\ mm$ < Span/240 = 25 mm Ok#

Hence the composite beam is structurally adequate for bending, shear and deflection checks.

The moment capacity of the bare steel beam (as per the manufacturer) used in this example is 18.5 kN.m. Considering the shear interaction due to mechanical

fasteners, the moment capacity of the composite system is calculated to be 25.6 kN.m. There is a 39% increase in the bending capacity of the system. As can be seen from the results of the worked example, the distinction between the bare steel joist and the composite beam suggests a sufficient justification for considering the composite behaviour in the composite CFST flooring system and the advantages to be gained in terms of strength and stiffness.

6.5 Concluding Remarks

In this chapter, a design method for the prediction of elastic bending moment capacity and deflection of composite CFST beam is presented. A relationship is also presented to determine the spacing of shear connectors to attain complete shear interaction. The design method is found to be capable of predicting moment capacity and flexural stiffness obtained from the experimental investigations. The calculation of the moment capacity of a composite CFST flooring system is based on the composite coefficient method, which is based on the attained degree of partial shear interaction. The magnitude of the moment capacity varies between the moment capacity of bare CFS joist and composite beam with full shear interaction. By using the shear bond coefficient based on the Gamma method, the effective flexural stiffness of the composite system was determined. The effective bending stiffness values of the composite CFST beams obtained experimentally and using the Gamma method were close. The moment capacity and deflection values determined through experimental testing were found to be, on average, 16% and 8% higher than those obtained from design equations, demonstrating a satisfactory agreement. The elastic analysis method yielded

slightly more conservative results than the plastic analysis method, but this methodology is anticipated to result in a safer design of composite flooring systems without significant experimental data. Finally, a simplified calculation example to predict the bending capacity and deflection of the composite system by utilizing the proposed design method is presented by considering the shear interaction between two components. Apparently, the proposed design method can be used by practising engineers to design composite CFST flooring systems.

7 Conclusions and Future Research

7.1 Conclusions

Cold-formed steel members are chosen to construct flooring systems because of their high strength-to-weight ratio, ease of fabrication, ease of transportation, and rapid installation. If an adequate interconnection between cold-formed steel joists and floorboard sheathing can be achieved, this type of composite flooring system has many benefits over traditional flooring systems with timber joists. Cold-formed steel composite flooring systems offer the advantage of a high strength-to-weight ratio, which eventually reduces the self-weight of floors and less imposed load on the foundation. This type of flooring system can be manufactured off-site and assembled on-site easily and quickly in a modular way, reducing construction time. The modular construction of the flooring system also helps to make the project cost-effective and better quality controlled. Therefore, the key focus of this thesis was to study the structural behaviour of prefabricated lightweight cold-formed steel and structural plywood flooring system both experimentally and numerically in terms of their attained degree of shear interaction and to quantify the benefits in terms of ultimate bending capacity and flexural stiffness.

An experimental investigation, discussed in Chapter 3, was conducted to investigate the load-slip response of different fasteners that can be used as shear connectors for composite cold-formed steel and timber (CFST) flooring systems. Material tests of plywood and cold-formed steel joists were carried out to determine their mechanical properties. Push-out tests were carried out on specimens with four different types of fasteners along with adhesives. Based on

the push-out test results, an analytical equation derived from the Foschi formula (Foschi, 1977) to get a load-slip relationship of fasteners in timber-based floorboards and cold-formed steel has been proposed, which can be used in numerical models. The full-scale testing of composite CFST beams, as described in Chapter 4, was carried out to study their structural performance. Four-point bending tests were conducted on twelve composite beam specimens and one bare steel system. In the proposed composite CFST flooring system, 45mm thick structural plywood panels were connected to the 2.4mm thick cold-formed steel C-section joist using self-drilling screws, coach screws, and nuts and bolts. The performance of different types of shear connectors on the composite action is experimentally investigated and compared with the theoretical plastic section. The ultimate moment capacity and flexural stiffness of the each of the examined composite beams normalised by theoretical plastic moment capacity and flexural stiffness as discussed in Chapter 4 highlighted the strength and stiffness capacity achieved in relation to the theoretical plastic capacity. It has been found that the spacing of the fasteners significantly influences the load-carrying capacity and stiffness of the examined composite floors. Furthermore, application of structural adhesives on the bottom surface of plywood panels and the top flange of the CFS joist enhances the flexural stiffness of the system under serviceability loading. Up to a 40% increase in the composite system's flexural stiffness was found compared to the bare steel system. The ductility of fasteners was found to have a substantial impact on the moment capacity and flexural stiffness of the examined system. In comparison to the bare CFS joist alone, the moment capacity of the composite CFST systems with 400mm fastener spacing was found to be increased by 6%, 47%, 54%, and 58% with SDS, M8 nuts and bolts,

M12 coach screws, and M12 nuts and bolts, respectively. For stiffer connections e.g. nuts and bolts and coach screws, the influence of closer fastener spacing (for example, 200 mm and 400 mm) on the moment capacity and flexural stiffness was not of too much difference as, in such cases, the capacity was found to be governed by the material strength of CFS or timber sheathing in comparison with the ductility of shear connectors.

As thoroughly discussed and presented in Chapter 5, three-dimensional finite element models are developed and validated against the experimental test results. All the validated models can predict the ultimate load capacity and flexural stiffness of the tested systems along with the exhibited failure modes. After the successful validation, parametric studies have been performed to investigate the influence of key parameters on the structural behaviour of composite CFST floors. The effect of CFS joist thickness, CFS web depth and fastener spacing on the flexural behaviour of composite floor was studied. Results from the conducted parametric studies have demonstrated that thicker steel sections and deeper web exhibited higher loading capacity and stiffness. The influence of fastener spacing on the ultimate strength capacity of composite CFST beams was found to be significant and in linear fashion. For example, a 4500 mm span composite beam with M8 nut and bolt at 600 mm and 200 mm spacing was found to have a load-carrying capacity of 68 kN and 87 kN, respectively. As a result of the mobilisation of composite action, substantial benefits in terms of strength and stiffness of composite CFST beams were demonstrated through the presented numerical studies.

Shear connection relationships to achieve complete shear interaction in composite CFST beam is thoroughly discussed. The proposed design equations

are presented to calculate the elastic bending capacity of examined composite systems taking into account the benefit of composite action. Since there will be a slip between two materials, partial shear interaction is assumed for the computation. Hence, the prediction of the moment capacity of the composite CFST flooring system is based on the attained degree of shear interaction, which varies between the moment capacity of the bare steel system and the equivalent composite system with full shear interaction. The effective flexural stiffness of the composite system was calculated based on the Gamma method by using the shear bond coefficient, as discussed in Chapter 6. The effective bending stiffness values of the composite CFST beams obtained experimentally and by using the Gamma method were close. The experimental results and calculated theoretical elastic values were compared in terms of moment capacity and deflection. On average, the moment capacity and deflection obtained from the experimental testing were 16% and 8%, respectively, higher than the one obtained from the design equations, which demonstrats a good agreement. Hence, the proposed analytical methods can reliably be used to calculate the ultimate elastic bending capacity and mid-span deflection of the composite CFST beams.

7.2 Recommendations for Future Research

The findings of this research have demonstrated the mobilisation of composite action through changes in a different types of fasteners as shear connectors leading to the substantial benefit in terms of the ultimate strength and flexural stiffness of cold-formed steel and timber flooring systems. Although the findings of this research are promising, improvements could be achieved for better

understanding of this type of system by conducting further studies which are not covered in this thesis.

Engineered timber floorboard of higher stiffness like cross-laminated timber (CLT), laminated veneer lumber (LVL) or laminated bamboo could be considered for the experimental testing of composite CFST flooring system. The necessity for using different timber floorboard sheathing for the construction of composite flooring systems should be based on the availability of timber in local regions around the world. Therefore, an extensive experimental analysis could be conducted with higher-stiffness timber sheathing as a way of improving the overall flexural stiffness of the composite system.

The effect of creep on the performance of the examined flooring system could be another factor to look into. Past studies have shown that creep can develop within timber-based floorboards, which might influence their flexural behaviour. Creep in timber can lead to loss of post-tensioning force in bolted shear connectors or grip of self-drilling screws, which can affect the strength and stiffness of the CFST floors. Additionally, long-term bending tests could be carried out to study the behaviour of the composite system under long-term service loading conditions.

Since the examined system is proposed for small to medium-scale construction to be used in residential buildings and industrial mezzanine floors, the flexural performance under ULS and SLS of composite CFST floors for larger span lengths (5.0 m to 6.0 m) shall be investigated. Accordingly, to accurately simulate the uniformly distributed loading on the CFS joist, six-point bending tests could be considered (instead of four-point bending), which can eliminate the need to stiffen the cross-sections due to more uniform loading distribution. Additionally,

rather than testing the specimen on simple supports like pin and roller, actual support conditions by using the angle brackets to fix the web of CFS joist to the primary steel supports as in real construction could be studied.

Finally, another factor that should be examined is the effect of concentrated loads (punching) at mid-span and close to web opening. Since CFS joists are thin-walled and susceptible to local instabilities, it is unclear whether the application of concentrated loads will reduce the capacity of the composite system and how other joists share the point load. Hence, it is imperative to consider the influence of point loads to better understand the structural performance of the composite CFST flooring systems to widen the existing design data source.

References

Abdel-Rahman, N. & Sivakumaran, K. S. 1997. Material Properties Models for Analysis of Cold-Formed Steel Members. *Journal of Structural Engineering,* 123**,** 1135-1143.

Ahmadi, B. H. & Saka, M. P. 1993. Behavior of Composite Timber-Concrete Floors. *Journal of structural engineering,* 119**,** 3111-3130.

Aisi 2007. American Iron and Steel Institute (AISI), North American Standard for Cold-Formed Steel Framing- General Provisions. Washington DC: American Iron and Steel Institute.

Al-Hunaity, S. A., Karki, D. & Far, H. 2023. Shear connection performance of cold-formed steel and plywood composite flooring systems: Experimental and numerical investigation. *Structures,* 48**,** 901-917.

Ansys Inc. Theory Reference for the Mechanical APDL and Mechanical Applications. Ansys Incorporation, Canonsburg, PA, 2009.

Arriaga-Martitegui, F., Peraza-Sánchez, F. & García-Esteban, L. 2008. Characteristic values of the mechanical properties of radiata pine plywood and the derivation of basic values of the layers for a calculation method. *Biosystems Engineering,* 99**,** 256-266.

Asiz, A. & Ahmed, D. 2013. Structural modeling and design of tall buildings composed of ultra-lightweight floor systems. 2013. Jeju, Korea.

Asiz, A. & Smith, I. 2009. Demands Placed on Steel Frameworks of Tall Buildings Having Reinforced Concrete or Massive Wood Horizontal Slabs. *Structural Engineering International,* 19**,** 395-403.

Ataei, A., Bradford, M. A. & Valipour, H. 2016. Sustainable Design of Deconstructable Steel-Concrete Composite Structures. *Procedia Engineering,* 145**,** 1153-1160.

Australian Steel Institute. 2019. *Growth in light gauge steel* [Online]. ASI. [Accessed 10/07/2019].

Bakker, M. C. M. & Peköz, T. 2003. The finite element method for thin-walled members—basic principles. *Thin-Walled Structures,* 41**,** 179-189.

Baleshan, B. & Mahendran, M. Improvements to the fire performance of light gauge steel floor systems. 20th International Specialty Conference on Cold-Formed Steel Structures - Recent Research and Developments in Cold-Formed Steel Design and Construction, 2010. 137-154.

Bamaga, S., Tahir, M. & Shek, P. N. 2019. Structural Behaviour of Cold-Formed Steel of Double C-Lipped Channel Sections Integrated with Concrete Slabs as Composite Beams. *Latin American Journal of Solids and Structures,* 16.

Bathon, L. & Graf, M. 2000. A continuous wood-concrete-composite system. World Conference of Timber Engineering, 2000 Whistler, BC. Whistler, BC.

Benítez, M. F. 2008. Development and testing of timber/concrete shear connectors. 2008. Concepcion, Chile.

British Standard 1991. BS EN 26891:1991 Timber structures-Joints made with mechanical fasteners.

Bsi 1998. BS 5950, Strucutral use of Steelwork in building- Part 5: Code of Practice for design of cold-formed thin gauge sections. London, UK: British Standard Institution.

Case 2006. THIN WALL 2, A Computer Program for Cross-section Analysis and Finite Strip Buckling Analysis and Direct Strength Design of Thin-walled Structures. Centre for Advanced Structural Engineering, School of Civil Engineering, The University of Sydney.

Ceccotti, A. 2002. Composite concrete-timber structures. *Progress in Structural Engineering and Materials,* 4**,** 264-275.

Cen 2004. EN 1995-1-1:2004 Eurocode 5: Design of timber structures-Part 1-1: General-Common rules and rules for buildings. European Committee for Standardization.

Cen 2005. BS EN 12512 Timber structures-Test methods-Cyclic testing of joints made with mechanical fasteners. European Committee for Standardization.

Chajes, A., Britvec, S. & Winter, G. 1963. Effects of cold-straining on structural sheet steels. *Journal of Structural Division,* 89**,** 1-32.

Chan, A. P. C., Darko, A. & Ameyaw, E. E. J. S. 2017. Strategies for promoting green building technologies adoption in the construction industry—An international study. 9**,** 969.

Chou, S. M., Chai, G. B. & Ling, L. 2000. Finite element technique for design of stub columns. *Thin-Walled Structures,* 37**,** 97-112.

Chu, X.-T., Kettle, R. & Li, L.-Y. 2004. Lateral-torsion buckling analysis of partial-laterally restrained thin-walled channel-section beams. *Journal of Constructional Steel Research,* 60**,** 1159-1175.

Couchman, G. H. 2016. Minimum degree of shear connection rules for UK construction to Eurocode 4. Steel Construction Institute.

Crisinel, M. & O'leary, D. 1996. Composite Floor Slab Design and Construction. *Structural Engineering International,* 6.

Deam, B. L., Fragiacomo, M. & Buchanan, A. H. 2008. Connections for composite concrete slab and LVL flooring systems. *Material and Structures,* 41**,** 495-507.

Dickof, C., Stiemer, S. F., Bezabeh, M. A. & Tesfamariam, S. 2014. CLT-Steel Hybrid System: Ductility and Overstrength Values Based on Static Pushover Analysis. 28**,** A4014012.

Dubina, D. & Ungureanu, V. 2002. Effect of imperfections on numerical simulation of instability behaviour of cold-formed steel members. *Thin-Walled Structures,* 40**,** 239-262.

Ellobody, E. & Young, B. 2006. Performance of shear connection in composite beams with profiled steel sheeting. *Journal of Constructional Steel Research,* 62**,** 682-694.

Far, H. 2020a. Flexural Behavior of Cold-Formed Steel-Timber Composite Flooring Systems. *Journal of structural engineering,* 146**,** 06020003.

Far, H. 2020b. Flexural Behaviour of Cold Formed Steel-Timber Flooring Systems. *Journal of Structural Engineering*.

Far, H., Saleh, A. & Firouzianhaji, A. 2017. A simplified method to determine shear stiffness of thin walled cold formed steel storage rack frames. *Journal of Constructional Steel Research,* 138**,** 799-805.

Foschi, R. O. 1977. Analysis of wood diaphragms and trusses. Part I: Diaphragms. *Canadian Journal of Civil Engineering,* 4**,** 345-352.

Gardner, L. & Ashraf, M. 2006. Structural design for non-linear metallic materials. *Engineering Structures,* 28**,** 926-934.

Gardner, L. & Yun, X. 2018. Description of stress-strain curves for cold-formed steels. *Construction and Building Materials,* 189**,** 527-538.

Gelfi, P., Giuriani, E. & Marini, A. 2002. Stud Shear Connection Design for Composite Concrete Slab and Wood Beams. *Journal of structural engineering,* 128**,** 1544-1550.

Gendy, B. L. & Hanna, M. T. 2017. Effect of geometric imperfections on the ultimate moment capacity of cold-formed sigma-shape sections. *HBRC Journal,* 13**,** 163-170.

Haidarali, M. R. & Nethercot, D. A. 2011. Finite element modelling of cold-formed steel beams under local buckling or combined local/distortional buckling. *Thin-Walled Structures,* 49**,** 1554-1562.

Hailu, M. 2015. *Long-term performance of timber-concrete composite flooring systems.* Master of Research Master of Research, University of Technology Sydney.

Hanaor, A. 2000. Tests of composite beams with cold-formed sections. *Journal of Constructional Steel Research,* 54**,** 245-264.

Hancock, G. J. 1998. *Design of Cold-formed Steel Structures: To Australian/New Zealand Standard AS/NZS 4600: 1996*, Australian Institute of Steel Construction.

Hancock, G. J. 2003. Cold-formed steel structures. *Journal of Constructional Steel Research,* 59**,** 473-487.

Hassanieh, A. 2017. *Development of steel-timber composite system for large scale construction.* PhD, University of New South Wales.

Hassanieh, A., Valipour, H. R. & Bradford, M. A. 2016a. Experimental and numerical study of steel-timber composite (STC) beams. *Journal of Constructional Steel Research,* 122**,** 367-378.

Hassanieh, A., Valipour, H. R. & Bradford, M. A. 2016b. Load-slip behaviour of steel-cross laminated timber (CLT) composite connections. *Journal of Constructional Steel Research,* 122**,** 110-121.

Hassanieh, A., Valipour, H. R. & Bradford, M. A. 2017a. Composite connections between CLT slab and steel beam: Experiments and empirical models. *Journal of Constructional Steel Research,* 138**,** 823-836.

Hassanieh, A., Valipour, H. R., Bradford, M. A. & Sandhaas, C. 2017b. Modelling of steel-timber composite connections: Validation of finite element model and parametric study. *Engineering Structures,* 138**,** 35-49.

Hsu, C.-T. T., Punurai, S., Punurai, W. & Majdi, Y. 2014. New composite beams having cold-formed steel joists and concrete slab. *Engineering Structures,* 71**,** 187-200.

Irwan, J. M., Hanizah, A. H. & Azmi, I. 2009. Test of shear transfer enhancement in symmetric cold-formed steel–concrete composite beams. *Journal of Constructional Steel Research,* 65**,** 2087-2098.

Irwan, J. M., Hanizah, A. H., Azmi, I. & Koh, H. B. 2011. Large-scale test of symmetric cold-formed steel (CFS)–concrete composite beams with BTTST enhancement. *Journal of Constructional Steel Research,* 67**,** 720-726.

Jatheeshan, V. & Mahendran, M. 2016. Experimental Study of Cold-Formed Steel Floors Made of Hollow Flange Channel Section Joists under Fire Conditions. *Journal of structural engineering,* 142**,** 04015134.

Johnson, R. P. & Molenstra, N. 1991. Partial shear connection in composite beams for buildings. *Proceedings - Institution of Civil Engineers. Part 2. Research and theory,* 91**,** 679-704.

Kalkert, R. E. & Dolan, J. D. 1997. Behavior of 8-D nailed stud-to-sheathing connections. *Forest Products Journal,* 47**,** 95-102.

Kankanamge, N. D. 2010. *Structural Behaviour and Design of Cold-formed Steel Beams at Elevated Temperatures.* Doctor of Philosophy, Queensland University of Technology.

Kankanamge, N. D. & Mahendran, M. 2012. Behaviour and design of cold-formed steel beams subject to lateral–torsional buckling. *Thin-Walled Structures,* 51**,** 25-38.

Karki, D., Al-Hunaity, S., Far, H. & Saleh, A. 2022. Composite connections between CFS beams and plywood panels for flooring systems: Testing and analysis. *Structures,* 40**,** 771-785.

Karki, D. & Far, H. 2021. State of the art on composite cold-formed steel flooring systems. *Steel Construction*.

Karki, D., Far, H. & Saleh, A. 2021. Numerical Studies into Factors Affecting Structural Behaviour of Composite Cold-Formed Steel and Timber Flooring Systems. *Journal of Building Engineering***,** 102692.

Keerthan, P. & Mahendran, M. 2013. Experimental studies of the shear behaviour and strength of lipped channel beams with web openings. *Thin-Walled Structures,* 73**,** 131-144.

Kieslich, H. & Holschemacher, K. Composite Constructions of Timber and High-Performance Concrete. 2010. Trans Tech Publications, 1171-1176.

Kwon, Y. B. & Hancock, G. J. 1993. Post-buckling analysis of thin-walled channel sections undergoing local and distortional buckling. *Computers & Structures,* 49**,** 507-516.

Kyvelou, P. 2017. *Structural Behviour of Composite Cold-Formed Steel Systems.* PhD, Imperial College London.

Kyvelou, P., Gardner, L. & Nethercot, D. A. 2017a. Design of Composite Cold-Formed Steel Flooring Systems. *Structures,* 12**,** 242-252.

Kyvelou, P., Gardner, L. & Nethercot, D. A. 2017b. Testing and Analysis of Composite Cold-Formed Steel and Wood−Based Flooring Systems. *Journal of Structural Engineering,* 143.

Kyvelou, P., Gardner, L. & Nethercot, D. A. 2018. Finite element modelling of composite cold-formed steel flooring systems. *Engineering Structures,* 158**,** 28-42.

Lacey, A. W., Chen, W., Hao, H. & Bi, K. 2018. Structural response of modular buildings – An overview. *Journal of Building Engineering,* 16**,** 45-56.

Laím, L., Rodrigues, J. P. C. & Silva, L. S. D. 2013. Experimental and numerical analysis on the structural behaviour of cold-formed steel beams. *Thin-Walled Structures,* 72**,** 1-13.

Lakkavalli, B. S. & Liu, Y. 2006. Experimental study of composite cold-formed steel C-section floor joists. *Journal of Constructional Steel Research,* 62**,** 995-1006.

Leborgne, M. R. & Gutkowski, R. M. 2010. Effects of various admixtures and shear keys in wood–concrete composite beams. *Construction and Building Materials,* 24**,** 1730-1738.

Li, Y., Shen, H., Shan, W. & Han, T. 2012. Flexural behavior of lightweight bamboo–steel composite slabs. *Thin-Walled Structures,* 53**,** 83-90.

Liu, J., Liu, R., Li, W., Wang, J. & Chen, L. 2022. Experimental Study on the Flexural Performance of Timber–Steel Composite (TSC) I-Beams. 12**,** 1206.

Liu, X., Bradford, M. A. & Lee, M. S. S. 2015. Behavior of High-Strength Friction-Grip Bolted Shear Connectors in Sustainable Composite Beams. 141**,** 04014149.

Loss, C. & Davison, B. 2017. Innovative composite steel-timber floors with prefabricated modular components. *Engineering Structures,* 132**,** 695-713.

Loss, C., Piazza, M. & Zandonini, R. 2016. Connections for steel–timber hybrid prefabricated buildings. Part I: Experimental tests. *Construction and Building Materials,* 122**,** 781-795.

Lukaszewska, E., Fragiacomo, M. & Johnsson, H. 2010. Laboratory Tests and Numerical Analyses of Prefabricated Timber-Concrete Composite Floors. *Journal of structural engineering,* 136**,** 46-55.

Majdi, Y., Hsu, C.-T. T. & Zarei, M. 2014. Finite element analysis of new composite floors having cold-formed steel and concrete slab. *Engineering Structures,* 77**,** 65-83.

Mirambell, E. & Real, E. 2000. On the calculation of deflections in structural stainless steel beams: an experimental and numerical investigation. *Journal of Constructional Steel Research,* 54**,** 109-133.

Mirza, O. & Uy, B. 2009. Behaviour of headed stud shear connectors for composite steel–concrete beams at elevated temperatures. *Journal of Constructional Steel Research,* 65**,** 662-674.

Nash 2007. General guide to steel- framed building. Victoria: National Association of Steel-Framed Housing.

Navaratnam, S., Ngo, T., Gunawardena, T. & Henderson, D. 2019. Performance Review of Prefabricated Building Systems and Future Research in Australia. 9**,** 38.

Navaratnam, S., Widdowfield Small, D., Gatheeshgar, P., Poologanathan, K., Thamboo, J., Higgins, C. & Mendis, P. 2021. Development of cross laminated timber-cold-formed steel composite beam for floor system to sustainable modular building construction. *Structures,* 32**,** 681-690.

Newton, P. W., Baum, S., Bhatia, K., Brown, S. K., Foran, B., Grant, T., Mak, S. L., Mitchell, V. G., Neate, K. & Smith, N. C. 2001. Human Settlements. *In:* Csiro Publishing on Behalf of the Department of the Environment and Heritage, C. (ed.) *Australia State of the Environment Report 2001.* CSIRO Publishing on behalf of the Department of the Environment and Heritage, Canberra.

Nie, J. & Cai, C. S. 2003. Steel-Concrete Composite Beams Considering Shear Slip Effects. 129**,** 495-506.

Oehlers, D. J. & Sved, G. 1995. Composite beams with limited-slip-capacity shear connectors. *Journal of Structural Engineering (United States),* 121**,** 932-938.

Omer, A. M. 2009. Energy use and environmental impacts: A general review. 1**,** 053101.

Originpro 2021. OriginPro-Graphing and Analysis Tool, Version number 2021. OriginLab Corporation, Northampton, MA, USA.

Parnell, R., Davies, B. W. & Xu, L. 2010. Vibration Performance of Lightweight Cold-Formed Steel Floors. *Journal of structural engineering,* 136**,** 645-653.

Pham, C. H. & Hancock, G. J. 2010. Numerical simulation of high strength cold-formed purlins in combined bending and shear. *Journal of Constructional Steel Research,* 66**,** 1205-1217.

Pham, C. H. & Hancock, G. J. 2013. Experimental Investigation and Direct Strength Design of High-Strength, Complex C-Sections in Pure Bending. 139**,** 1842-1852.

Quach, W. M., Teng, J. G. & Chung, K. F. 2006. Finite element predictions of residual stresses in press-braked thin-walled steel sections. *Engineering Structures,* 28**,** 1609-1619.

Rackham, J. W., Couchman, G. H. & Hicks, S. J. 2009. Composite slabs and beams using steel decking: Best practice for design and construction. *MCRMA Technical paper No.13.* Steel Construction Institute.

Raffoul, S., Heywood, M., Moutaftsis, D. & Rowell, M. 2019. Experimental Investigation of Cold-Formed Steel-Timber Board Composite Floor Systems. *International Journal of Structural and Construction Engineering,* 13**,** 509-514.

Rasmussen, K. J. R. 2003. Full-range stress–strain curves for stainless steel alloys. *Journal of Constructional Steel Research,* 59**,** 47-61.

Ren, W.-X., Fang, S.-E. & Young, B. 2006. Analysis and design of cold-formed steel channels subjected to combined bending and web crippling. *Thin-Walled Structures,* 44**,** 314-320.

Rondal, J. 2000. Cold formed steel members and structures: general report. *Journal of constructional steel research,* 55**,** 155-158.

Sakumoto, Y., Hirakawa, T., Masuda, H. & Nakamura, K. 2003. Fire resistance of walls and floors using light-gauge steel shapes. *Journal of Structural Engineering,* 129**,** 1522-1530.

Saleh, A., Far, H. & Mok, L. 2018. Effects of different support conditions on experimental bending strength of thin walled cold formed steel storage upright frames. *Journal of constructional steel research,* 150**,** 1-6.

Schafer, B. W. 2008. Review: The Direct Strength Method of cold-formed steel member design. *Journal of Constructional Steel Research,* 64**,** 766-778.

Schafer, B. W. & Pekoz, T. 1998a. Computational modelling of cold-formed steel characterising geometric imperfections and residual stresses. *Journal of Constructional Steel Research,* 47**,** 193-210.

Schafer, B. W. & Pekoz, T. 1998b. Direct strength prediction of cold-formed steel members using numerical elastic buckling solutions. *International Speciality Conference on Cold-Formed Steel Structures.* St.Louis, Missouri.

Schafer, B. W. & Peköz, T. 1999. Laterally Braced Cold-Formed Steel Flexural Members with Edge Stiffened Flanges. *Journal of structural engineering,* 125**,** 118-127.

Seo, J. K., Anapayan, T. & Mahendran, M. Initial Imperfection Characteristics of Mono-Symmetric LiteSteel Beams for Numerical Studies. Proceedings 5th International Conferance on Thin-Walled Structures:ICTWS 2008, 2008. Brisbane.

Shamayleh, O. & Far, H. 2022. Investigation on Structural Behaviour of Composite Cold-formed Steel and Reinforced Concrete Flooring Systems. *Steel and Composite Structures: an international journal*.

Shi, Y., Yang, K., Guan, Y., Yao, X., Xu, L. & Zhang, H. 2020. The flexural behavior of cold-formed steel composite beams. *Engineering Structures,* 218**,** 110819.

Standard Australia 1996. AS1393:1996 Coach screws-Metric series with ISO hexagon heads. SAI Global.

Standard Australia 2000. AS1110.1-2000 ISO Metric hexagon bolts and screws. SAI Global.

Standard Australia 2002. AS3566.1-2002; Self-drilling screws for buidling and construction industries-Part 1. SAI Global.

Standard Australia 2007. AS 1391-2007 Metallic materials -Tensile testing at ambient temperature. Standard Australia: SAI Global.

Standard Australia 2012. AS/NZS 2269.1:2012 Plywood-Structural, Part 1: Determination of structural properties-Test methods. Australia: SAI Global.

Standard Australia 2017. AS/NZS 2327:2017 Composite Structures-Composite steel-concrete construction in buildings. Australia: SAI Global.

Standard Australia 2018. AS/NZS: 4600-2018 Cold-formed steel structures. Australia: SAI Global.

Steinberg, E., Selle, R. & Faust, T. 2003. Connectors for Timber-Lightweight Concrete Composite Structures. *Journal of structural engineering,* 129**,** 1538-1545.

Stratco Australia. 2019. *Steel framing-Tuffloor framing* [Online]. [Accessed 1 October 2019].

Valente, I. & Cruz, P. J. S. 2004. Experimental analysis of Perfobond shear connection between steel and lightweight concrete. *Journal of Constructional Steel Research,* 60**,** 465-479.

Vella, N., Gardner, L. & Buhagiar, S. 2020. Experimental analysis of cold-formed steel-to-timber connections with inclined screws. *Structures,* 24**,** 890-904.

Von Karman, T., Sechler, E. E. & Donnel, L. H. 1932. Strength of thin plates in compression. *Transaction ASME,* 54(5).

Wang, H. & Zhang, Y. 2009. Experimental and numerical investigation on cold-formed steel C-section flexural members. *Journal of Constructional Steel Research,* 65**,** 1225-1235.

Wang, L. & Young, B. 2014. Design of cold-formed steel channels with stiffened webs subjected to bending. *Thin-Walled Structures,* 85**,** 81-92.

Wehbe, N., Wehbe, A., Dayton, L. & Sigl, A. 2011. Development of Concrete/Cold Formed Steel Composite Flexural Members. *Structures Congress 2011.*

Winter, G. 1947. Strength of thin steel compression flanges. *Transaction ASCE,* 112**,** 527-554.

Xu, L., Ling, Z., Xie, W. & Schuster, R. 2000. Dynamic behaviour of floors with cold-formed steel joists. International Speciality Conference on Cold-Formed Steel Structures, 2000.

Xu, L., Sultana, P. & Zhou, X. 2009. Flexural strength of cold-formed steel built-up box sections. *Thin-Walled Structures,* 47**,** 807-815.

Xu, L. & Tangorra, F. M. 2007. Experimental investigation of lightweight residential floors supported by cold-formed steel C-shape joists. *Journal of Constructional Steel Research,* 63**,** 422-435.

Yam, L. C. P. 1981. *Design of composite steel-concrete structures,* Guildford, Surrey, Surrey University Press.

Yang, J. & Liu, Q. 2012. An experimental study into flexural behaviour of sigma purlins attached with roof sheets. *Engineering Structures,* 45**,** 481-495.

Yang, R., Li, H., Lorenzo, R., Ashraf, M., Sun, Y. & Yuan, Q. 2020. Mechanical behaviour of steel timber composite shear connections. *Construction and Building Materials,* 258**,** 119605.

Yang, R., Li, H., Lorenzo, R., Sun, Y. & Ashraf, M. 2021. Flexural behaviour of steel timber composite (STC) beams. *Steel and Composite Structures,* 41**,** 193-207.

Yeoh, D., Fragiacomo, M., Franceschi, M. D. & Boon, K. H. 2011. State of the Art on Timber-Concrete Composite Structures: Literature Review. 137**,** 1085-1095.

Young, B. & Rasmussen, K. J. R. 1998. Tests of Fixed-Ended Plain Channel Columns. *Journal of structural engineering,* 124**,** 131-139.

Yu, C. & Schafer, B. W. 2003. Local Buckling Tests on Cold-Formed Steel Beams. *Journal of structural engineering,* 129**,** 1596-1606.

Yu, C. & Schafer, B. W. 2006. Distortional Buckling Tests on Cold-Formed Steel Beams. *Journal of structural engineering,* 132**,** 515-528.

Yu, C. & Schafer, B. W. 2007. Simulation of cold-formed steel beams in local and distortional buckling with applications to the direct strength method. *Journal of Constructional Steel Research,* 63**,** 581-590.

Yu, M., Wiedmann, T., Crawford, R. & Tait, C. 2017. The Carbon Footprint of Australia's Construction Sector. *Procedia Engineering,* 180**,** 211-220.

Yu, W. W. 1999. Cold-formed steel structures. *Principles of Structural Design.* CRC Press.

Zhou, X., Shi, Y., Xu, L., Yao, X. & Wang, W. 2019. A simplified method to evaluate the flexural capacity of lightweight cold-formed steel floor system with oriented strand board subfloor. *Thin-Walled Structures,* 134**,** 40-51.

Appendix

The work presented in this thesis contains material published or submitted for publication, for which I am the main author.

Journal Papers

Karki, D. and Far, H., "State of the art on composite cold-formed steel flooring systems," ***Steel Construction****,* 2021.https://doi.org/10.1002/stco.202000026

Karki, D., Far, H., and Saleh, A., "Numerical Studies into Factors Affecting Structural Behaviour of Composite Cold-Formed Steel and Timber Flooring Systems," ***Journal of BuildingEngineering****,*p.102692,2021/05/09/2021.https://doi.org/10.1016/j.jobe.2021.102692

Karki, D., Al-Hunaity, S., Far, H., and Saleh, A., "Composite connections between CFS beams and plywood panels for flooring systems: Testing and analysis," ***Structures****,* vol. 40, pp. 771-785, 2022/06/01/ 2022.https://doi.org/10.1016/j.istruc.2022.04.064

Karki, D., Far, H., and Al-Hunity, S., "Determination of Slip Modulus of Cold-Formed Steel Composite Members Sheathed with Plywood Structural Panels," ***Steel and Composite Structures:*** *an international journal,* vol. 43, pp. 511-522, 2022/05/26 2022.https://doi.org/10.12989/scs.2022.43.4.511

Karki, D., Far, H., Nejadi, S., “Structural Behaviour of Prefabricated Composite Cold-formed Steel and Timber Flooring Systems”, Under review in ***ASCE Journal of Structural Engineering***

Karki, D., Far, H., Nejadi, S., “Analysis and Design of Lightweight Cold-formed Steel and Plywood Sheathed Composite Flooring Systems”, Under review in ***Finite Elements in Analysis and Design***